Università degli Studi di Ferrara

DOTTORATO DI RICERCA IN
"MEDICINA MOLECOLARE E FARMACOLOGIA"

CICLO XXX

COORDINATORE Prof. Francesco Di Virgilio

TFEB and AGC1 as homeostasis regulators: SOCE modulation and cell proliferation control

Settore scientifico disciplinare MED/04

Dottorando
Dott. Luigi Sbano

Tutore
Prof. Alessandro Rimessi

Cotutore
Prof. Paolo Pinton

Anni 2014/2017

Table of Contents

Chapter 1. TFEB-mediated increase in peripheral lysosomes regulates store-operated calcium entry

Abstract

Lysosomes are membrane-bound organelles mainly involved in catabolic processes. In addition, lysosomes can expel their contents outside of the cell via lysosomal exocytosis. Some of the key steps involved in these essential cellular processes, such as vesicular fusion and trafficking, require calcium (Ca^{2+}) signalling. Recent data show that lysosomal functions are transcriptionally regulated by transcription factor EB (TFEB) through the induction of genes involved in lysosomal biogenesis and exocytosis. Given these observations, we investigated the roles of TFEB and lysosomes in intracellular Ca^{2+} homeostasis. We studied the effect of transient modulation of TFEB expression in HeLa cells by measuring the cytosolic Ca^{2+} response after capacitative Ca^{2+} entry activation and Ca^{2+} dynamics in the endoplasmic reticulum (ER) and directly in lysosomes. Our observations show that transient TFEB overexpression significantly reduces cytosolic Ca^{2+} levels under a capacitative influx model and ER re-uptake of calcium, increasing the lysosomal Ca^{2+} buffering capacity. Moreover, lysosomal destruction or damage abolishes these TFEB-dependent effects in both the cytosol and ER. These results suggest a possible Ca^{2+} buffering role for lysosomes and shed new light on lysosomal functions during intracellular Ca^{2+} homeostasis.

Introduction

1. Lysosomes: structure and functions

Lysosomes are ubiquitous organelles that constitute the primary degradative compartments of the cell. They receive their substrates through endocytosis, phagocytosis or autophagy (Fig. 1) (Saftig and Klumperman 2009).

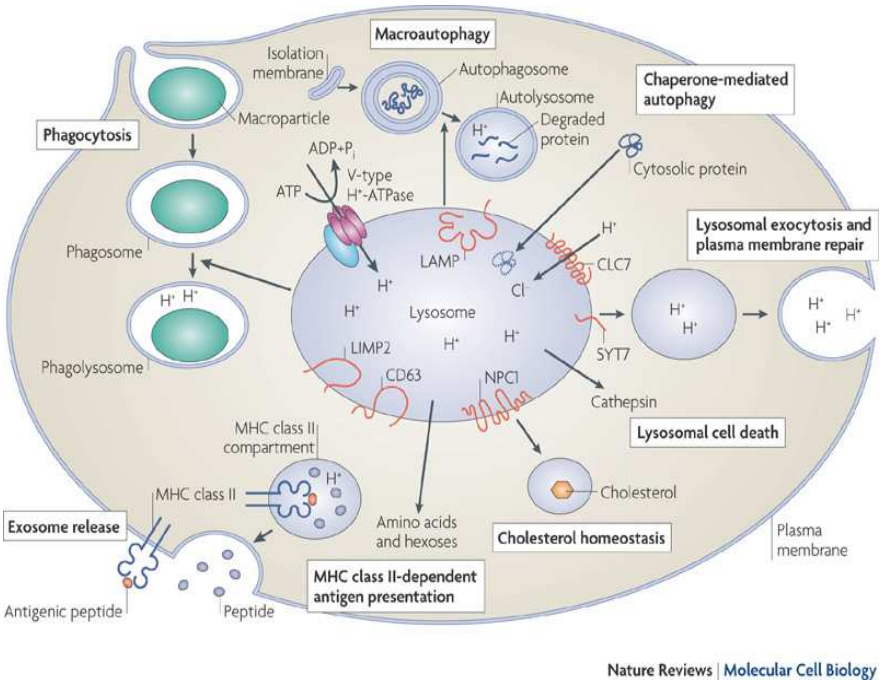

Fig. 1. Significant functions of lysosomal membrane proteins. The lysosome is a central, acidic organelle that is involved in the degradation of macromolecules through the activity of lysosomal hydrolases. Lysosomes are crucial for the maturation of phagosomes to phagolysosomes in phagocytosis, which is important for cellular pathogen defence. The macroautophagy pathway mediates the turnover of cytoplasmic components, such as organelles and large complexes, and is involved in cell death and proliferation. Macroautophagy depends on the fusion of lysosomes with autophagosomes to create autolysosomes, in which degradation occurs. Lysosomal exocytosis and plasma membrane repair are Ca2+ and synaptotagmin 7 (SYT7)-dependent fusion events, which are possibly involved in pathogen entry, autoimmunity and neurite outgrowth. The lysosomal cell death pathway is triggered by a release of lysosomal cathepsins through an unknown mechanism. Cellular cholesterol homeostasis is controlled by lysosomal cholesterol efflux through Niemann–Pick C1 protein (NPC1). Major histocompatibility complex (MHC) class II-dependent antigen presentation requires lysosomal proteases and membrane proteins. The release of exosomes is thought to be involved in adaptive immune responses. Lysosomal membrane proteins are also involved in the transport of newly synthesized hydrolases to the lysosome and across the lysosomal membrane (Saftig and Klumperman 2009).

They are membrane-bound organelles that constitute up to 5% of the intracellular volume of eukaryotic cells. Lysosomes were discovered in 1955 from Christian Duve that observed the "latency" acid phosphatase activity and postulated the presence of this enzyme in e membrane-enclosed compartment (de Duve 2005) and after a year Alex Novikoff observed for the first time their structure by electron microscopy (Bainton 1981). Today is well known from the literature, in agreement with these initial observations, their existence, biogenesis, morphology, diverse functions and failure in disease.

Lysosomes are limited by a single phospholipid bilayer and their shape varies between globular and tubular patterns of ~ 0,5µm diameter. As the same, their content can be heterogeneous: usually they appear electron-dense but often include irregularities and membrane sheets (Saftig and Klumperman 2009). Acidic interior with a pH of 4.5-5, is a common characteristic: it is maintained by the vacuolar V-H^+-ATPase, a transmembrane multiprotein complex that use energy derived from ATP hydrolysis to transport in protons across the lysosomal membrane (Nishi and Forgac 2002), (Hinton, Bond et al. 2009). Additional lysosomal membrane channels are probably involved in lysosomal acidification, such as the anion transporter cloride channel 7 (ClC7), the cation transporters mucolipin 1 (MCOLN1 or TRPML1) and the two pore channel 1 (TPC) 1 and 2, which mediate Ca^{2+} and Na^+ release from the lysosomes (Kasper, Planells-Cases et al. 2005, Graves, Curran et al. 2008, Calcraft, Ruas et al. 2009, Zhang, Jin et al. 2009, Mindell 2012). The precise mechanisms that involve TPC2 and MCOLN1 in the complex regulation of lysosomal acidification and ion balance are still controversial and require further investigation.

Segregate the 'aggressive' acidic environment of the lumen from the rest of the cell, is the primary function of lysosomal membrane. This is ensured by the presence of a thick glycocalyx, the polysaccharide-based coating that lines the internal perimeter to prevent the lysosomal membrane being degraded. The lysosomal membrane also actively mediates the fusion of lysosomes with other structures, such as endosomes, autophagosomes and plasma membrane, as well as the transport of metabolites, ions and soluble substrates into and out of the organelle. Lysosomal trafficking and fusion are mediated by specific sets of membrane-associated Rab GTPases (Rojas, van Vlijmen et al. 2008, Wang, Ming et al. 2011) and a particular combinatorial set of N-ethylmaleimide-sensitive factor attachment protein receptors (SNARE) (Pryor, Mullock et al. 2004), including vesicle-associated membrane protein (VAMP) (see below).

Into their acid matrix, lysosomes contain more than 50 different acid hydrolases (proteinase, peptidase, phosphatases, nucleases, glycosidases, sulphatase, lipases) and several activator

proteins that are localized mainly in the matrix (de Duve 2005). In a concerted action, this hydrolases are able to decompose simple and complex macromolecules and even membranes into their monomeric constituents, which are either recycled through biosynthetic pathways or further degraded to generate energy. The targeting of lysosomal matrix enzymes to lysosomes, as well as their ability to be secreted and taken up again by cells, is mediated by a mannose-6-phosphate (MP6) modification that they undergo in the late Golgi compartments (Braulke and Bonifacino 2009), (Ghosh, Dahms et al. 2003). The MP6 tags are recognized and bound in the *trans*-Golgi network (TGN) by two different mannose-6-phosphate receptors (M6PR) that cycle between the TGN end endosomes (Schroder, Wrocklage et al. 2010). Unlike soluble hydrolase, the delivery of newly synthesized lysosomal membrane proteins from the TGN occurs either by an indirect route via plasma membrane or by a direct intracellular rout (Luzio, Pryor et al. 2007).

The question of how lysosomes form, has captivated the interest of cell biologists for decades (see Fig. 2). Early microscopy studies suggested lysosomes form by direct budding from the Golgi complex. Later studies led to models proposing lysosome maturation from endosomal compartments (Mullins and Bonifacino 2001). The "maturation" model involves the formation of early endosomes by coalescence of vesicles and addition of TGN-derived vesicles converts these endosomes to late endosomes, and eventually to lysosomes. Alternatively, there are three more possible models known from literature: "vesicle-transport", "kiss and run" and "fusion-fission". The "vesicle-transport" model postulates that early endosomes, late endosomes and lysosomes are stable compartments and the transport proceeds from early to late endosomes and then to lysosomes. The "kiss and run" model proposes that endosomes and lysosomes undergo repeated cycles of fusion and fission allowing transfer of materials and maintenance of mature lysosomes. The "fusion-fission" model is a variation of the "kiss and run" in which late endosomes and lysosomes undergo heterotypic fusion producing a hybrid organelle containing markers of both compartments (Mullins and Bonifacino 2001).

The view that lysosomes are merely a 'garbage-disposal-units' has been challenged. Lysosomal functions are several and they can be schematically divided into three main types: degradation, secretion and signalling.

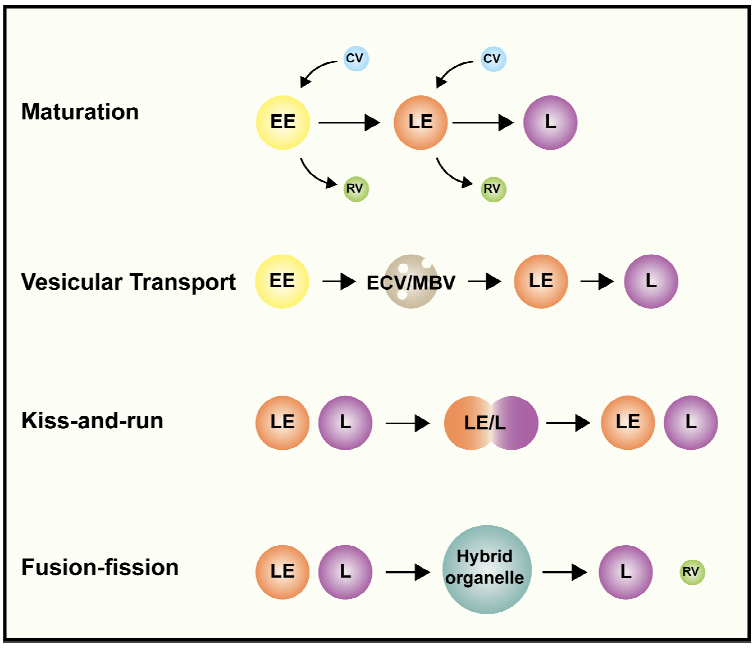

Fig. 2. Models for lysosomal biogenesis requiring endosomal compartments. Abbreviations: EE, early endosome; LE, late endosome; L, lysosome; ECV, endosomal carrier vesicle; MVB, multivesicular body; CV, cargo vesicle; RV, recycling vesicle.

2. Lysosomal degradation programme

Lysosomes receive intracellular or extracellular waste through various pathways including endocytosis and autophagy. Extracellular material reaches the lysosomes mainly by endocytosis and occurs through specific mechanism according to the nature of the cargo. Prominent examples of endocytosis are phagocytosis, macropinocytosis, clathrin-mediated endocytosis, caveolin-mediate endocytosis and clathrin- and caveolin-mediated endocytosis (Conner and Schmid 2003). A generalized route map for the passage of endocytosed material to lysosomes has been established. By definition, this material is delivered first to early endosomes, then to late endosome and subsequently to lysosomes; the time of delivery to each endosomal compartment varying between cell types (Mullock, Perez et al. 1994). The early endosome is the major sorting compartment of the endocytic pathway, in which many ligands dissociate from their receptor in the pH of the lumen and from which many of the receptors recycle to the cell surface (Mellman 1996, Mukherjee, Ghosh et al. 1997). The membrane traffic pathway from early to late endosomes has been well clarified (Gruenberg and Maxfield 1995), in contrast, different models have been proposed to explain how cargo is trafficked from late endosomes to lysosomes. A known hallmark of endosome-to-lysosome maturation is the progressive decrease of the internal pH to pH ~ 5 in the mature lysosomes, crucial for the uptake of acid hydrolase (Ohkuma, Moriyama et al. 1982).

Intracellular materials reach the lysosomes trough the process of autophagy, a 'self-eating' catabolic pathway and evolutionarily conserved, that is used by the cell to degrades cytoplasmic components, thus contributing to cell survival and tissue homeostasis. Three type of autophagy have been identified: microautophagy, cytosolic proteins are engulfed in the lysosome through direct lysosomal membrane invagination; chaperone-mediated autophagy (CMA), cytosolic proteins are transported into the lysosome lumen through chaperone- and receptor-mediated internalization; macroautophagy, relies on the biogenesis of autophagosomes that sequesters cytoplasmic material and then fuses with lysosomes. Thus, the role of all three types of autophagy is strictly dependent on lysosomal function.

3. Lysosomal exocytosis

Lysosomes can secrete their content through a process called exocytosis. Contrary to what was thought at the beginning, not only 'professional secretory cells', but any cell type can perform lysosomal exocytosis. Lysosomal exocytosis mediates several physiological process, such as degranulation in cytotoxic T lymphocytes (Stinchcombe and Griffiths 2007), bone resorption by osteoclasts (Mostov and Werb 1997), parasite defence by mast cells and eosinophils (Logan, Odemuyiwa et al. 2003) (Wesolowski and Paumet 2011), melanocyte function in pigmentation (Stinchcombe, Bossi et al. 2004), platelet function in coagulation (Ren, Ye et al. 2008), and hydrolase release by spermatozoa during fertilization (Tulsiani, Abou-Haila et al. 1998).

In this process, lysosomes fuse with the plasma membrane in response to an increased in the concentration of cytosolic Ca^{2+} that leads to a bulk release of the lysosomal content into the extracellular matrix (Rodriguez, Webster et al. 1997) (Jaiswal, Andrews et al. 2002). It can be detected by the translocation of lysosomal membrane marker protein, like lysosomal-associated membrane 1 (LAMP1), to the plasma membrane (Chieregatti and Meldolesi 2005) (Verhage and Toonen 2007). As mentioned above, lysosomes fusion with the plasma membrane, also with endosomes and phagosomes, is controlled by SNARE. The molecular machinery mediating Ca^{2+}-regulated exocytosis of conventional lysosomes includes the vesicle SNARE (v-SNARE) VAMP7, that forme a *trans*-SNARE complex with syntaxin 4 and the target SNAREs (t-SNARE) synaptosome-associated protein of 23kDa (SNAP23) on the plasma membrane, allowed by several Rab protein on the lysosomal surface (Rao, Huynh et al. 2004) (Bossi and Griffiths 2005). The Ca^{2+} sensor synaptotagmin VII (SYTVII) on lysosomes regulates lysosomal exocytosis and restrict both the kinetics and the extent of Ca^{2+}-

dependent fusion (Rao, Huynh et al. 2004). Another important mediator of lysosomal exocytosis is the lysosomal membrane Ca^{2+} channel MCOLN1 (LaPlante, Sun et al. 2006) (Medina, Fraldi et al. 2011).

Additionally, lysosomal exocytosis provides the extra membrane for plasma-membrane wound repair (McNeil and Kirchhausen 2005) and allows the formation of a parasitophorous vacuole, a membrane-bound organelle that contains an intracellular parasite. Plasma membrane injuries induce the rapid migration of lysosomes to the damaged site. Lysosomes than fuse with the plasma membrane and efficiently reseal the damaged sites, a process important in defence mechanism against bacterial infection (Roy, Liston et al. 2004).

4. Lysosome in autophagy

The involvement of the lysosomes in nutrient sensing is a new concept that expands our view of this organelle from simply being an effector of cellular clearance to being a sensor and regulator of various cellular functions including, cell cycle progression, growth, macromolecules biosynthesis and autophagy.

The kinase complex mammalian target of rapamycin complex 1 (mTORC1), a master controller of cell and organism growth (Laplante and Sabatini 2012), exert its activity on the lysosomal surface (Sancak, Bar-Peled et al. 2010). Growth factor, hormones, amino acids, glucose, oxygen, and stress are the primary activator of mTORC1, which in turn positively regulates proteins, mRNAs, lipid biosynthesis and ATP production. When nutrients are present, mTORC1 directly phosphorylates and suppresses the activity of the kinase complex ULK1-ATG13-FIP200, required to induce autophagosome biogenesis (Chan, Kir et al. 2007). The inhibition of mTORC1, either by starvation or drugs, leads to the activation of ULK1-ATG13-FIP200 and autophagy. It was recently shown that the level of amino acids inside the lysosomal lumen controls mTORC1 docking on the lysosomal surface, which is a prerequisite for its activity, and that amino acids must accumulate in the lysosomal lumen in order for mTORC1 to bind and become activated (Zoncu, Bar-Peled et al. 2011). These observations support the idea that mTORC1activity is dependent on the lysosomes. Another study demonstrates the presence of an interaction between an endolysosomal ATP-sensitive Na^+-permeable channel, $lysoNa_{ATP}$, and mTORC1, on the lysosomal membrane. Thus, $lysoNa_{ATP}$ regulates lysosomal pH stability and amino acid homeostasis by responding to ATP levels (Cang, Zhou et al. 2013). Thus, complex signalling machinery, which involves mTORC1 and other protein complexes is located on the lysosomal surface. This machinery herein referred

like LYNUS, lysosomal nutrient sensing, responds to the lysosomal amino acid content and signals the information both cytoplasm and the nucleus.

It's also important to mention the involvement of lysosomes in the apoptotic process. For many years, lysosomes have played a limited role in the digestion of engulfed apoptotic bodies (Ferri and Kroemer 2001). These concepts now seem to be outdated. Indeed, partial lysosomal permeabilization with subsequent release of proteolytic enzymes into the cytosol and their active contribution to the signalling pathways has been recently described in several models of apoptosis (Guicciardi, Leist et al. 2004). The critical factor in determining the type of the cell death (necrosis versus apoptosis) mediated by lysosomes enzymes seems to be the magnitude of lysosomal permeabilization, and, consequently, the number of proteolytic enzymes released into the cytosol (Li, Yuan et al. 2000). A complete breakdown of the organelle with the release of high concentration of lysosomal enzymes into the cytosol, results in unregulated necrosis, whereas partial, selective permeabilization trigger apoptosis (Bursch 2001). Once in the cytosol, the amount of lysosomal enzymes is sufficient to overcome the protective barrier of the endogenous inhibitors (i.e. cystatins), and contribute to the execution of apoptotic program either by direct cleavage of key cellular substrates, or by acting in concert with caspases in the signaling pathway (Berg, Gjoen et al. 1995, Leist and Jaattela 2001).

5. Lysosomal dysfunction

Seen the involvement of lysosomes in several processes that take part in the cell, it does not surprise the existence of many pathologies due to their disorders. Indeed, lysosomal disfunction has been associated with several human diseases, as well as the process of ageing. In particular, lysosomal storage diseases (LSDs) are a group of rare and recessively inherited metabolic dysfunction of more than 50 genetic disorders caused by a deficiency of lysosomal proteins or non-lysosomal proteins, but that contributes to lysosomal function (Ballabio and Gieselmann 2009). These disorders are due to genetic defects, that lead to the accumulation of substrates that are not degraded in the lysosomal lumen, followed by progressive lysosomal dysfunction in several tissue and organs. Most LSDs are caused by deficiency of soluble lysosomal proteins residing in the lumen of the lysosome. A minority is caused by defects in lysosomal membrane protein. It must be emphasized that in most lysosomal diseases more than one compound accumulates and in some disorder for various reasons the stored material can be slightly heterogeneous (Ballabio and Gieselmann 2009). A generic pathway is

presented: mutations of genes that encode for proteins involved in lysosomal functions result in an accumulation of specific substrates that have not been degraded in lysosome (primary storage). This lead to the accumulation of additional lysosomal substrate (secondary storage) due to a blockage in lysosomal trafficking. Excessive lysosomal storage has a broad impact on lysosomal functions by causing defects in Ca^{2+} homeostasis, signally abnormalities and lysosomal membrane permeabilization. In addition, lysosomal dysfunction is associated with autophagy impairment, due to defective fusion between lysosomes and autophagosomes. This causes the accumulation of autophagic substrates such as aggregate-prone proteins and dysfunctional mitochondria (Settembre, Fraldi et al. 2013). LSDs are most frequently classified according to the principal storage compound.

6. The concept of Ca^{2+} as a cellular signal

In the past two decades, our understanding of how extracellular signals are conveyed to eukaryotic cells via an increase in intracellular Ca^{2+} concentration has widely expanded. It is today common knowledge that a variety of extracellular stimuli (ranging from the binding of hormones, neurotransmitters, growth factors to phenomena such as cell-cell interactions), through diverse mechanisms (e.g. receptors that are themselves ion channels, or have an intrinsic enzymatic activity or are coupled to enzymatic effectors via G proteins) induce a rise in cytoplasmic Ca^{2+} concentration ($[Ca^{2+}]_c$) with defined amplitude and kinetics (Berridge, Lipp et al. 2000) (Clapham 1995).

In eukaryotic cells, a significant electrochemical Ca^{2+} gradient exists across the plasma membrane (PM) (approximately 70 to 90 mV), but the $[Ca^{2+}]_c$ is less than 1/10,000 that of the extracellular milieu. However, eukaryotic cells can store Ca^{2+} in many organelles and can mobilize the ion in response to endogenous and extracellular stimuli. The major intracellular Ca^{2+} storage unit is the ER (luminal $[Ca^{2+}]_{ER}$ 500 μM-1 mM)(Berridge, Bootman et al. 2003), which exhibits significant heterogeneity in the Ca^{2+} level among its sub-regions. Upon stimulation with agonists such as histamine or ATP, the ER rapidly releases Ca^{2+} through the inositol 1,4,5-trisphosphate receptor (IP3R), thereby generating transient waves in the cytoplasm and mitochondria to promote cell activities (Bonora, Giorgi et al. 2015) (Fig. 3). Upon ER Ca^{2+} depletion, the luminal sensor protein STIM1 oligomerizes on the ER membrane and migrates to sites of ER/PM interaction to activate the highly Ca^{2+}-selective ORAI channels located on the PM (Koziel, Lebiedzinska et al. 2009, Smyth, Hwang et al. 2010). Thus, the ER Ca^{2+} store is replenished via the sarco-endoplasmic reticulum Ca^{2+}-

ATPase (SERCA) pump(Clapham 2007, Lewis 2007, Berridge 2012, Marchi, Patergnani et al. 2014) in a process known as capacitative Ca^{2+} entry or store-operated Ca^{2+} entry (SOCE) (see Fig. 4).

Moreover, the technological advancements in probe design and imaging systems, by allowing the accurate measurement [Ca^{2+}] at the single cell level, have revealed marked asynchronicity in cell response and a high spatiotemporal complexity of the intracellular Ca^{2+} signal. We now know that the Ca^{2+} signal can be conveyed as repetitive $[Ca^{2+}]_c$ spikes (commonly referred to as Ca^{2+} oscillations) (Morgan and Thomas 1999) as well as localised $[Ca^{2+}]_c$ increases that may either be confined or gradually propagate to the rest of the cell ("Ca^{2+} waves") (Jaffe and Creton 1998) (Petersen, Burdakov et al. 1999).

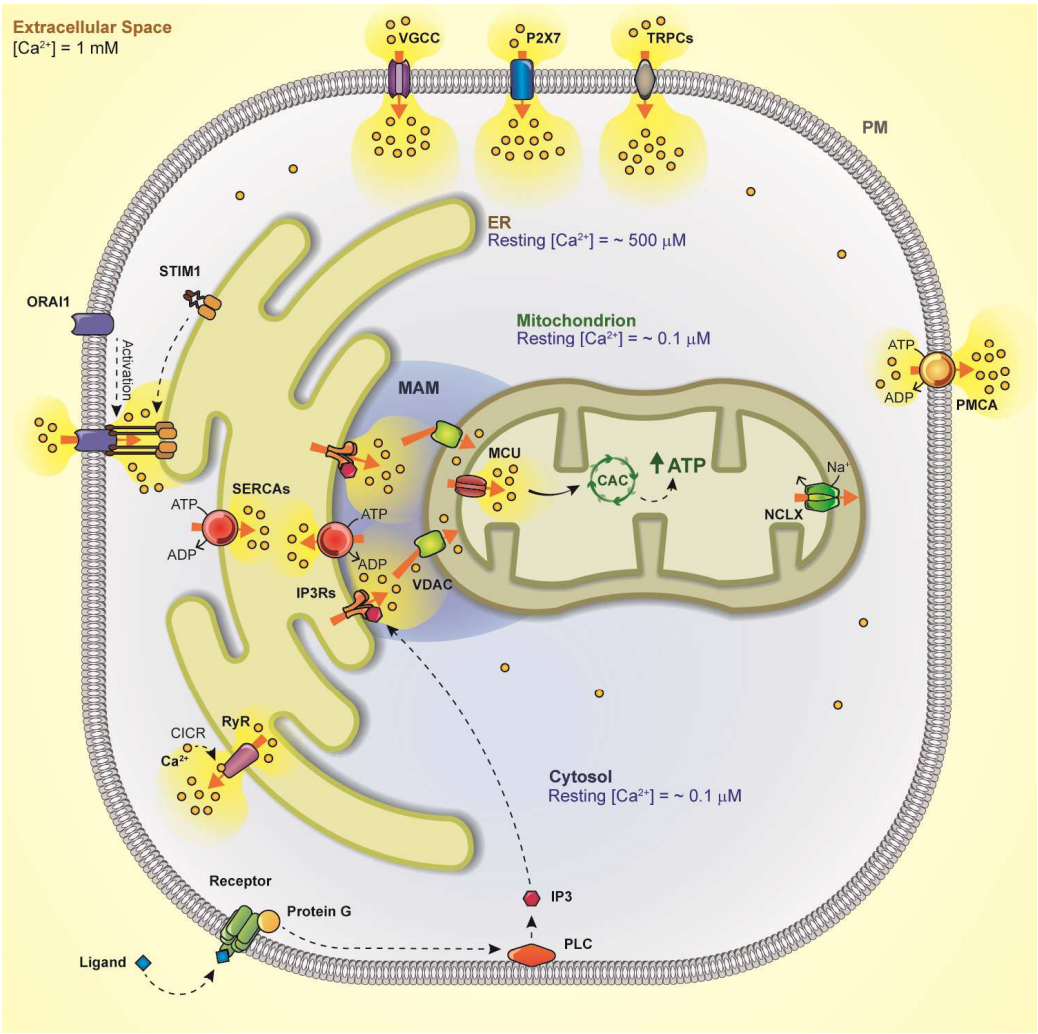

Fig. 3. Summary of the principal effectors involved in inter-organelle Ca^{2+} transfer. Abbreviations: PM, plasma membrane; ER, endoplasmic reticulum; IP3, inositol 1,4,5 trisphosphate; IP3Rs, inositol 1,4,5 trisphosphate receptors; MCU, mitochondrial calcium uniporter; VGCC, voltage gated Ca^{2+} channel; TRPC, transient receptor potential cation channel; PMCA, plasma membrane Ca^{2+} ATPase; PLC, phospholipase c; RyR, ryanodine receptor; NCLX, Na^+/Ca^{2+} exchanger; SERCA, sarco/endoplasmatic reticulum Ca^{2+} ATPase; VDAC, voltage-dependent anion channel.

An extensive Ca^{2+}-signalling toolkit is used to assemble signalling systems with very different spatial and temporal dynamics. Rapid highly localized Ca^{2+} spikes regulate fast responses, whereas slower responses are controlled by repetitive global Ca^{2+} transients or intracellular Ca^{2+} waves. The Ca^{2+} has a direct role in managing the expression patterns of its signalling systems that are constantly being remodelled in both health and disease. During the *on reaction*, stimuli induce both the entry of external Ca^{2+} and the formation of second messengers that release internal Ca^{2+} that is stored within the endoplasmic reticulum or Golgi apparatus. Most of this Ca^{2+} is bound to buffers, whereas a small proportion binds to the effectors that activate various cellular processes. Calcium can enter cells across the plasma membrane by any of several general classes of channels, including voltage-operated channels (VOC), second messenger-operated channels (SMOC), store-operated calcium entry (SOCE) channels and receptor-operated channels (ROC). VOCs are activated by membrane depolarization, and SMOCs are activated by any of a number of small messenger molecules, the most common being inositol phosphates, cyclic nucleotides, and lipid-derived messengers. SOCs are activated by the depletion of the intracellular Ca^{2+} store, and ROCs are activated by direct binding of a neurotransmitter or hormone agonist (Parekh and Putney 2005). During the *off reactions*, Ca^{2+} leaves the effectors and buffers and is removed from the cell by various exchangers and pumps. The Na^{+}/Ca^{2+} exchanger (NCX) and the plasma membrane Ca^{2+}-ATPase (PMCA) extrude Ca^{2+} to the outside, whereas the sarco-endoplasmic reticulum Ca^{2+}-ATPase (SERCA) pumps Ca^{2+} back into the ER.

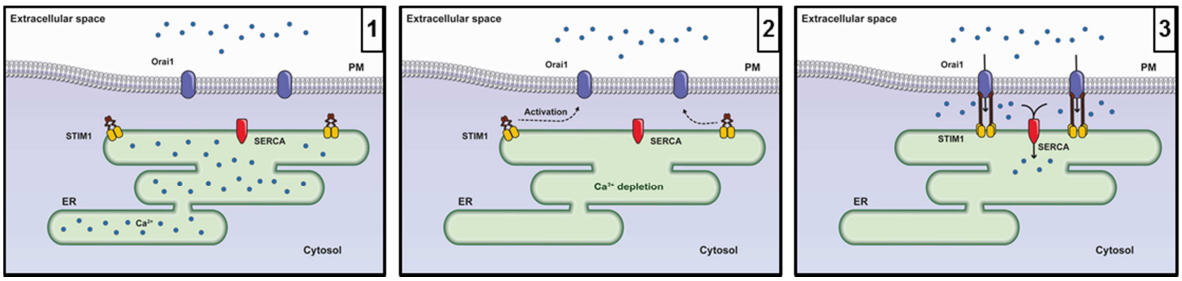

Fig. 4. The functional units of store-operated Ca^{2+} entry assemble in response to store depletion. (1) In resting cells with replete Ca^{2+} stores, STIM1 and Orai1 are dispersed throughout the ER and plasma membrane, respectively. (2) Store depletion causes STIM1 to accumulate at locations where the ER is juxtaposed to the plasma membrane, and to a limited extent increases the number of these close contacts. At the same time, Orai1 accumulates in regions of the plasma membrane directly opposite the STIM1 clusters. (3) The co-localization of STIM1 and Orai1 restricts channel activation and Ca^{2+} entry to these sites favouring the replenishment of the endoplasmic reticulum.

Mitochondria also have an active function during the recovery process in that they sequester Ca^{2+} rapidly through a uniporter, and release more slowly back into the cytosol to be dealt

with by the SERCA and the PMCA. Cell survival is dependent on Ca^{2+} homeostasis, whereby the Ca^{2+} fluxes during the *off reactions* exactly match those during the *on reaction.*

7. Lysosomal Ca^{2+} regulation

Lysosomes have a high intravesicular Ca^{2+} concentration estimated to be in the region of 500-600μM (Christensen, Myers et al. 2002) that is maintained an unidentified H^{+}-Ca^{2+} exchanger. Better known are the proteins involved in the lysosomal Ca^{2+} release.

The role of Ca^{2+} in lysosomal function is supported by the well-established paradigm of its role in organellar and plasma membrane fusion (Kiselyov, Yamaguchi et al. 2010) but only recently the lysosomes are considered emerging Ca^{2+} signalling centre of the cell (Galione, Morgan et al. 2010). Starting from identification of nicotinic acid adenine dinucleotide phosphate (NAADP), a metabolite of NADP (Lee 1997), as a potent Ca^{2+}- mobilizing messenger that did not require activation of IP_3R or RyR (Clapper, Walseth et al. 1987), than other substantial evidence established that NAADP-evoked Ca^{2+} is distinguishable from that mediated by IP_3R or RyR (Naylor, Arredouani et al. 2009). A significant step was the discovery that in the sea urchin eggs, the effects of NAADP are selectively abolished by disruption of acidic organelles, most notably by glycyl-phenylalanyl-naphthylamide (GPN) which selectively destroy lysosomes (Galione, Morgan et al. 2010). Thus, many studies focused attention on endo-lysosomal Ca^{2+} channels as candidates for the NAADP-gated channel; the more persuasive and extensive evidence suggests that NAADP-gated channel are formed by oligomeric assemblies of two-pore channel, TPC, proteins (Brailoiu, Hooper et al. 2010) recently emerged as a novel intracellular calcium release channel (Peiter, Maathuis et al. 2005). At the presence, the strongest evidence support TPC2 as the lysosomal Ca^{2+} channel and TPC1 as the endosomal Ca^{2+} channel. TPCs have a domain structure similar to one-half of voltage-sensitive Ca^{2+} channels and they are composed of two repeats of six trans-membrane helices each encompassing a putative pore (Peiter, Maathuis et al. 2005).

Another candidate is MCOLN1, also known as the member of the mucolipin family of transient receptor potential (TRP) channel TRPML1, a lysosomal nonselective cation channel (Bargal, Goebel et al. 2002). MCOLN1 plays a role in lysosomal Ca^{2+} release (Zhang, Jin et al. 2009) and in the lysosomal-endosomal fusion (LaPlante, Falardeau et al. 2002). The TRP channels are tetrameric cation channels and are activated by a wide range of stimuli, including G protein-coupled receptor interaction, ligand activation and temperature (Ramsey, Delling et

al. 2006). MCOLN1 protein is localized to lysosomes and it is encoded by the MCOLN1 gene (mutated in the lysosomal storage disorder mucolipidosis type IV).

8. Lysosomal biogenesis regulation

Cell metabolism is controlled by complex networks of genes, proteins and metabolites, which sense the cellular environment and organize the appropriate responses. In the past two decades, the importance of regulatory gene networks in cell metabolism has become evident in every aspect of cell function. In this context, the transcriptional networks associated with biogenesis and function organelles are of particular interest.

Sardiello et al. observed how genes encoding lysosomal proteins tend to have coordinated expression (Sardiello, Palmieri et al. 2009). Pattern discovery analysis of the promoter region of the 96 known lysosomes genes (Lubke, Lobel et al. 2009) resulted in the identification of a palindromic 10-base pair (bp) GTCACGTGAC motif highly enriched in this promoter set. This motif is preferentially located within 200bp from the transcription start site (TSS), either in a single sequence or in tandem multiple copies. They named this motif coordinated lysosomal expression and regulation (CLEAR) element (Sardiello, Palmieri et al. 2009). The CLEAR consensus sequence overlaps that of the E-box (CANNTG), a known target site for basic helix-loop-helix (bHLH) transcription factors (Massari and Murre 2000). In particular, members of the microphthalmia-transcription factor E (MiT/TFE) subfamily of bHLH factors were found to bind sequence similar to the CLEAR consensus (Meadows, Sharma et al. 2007). The MiT/TFE subfamily is composed of four members in humans: MITF, TFE3,TFEB, and TFEC (Steingrimsson, Copeland et al. 2004). In their work Sardiello et al. demonstrate that only TFEB is responsible of an increase of mRNA level of lysosomes genes. Moreover, an expansion of the lysosomes compartment was detected by stable overexpression of TFEB. Accordingly, ultrastructural analysis revealed a significant increase in the number of lysosomes per cell, indicating the involvement of TFEB in lysosomal biogenesis (Sardiello, Palmieri et al. 2009). This discovery, of a ‘lysosomes gene network’, and of its master regulator TFEB has revealed that lysosomal function can be coordinated.

9. Transcription factor EB: TFEB

The transcription factor EB, TFEB, is a member of the bHLH leucine-zipper family of TFs. TFEB recognize E-box sequence, the site presents also in the CLEAR consensus sequence.

TFEB binding CLEAR site promotes lysosomal genes expression (Sardiello, Palmieri et al. 2009).

Under basal conditions, in most cell types, TFEB is phosphorylated and located in the cytoplasm. TFEB translocation's to the nucleus is a process controlled by its phosphorylation status, the dephosphorylated form is found in the nucleus (Settembre, Di Malta et al. 2011). Phosphoproteomic studies identified at least ten different phosphorylation sites in the TFEB protein and at least three different kinases: extracellular signal-regulated kinase (ERK2) (Settembre, Di Malta et al. 2011) (Cea, Cagnetta et al. 2012), mTORC (Cea, Cagnetta et al. 2012, Roczniak-Ferguson, Petit et al. 2012, Settembre, Zoncu et al. 2012) and protein kinase Cβ (PKCβ) (Ferron, Settembre et al. 2013). Interestingly, cytoplasmic TFEB is located both in the cytosol and on the lysosomal surface, where it interacts with mTORC1 and LYNUS machinery (Settembre, Zoncu et al. 2012).

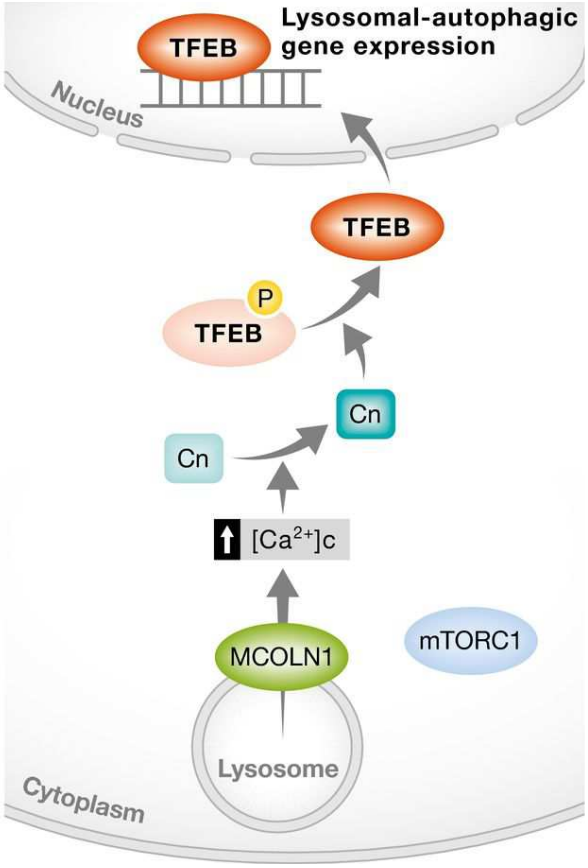

Fig. 5. Ca^{2+}-mediated regulation of TFEB. Under normal feeding conditions, TFEB is phosphorylated by mTORC1 on the lysosomal surface and is sequestered in the cytoplasm. During starvation, Ca^{2+} is released from the lysosome through MCOLN1 leading to local calcineurin (Cn) activation and TFEB dephosphorylation. Dephosphorylated TFEB can freely translocate to the nucleus where it transcriptionally activates the lysosomal/autophagic pathway (Ballabio 2016).

This observation suggests a mechanism by which the lysosomes regulates its own biogenesis by controlling TFEB subcellular localization. More recently, TFEB was shown to interact

with active RAG GTPases. This interaction promotes the lysosomal localization of TFEB and its mTORC1-dependent phosphorylation (Martina and Puertollano 2013).

Not only biogenesis and lysosome-to nucleus signalling are controlled by TFEB, but also exocytosis and fusion of lysosome with the plasma membrane, and lipidic catabolism (Settembre, Fraldi et al. 2013). In lysosomal exocytosis, TFEB induces both docking and fusion of lysosomes with plasma membrane by regulating the expression of specific genes, the protein products of which increase lysosomal dynamics and cause an MCOLN1-mediated increase in intracellular Ca^{2+} (Medina, Fraldi et al. 2011). Interestingly, TFEB-mediated regulation of lysosomal exocytosis has an essential role in osteoclast differentiation and bone resorption (Ferron, Settembre et al. 2013).

Moreover, TFEB was found to regulate lipid metabolism (Settembre, De Cegli et al. 2013). The trascriptome analysis in the mouse liver after viral-mediated TFEB overexpression revealed that this transcription factor positively regulates the expression of genes involved in several steps of lipid breakdown, such as lipophagy, fatty acid oxidation and ketogenesis. Interestingly, peroxisome proliferator-activated receptor-α (PPARα) and PPARγ coactivator 1α (PG1α), which are critical regulators of lipid metabolism in response to starvation (Finck and Kelly 2006), are significantly induced by TFEB. The recent discovery of starvation-induced lysosome-to-nucleus signalling mechanism, support this concept (Settembre, Zoncu et al. 2012).

Recently, a new lysosomal signalling pathway activated by lysosomal calcium release through MCOLN1 has been shown to be involved in the activation of TFEB via de-phosphorylation (Settembre, Di Malta et al. 2011, Medina, Di Paola et al. 2015, Medina, Di Paola et al. 2015).

Ca^{2+} is a versatile and ubiquitous intracellular messenger in eukaryotic cells since can be rapidly moved across biological membranes to generate spatially organized increased in cytosolic free ($[Ca^{2+}]_c$). Most intracellular Ca^{2+} signals result from the opening of Ca^{2+} channels in the plasma membrane or endoplasmic reticulum in response to precise stimuli, and they are reversed by active transport across these membranes or by shuttling Ca^{2+} in mitochondria and other organelles. The recent identification of regulated Ca^{2+} channels in lysosomes, suggests that they too may contribute to intracellular Ca^{2+} signalling. As previously stated, TFEB overexpression elicits a significant increase in lysosomes content and their motility closer to the plasma membrane. Based on these observations, we investigated the contribution of TFEB expression and lysosomes to intracellular Ca^{2+} homeostasis with the goal of characterizing Ca^{2+} dynamics in both the cytosol and ER upon the induction of SOCE.

Results

1. TFEB overexpression promotes lysosomal localization to the PM to decrease capacitative Ca^{2+} influx

To investigate the role of TFEB and lysosomes in intracellular Ca^{2+} homeostasis, we first evaluated the effects manipulating its expression. We transiently overexpressed TFEB (TFEB-3xflag) for 48 h in human cervical carcinoma (HeLa) cells (Fig. 1A), revealing an increase in protein expression compared with control cells transfected with pcDNA3.

As previously demonstrated by Sardiello et al.(Sardiello, Palmieri et al. 2009), the primary consequence of this modified genetic control is increased lysosomal biogenesis due to the upregulation of most lysosomal proteins modulated by the CLEAR consensus sequence in promoter regions(Settembre, Fraldi et al. 2013). To verify these data and validate our experimental setup, we analysed lysosomal morphology using 3D imaging deconvolution. The lysosomal compartment was marked by the overexpression of Lysosomal-associated membrane protein 1 associated with green fluorescence protein (LAMP1-GFP). Imaging analysis revealed a significant expansion of the lysosomal compartment (see Fig. 1B) in HeLa cells overexpressing TFEB.

It has been suggested that TFEB overexpression increases the pool of lysosomes proximal to the PM and promotes their fusion with the PM(Medina, Fraldi et al. 2011). To confirm these observations, we performed experiments aimed at assessing the location of the lysosomes. We analyzed the distance of LAMP1-GFP-marked lysosomes from the FM4-64fx dye-stained PM (Fig. 1C), which revealed that these organelles are proximal to the PM (Fig. 1C) in HeLa cells transfected with TFEB-3xFLAG compared with the control.

Next, we considered the possibility that an increased number of lysosomes and their proximity to the PM might contribute to intracellular Ca^{2+} homeostasis, particularly for phenomena occurring near the PM. We took advantage of aequorin technology(Bonora, Giorgi et al. 2013) to assess the level of accumulated cytosolic Ca^{2+} entering the cell across the PM via SOCE in the cell models previously described. To induce capacitative Ca^{2+} influx via the activation of SOCE, HeLa cells were pre-treated with a SERCA blocker (thapsigargin; 200 nM) for 15 min in a Ca^{2+} free medium (KRB/EGTA) to encourage the depletion of ER Ca^{2+} stores. When the release of stored ER Ca^{2+} was complete, Ca^{2+} was added to the KRB

perfusion. A major increase in $[Ca^{2+}]_c$ due to Ca^{2+} influx through plasma membrane channels was observed when the perfusing buffer was supplemented with 1 mM $CaCl_2$.

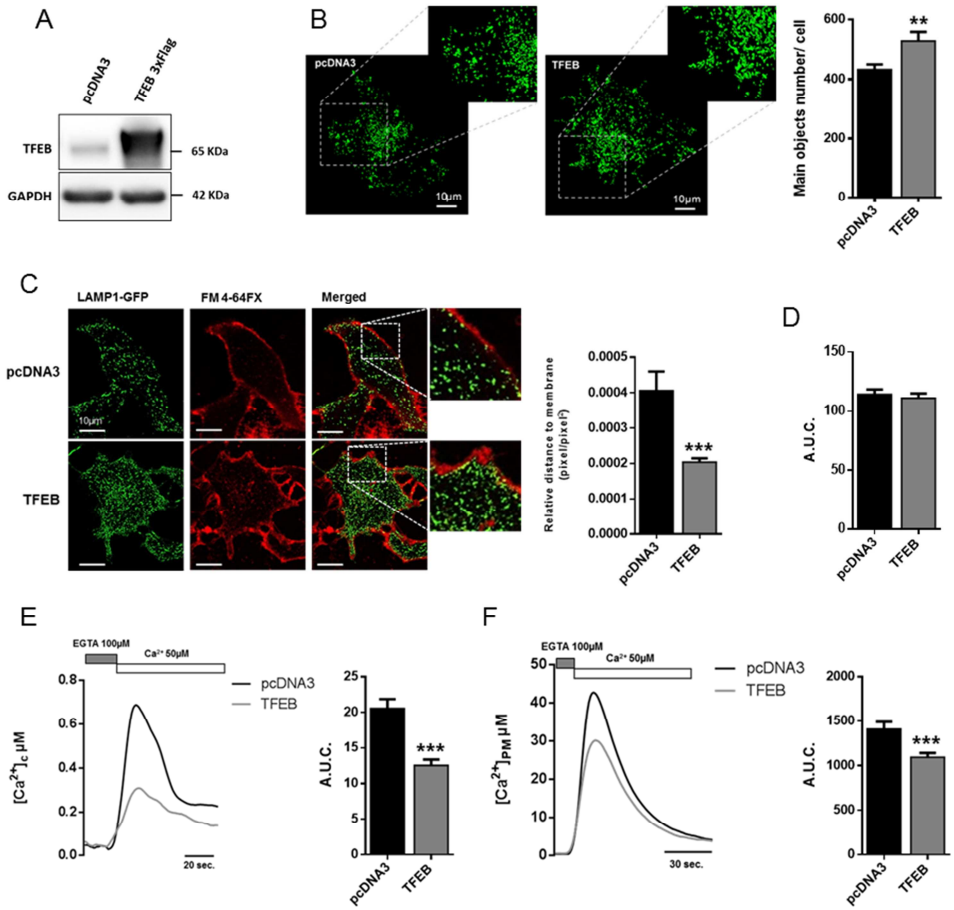

Fig. 1. Overexpression increases lysosomal localization to the plasma membrane, decreasing capacitative Ca^{2+} entry. (A) Representative immunoblot images of TFEB protein abundance in HeLa cells transfected for 48 h with the empty vector (pCDNA3) or plasmid encoding TFEB 3xflag (TFEB). (B) Representative images of lysosomal morphology and quantification of the lysosomal number in HeLa cells co-transfected for 48 h with LAMP1-GFP (green) and pcDNA3 (Control) or TFEB 3xflag (TFEB). (C) Representative images and quantification of the distance of lysosomes from the plasma membrane, normalized to the cellular area, in HeLa cells co-transfected with pcDNA3 (control) or TFEB3xflag (TFEB) and LAMP1-GFP (green) for 48 h; the plasma membrane is stained with the FM4-64fx colourant (red). (D) Cytosolic Ca^{2+} measurements of capacitative Ca^{2+} entry measured by cytosolic aequorin in HeLa cells transfected with pcDNA3 or TFEB 3xflag (TFEB). After intracellular Ca^{2+} store depletion, 1 mM Ca^{2+} was perfused in solution. (E) Representative traces and histogram of capacitative Ca^{2+} entry measured using cytosolic aequorin in control HeLa cells (pcDNA3) or HeLa cells overexpressing TFEB for 48 h after Ca^{2+} ($CaCl_2$ 50 µM) administration. (F) Representative traces and histogram of capacitative Ca^{2+} entry measured using PM-targeted aequorin in control HeLa cells (pcDNA3) or HeLa cells overexpressing TFEB after Ca^{2+} (50 µM) administration. Data are presented as the means ± SEM, **p<0.01, ***p<0.001. a.u.c. = area under the curve.

Under these conditions, TFEB overexpression did not significantly influence SOCE (Fig. 1D). However, because of the influx of massive amounts of Ca^{2+} into the subplasmalemmal region (not physiological, but due to the Ca^{2+}-free pre-treatment) and the discharge of the aequorin

probe due to the high Ca^{2+} affinity that has been ascribed to lysosomes(Christensen, Myers et al. 2002), the $[Ca^{2+}]_c$ values obtained under these conditions were largely artifactual, as reported previously (Marsault, Murgia et al. 1997). To avoid saturation of the aequorin probe in subsequent experiments, cells were therefore challenged with a lower extracellular $[Ca^{2+}]$ of 50 μM.

In our experimental setting, this procedure evoked an increase in the $[Ca^{2+}]_c$ followed by a gradual decline, providing evidence for the presence of an abundance of SOCE in HeLa cells (Fig. 1E).

Samples transfected with the TFEB construct displayed a consistent and significant reduction of cytosolic Ca^{2+} accumulation after the activation of capacitative Ca^{2+} influx compared with the control samples.

To confirm that the presence of lysosomes in the proximity of the PM might modulate SOCE, we measured the Ca^{2+} influx using a different aequorin probe targeting the cytosolic side of the PM (PM-Aeq) (Marsault, Murgia et al. 1997). After the activation of SOCE via depletion of ER Ca^{2+} stores, Ca^{2+} ($CaCl_2$ 50 μM) was added to the KRB perfusion (Fig. 1E). In our experimental setting, HeLa cells transfected with the TFEB construct displayed a consistent and significant reduction of Ca^{2+} accumulation in close proximity to the PM compared with the control cells.

Overall, these data suggest a specific role for TFEB in regulating SOCE, likely due to increased lysosomal localization at the PM.

2. Impairment of lysosomal activity restores regular capacitative Ca^{2+} influx in TFEB-expressing cells

To determine whether the TFEB-dependent effects on SOCE are strictly related to altered lysosomal activity, we used different pharmacological approaches that compromise lysosomal structure and function through different modes of action.

The first compound was the membrane-permeable di-peptide glycyl-L-phenylalanine 2-naphthylamide (GPN), which causes selective osmotic lysis of the lysosomal membrane triggered by cleavage of the lysosomal enzyme cathepsin C (Berg, Stromhaug et al. 1994). Its specific lysosome-perforating activity allows it to be used for mobilizing lysosome-specific Ca^{2+} stores (Jadot, Colmant et al. 1984, Haller, Dietl et al. 1996, Haller, Volkl et al. 1996, Srinivas, Ong et al. 2002, Morgan, Platt et al. 2011).

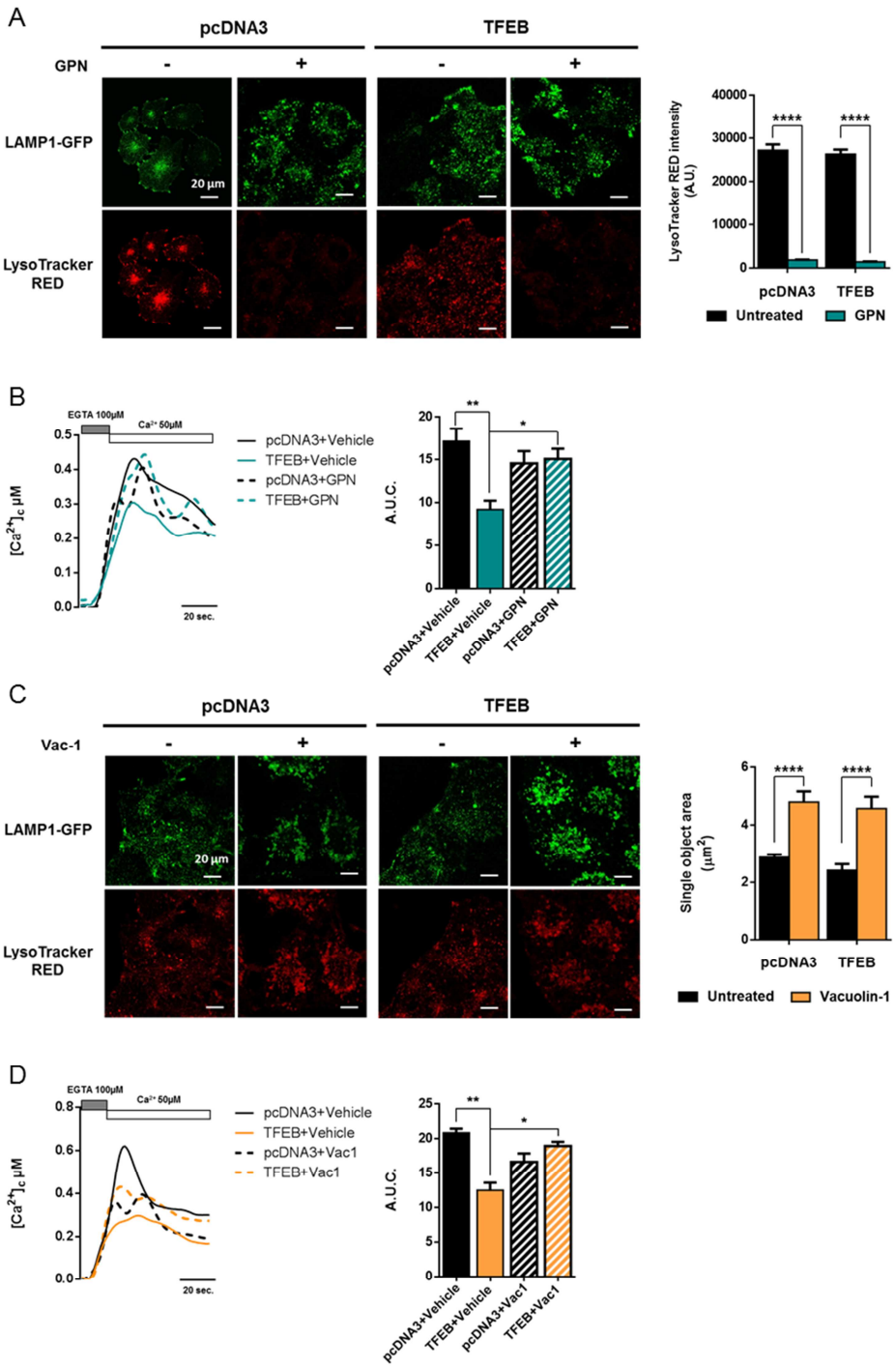

Fig. 2. Impairment of lysosomal activity restores capacitative Ca^{2+} influx. (A) Representative images and quantification of the LysoTracker RED (red) dye intensity after treatment of HeLa cells with 200 nM thapsigargin for 30 min in the absence of Ca^{2+}, with or without GPN 200 µM; the cells were transfected with LAMP1-GFP (green) to highlight lysosomes. (B) Cytosolic Ca^{2+} measurements after SOCE activation, with aequorin in control HeLa cells (pcDNA3) or HeLa cells overexpressing TFEB, pretreated with GPN 200 µM or DMSO (vehicle) for 30 min. (C) Representative images and quantification of the area of single lysosomes after treatment of HeLa cells with 10 µM Vac-1 or DMSO (vehicle) for 1 h, causing fusion of lysosomes (enlargeosomes); the cells were transfected with LAMP1-GFP (green) to highlight lysosomes and stained with LysoTracker RED (red) dye. (D) Cytosolic Ca^{2+} measurements after SOCE activation, using aequorin in control HeLa cells (pcDNA3) or HeLa cells overexpressing TFEB, pretreated with 10 µM Vac-1 or vehicle for 1 h. Data are presented as the means ± SEM; *p<0.05, **p<0.01, ***p<0.001, ****p<0.0001. a.u.c. = area under the curve, a.u. = arbitrary units.

Following treatment with GPN, LysoTracker RED staining was abolished in both pcDNA3-transfected cells and TFEB-overexpressing HeLa cells, without affecting the distribution of LAMP1-GFP (Fig. 2A), indicating permeabilization of the lysosomal membrane.

Activation of SOCE after pre-treatment with GPN (200 μM) did not affect cytosolic Ca^{2+} accumulation in HeLa cells compared with the untreated condition (Fig. 2B). Conversely, GPN treatment abolished the alterations induced by TFEB overexpression, suggesting a possible buffering role for the lysosome.

The second compound, vacuolin-1 (Vac-1), promotes the alteration of lysosomal morphology, resulting in the fusion of acidic organelles without affecting the pH of the lysosomal lumen(Cerny, Feng et al. 2004). Nevertheless, Vac-1 blocks lysosomal exocytosis induced by Ca^{2+} ionophores and by membrane wounding(Cerny, Feng et al. 2004). Although the mechanism of action is unknown, previous studies have revealed that Vac-1 does not affect lysosomal ion transport mechanisms and only changes the surface area available to lysosomes, thereby perturbing their interactions with other organelles(Lopez-Sanjurjo, Tovey et al. 2013). Thus, in the presence of Vac-1, lysosomes cannot fuse with the PM(Huynh and Andrews 2005). To confirm these data, we treated HeLa cells transiently expressing LAMP1-GFP and stained with LysoTracker RED with Vac-1 (10 μM for 1 h). We observed an altered and hyper-fused lysosomal compartment (Fig. 2C) without an evident modification in lysosomal permeability to LysoTracker RED in cells transfected with either the empty vector or the TFEB construct.

Then, we performed capacitative Ca^{2+} influx experiments on HeLa cells transiently transfected with empty vector (pcDNA3) or TFEB after pretreatment with Vac-1 (10 μM for 1 h) or DMSO (vehicle). Under experimental conditions including the only vehicle, we observed maintenance of the differences in capacitative Ca^{2+} influx between control and TFEB-overexpressing samples (Fig. 2D). In contrast, Vac-1 treatment abolished the TFEB-related effects on SOCE.

3. TFEB knockdown increases Ca^{2+} influx via SOCE

To determine whether the effects of altered lysosome activity on SOCE are mediated by TFEB-dependent alteration of the lysosomal compartment, we transiently inhibited the expression of the transcription factor with a specific siRNA for TFEB (siRNA-TFEB) (see Materials and Methods) in HeLa cells for 72 h (Fig. 3A). To validate our experimental setup, we analyzed lysosomal morphology using 3D imaging deconvolution. As expected, imaging

revealed a significant reduction in the number of lysosomes (Fig. 3B) in TFEB-silenced cells. Furthermore, to consolidate our experimental model and confirm the role of TFEB as a critical regulator of lysosomal localization to the PM, we analyzed the intracellular distribution of lysosomal compartments (as previously described) by measuring their distance from the PM (Fig. 3C). Compared to the control, we observed that lysosomes were located farther from the PM (Fig. 3C) in TFEB-depleted HeLa cells.

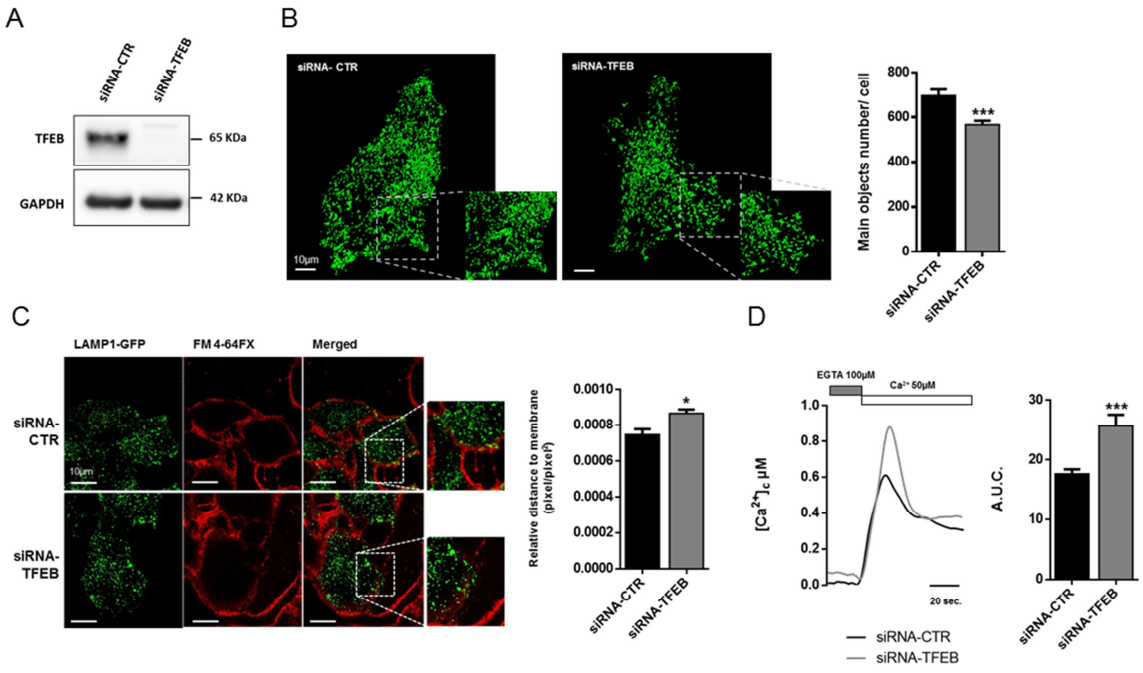

Fig. 3. Downregulation of TFEB decreased the lysosomal network and lysosomal localization to the PM, thereby increasing capacitative Ca^{2+} entry in HeLa cells. (A) Representative immunoblot images of TFEB protein abundance in HeLa cells transfected for 72 h with control siRNA (siRNA-CTR) or siRNA for TFEB (siRNA-TFEB). (B) Representative images of lysosomal morphology and quantification of the lysosomal number in HeLa cells transfected for 48 h with LAMP1-GFP (green) and silenced for 72 h with control siRNA (siRNA-CTR) or siRNA for TFEB (siRNA-TFEB). (C) Representative images and quantification of lysosomal distance to the plasma membrane normalized on the cellular area in HeLa cells transfected for 48 h with LAMP1-GFP (green) and silenced for 72 h with siRNA control (siRNA-CTR) or siRNA for TFEB (siRNA-TFEB); the plasma membrane is stained with FM4-64fx dye (red). (D) Cytosolic Ca^{2+} measurements of capacitative Ca^{2+} entry measured by cytosolic aequorin in HeLa cells transfected with control siRNA (siRNA-CTR) or siRNA for TFEB (siRNA-TFEB). Data are presented as the means ± SEM; *p<0.05, ***p<0.001. a.u.c. = area under the curve.

Subsequently, we assessed the level of cytosolic Ca^{2+} entering the cell across the PM via SOCE employing the same experimental setting used for TFEB-overexpressing HeLa cells. After induction of capacitative Ca^{2+} influx, Ca^{2+} ($CaCl_2$ 50 µM) was added to the KRB perfusion, and we observed that TFEB-silenced cells (Fig. 3D) displayed a significant increase in cytosolic Ca^{2+} uptake compared with the control samples. Overall, these data

suggest that the effect of TFEB activity on SOCE is strictly dependent on both lysosomal activity and the PM-specific positioning of lysosomes.

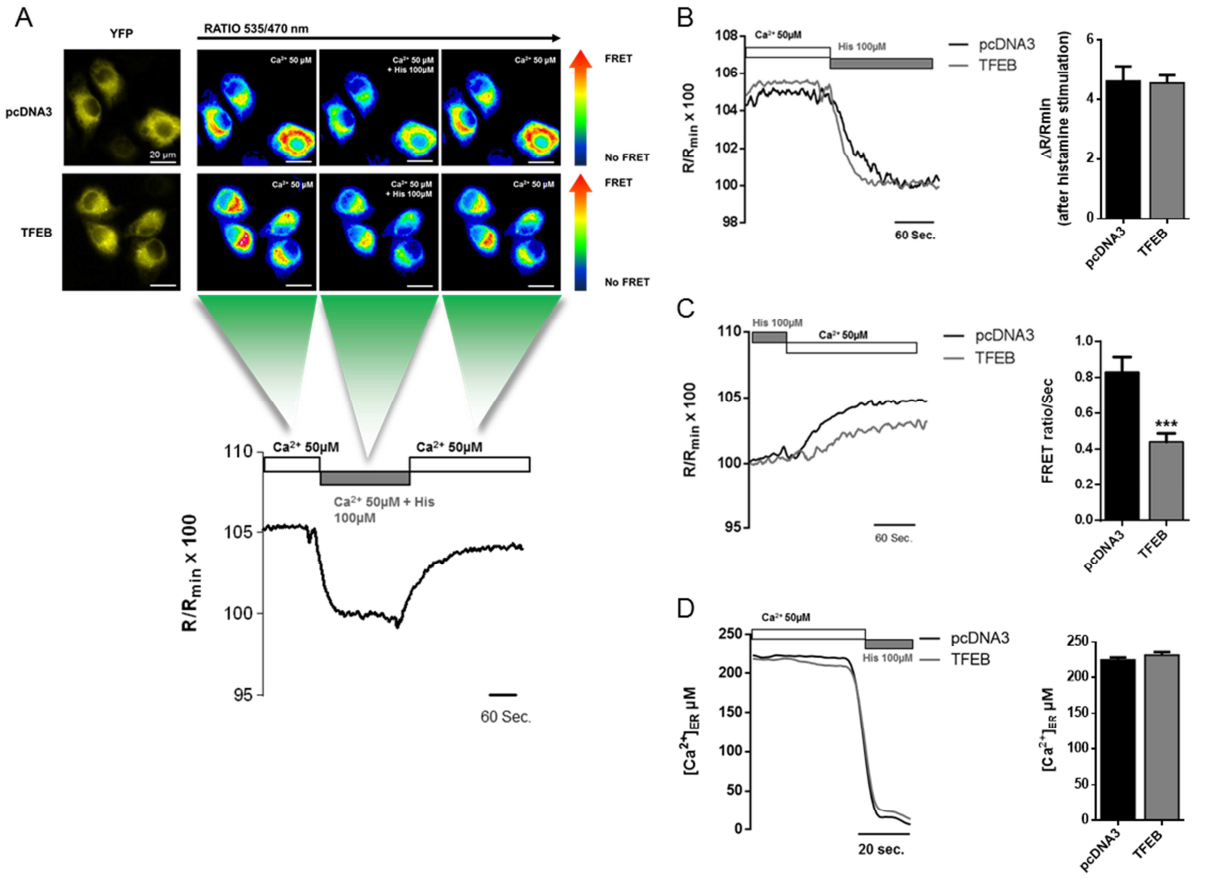

Fig. 4. TFEB reduces Ca^{2+} re-uptake in the endoplasmic reticulum. (A) Representative images of D1ER probe yellow fluorescence (YFP), FRET ratio images and of phases of FRET experiments of HeLa cells transfected with pcDNA3 (up) or TFEB (below), before and after stimulation with histamine (100 µM) and after washout of the perfused ER Ca^{2+}-releasing stimulus. (B) Measurements of the Δ FRET ratio ($\Delta R/R_{min}$) in HeLa cells co-transfected with pcDNA3 (control) or TFEB3xflag (TFEB) for 48 h during lysosomal emptying after histamine (100 µM) stimulation. (C) Ca^{2+} re-uptake rate measurements in pcDNA3 (control) or TFEB3xflag (TFEB)-transfected cells during washout of the agonist (histamine 100 µM). (D) The ER Ca^{2+} concentration measured with ER-targeted aequorin in control (pcDNA3) or overexpressing TFEB 3xflag (TFEB) HeLa cells in the presence of a low extracellular Ca^{2+} concentration ($CaCl_2$ 50 µM). Administration of histamine (100 µM) resulted in comparable ER emptying under both conditions. Data are presented as the means ± SEM; ***p<0.001.

4. TFEB reduces SOCE-dependent Ca^{2+} refilling in the ER

As seen above, the capacitative influx is activated in response to the depletion of intracellular Ca^{2+} in the ER, and it represents the primary path for the maintenance of Ca^{2+} levels in the ER during stimulation.

Therefore, we determined whether lysosomes affect ER Ca^{2+} dynamics in response to stimuli. Reticular Ca^{2+} measurements were performed using the genetically encoded fluorescence

resonance energy transfer (FRET)-based probe D1ER chameleon, which is targeted to the ER via a KDEL retention sequence(Palmer, Jin et al. 2004). This probe contains a Ca^{2+}-binding domain that, once Ca^{2+} is bound, allows the highly efficient excitation transfer from a donor cyan fluorescent protein to an acceptor yellow fluorescent protein. The degree of FRET provides a ratiometric indicator of the Ca^{2+} level within the ER(McCombs and Palmer 2008) (Fig. 4A).

We performed FRET experiments in HeLa cells transfected with D1ER. When the cells were perfused with KRB and Ca^{2+} (50 μM) at the start of the test, we measured the baseline FRET ratio, which corresponds to the resting Ca^{2+} level (see Fig. 4A and B). Subsequently, we added an agonist (histamine 100 μM) that acts on Gq-coupled PM receptors triggering the production of IP3, thereby stimulating Ca^{2+} release from the ER through IP3Rs. Ca^{2+} depletion in the ER leads to the activation of Ca^{2+} channels, resulting in Ca^{2+} influx from the extracellular medium through the PM. At this point, the rate of Ca^{2+} re-uptake in the ER was measured (Fig. 4A and C).

HeLa cells transiently overexpressing TFEB did not display any difference in ER Ca^{2+} concentration at baseline compared with control (pcDNA3) cells (Fig. 4B). These data were also confirmed through an ER-targeted aequorin-based approach. After the induction of ER Ca^{2+} emptying with ionomycin (3 μM) and EGTA (600 μM) (see material and methods), the cells were perfused with Ca^{2+} at an extracellular concentration of 50 μM, and the maximum basal level of accumulated Ca^{2+} was measured (Fig. 4D). We did not observe any difference in ER baseline Ca^{2+} levels in TFEB-overexpressing cells compared with control cells. However, TFEB-overexpressing cells showed a significant reduction in the Ca^{2+} re-uptake rate (Fig. 4A and C) after agonist washout compared with control cells, supporting the notion that TFEB-mediated SOCE inhibition could reduce Ca^{2+} refilling within the ER.

5. Impairment of lysosomal activity or TFEB knockdown promotes the recovery or an increase of the Ca^{2+} re-uptake rate in the ER, respectively

We thus hypothesized that the increased quantity of lysosomes near the PM induced by TFEB overexpression might be responsible for the reduction in SOCE, thus delaying its sequestration by the ER. To confirm our hypothesis, we performed FRET measurements of Ca^{2+} reuptake to evaluate ER Ca^{2+} dynamics after pre-treatment of HeLa cells with functional inhibitors of lysosomes.

GPN treatment (200 µM for 30 min) minimized the effects of TFEB overexpression on the ER Ca^{2+} re-uptake rate (Fig. 5A). Moreover, upon Vac-1 treatment (10 µM for 1 h) (Fig. 5B), we observed a restoration of the ER Ca^{2+} re-uptake rate in HeLa cells expressing TFEB.

Taken together, these results confirm the effect of TFEB overexpression on the rate of ER Ca^{2+} re-uptake due to the Ca^{2+} buffering capacity of PM-located lysosomes.

To verify the effect of TFEB on SOCE modulation, we performed similar FRET experiments in TFEB-depleted cells measuring the rate of ER Ca^{2+} re-uptake (Fig. S5C).

Down-regulation of TFEB induced a significant increase in the rate of Ca^{2+} re-uptake compared to control cells, supporting a specific role for TFEB in regulating SOCE.

To further confirm our results regarding lysosome-mediated Ca^{2+} regulation and to exclude a direct effect of TFEB overexpression on SOCE molecular machinery, we first examined the protein expression levels of two main modulators of the capacitative Ca^{2+} influx pathway: STIM1 and ORAI1. TFEB did not affect the expression level of either STIM1 or ORAI1 (as shown in Fig. 6A). We then investigated the formation of STIM1 and ORAI1 clusters to clarify whether overexpression of TFEB can influence the contact sites between two proteins involved in the activation of SOCE.

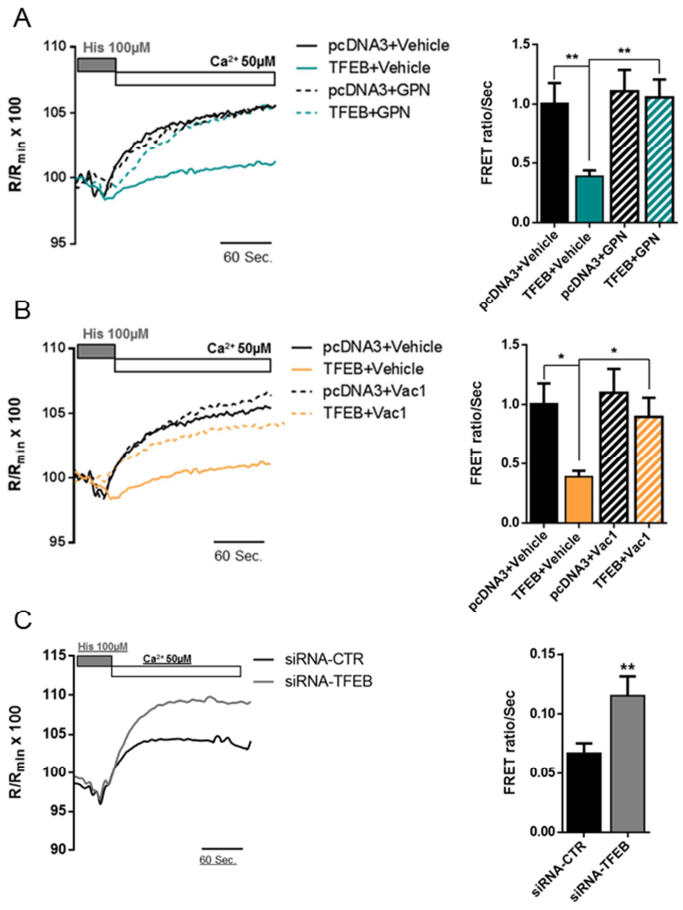

Fig. 5. Lysosomal impairment promotes recovery of the rate of Ca^{2+} re-uptake in the endoplasmic reticulum, without affecting SOCE protein expression. (A) and (B) Measurement of the Ca^{2+} re-uptake rate in the ER after depletion with an agonist (histamine 100 µM) using the ER-targeted chameleon (D1ER) probe in HeLa cells co-transfected with pcDNA3 (control) or TFEB3xflag (TFEB) for 48 h. As previously described for the aequorin experiments, cells were pretreated with 200 µM GPN (A) for 30 min or 10 µM Vac-1 (B) for 1 h, or with DMSO as a control. In both experiments, the rate of Ca^{2+} re-uptake into the ER was significantly recovered in HeLa cells overexpressing TFEB. (C) Ca^{2+} re-uptake rate measurement using the ER-targeted Cameleon (D1ER) probe in HeLa cells transfected for 72 h with control siRNA (siRNA-CTR) or siRNA for TFEB (siRNA-TFEB) during washout of agonist (histamine 100 µM). Data are presented as the means ± SEM; *p<0.05, **p<0.01.

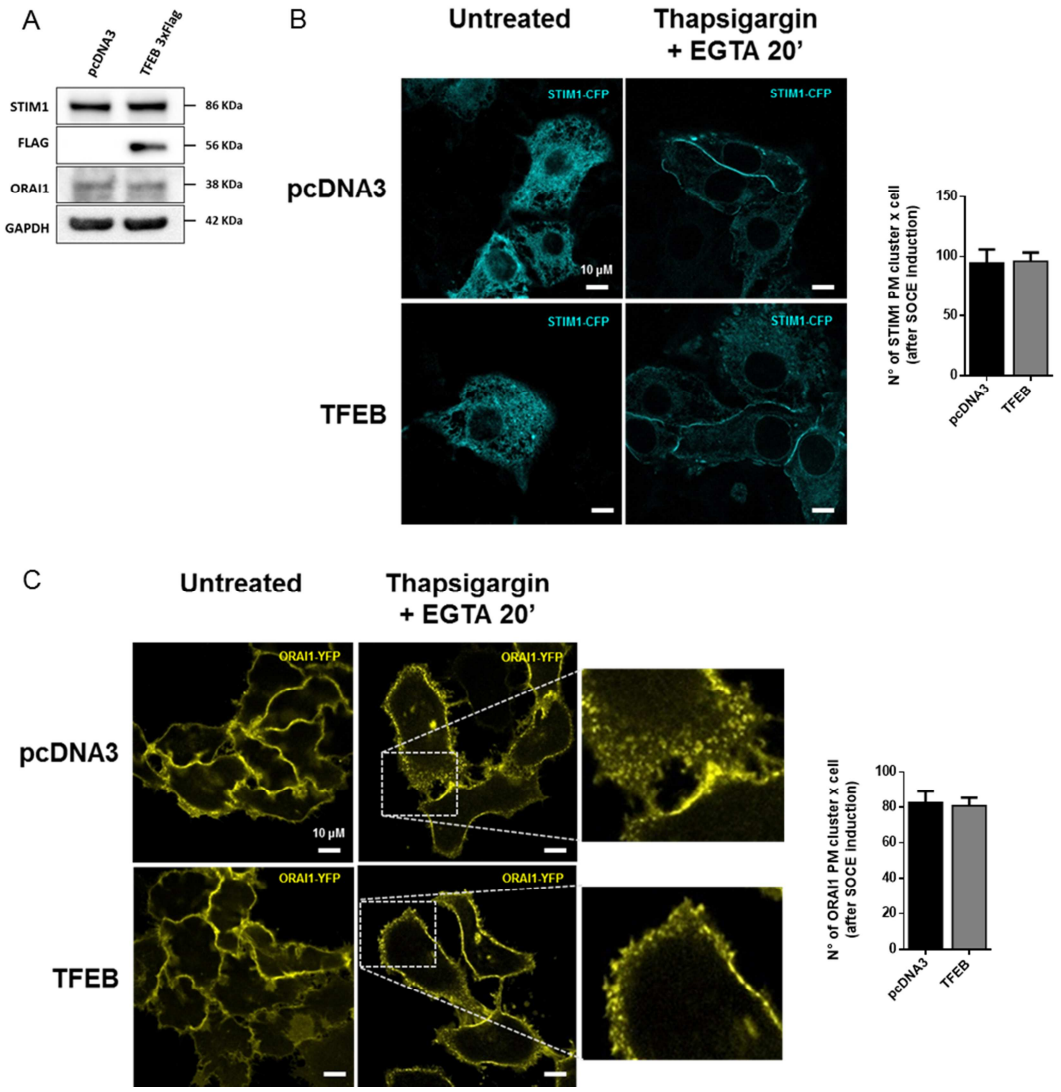

Fig. 6. TFEB overexpression did not influence STIM1 and ORAI1 expression or punctae formation. (A) Representative immunoblot images of protein expression levels of STIM1 and ORAI1 in HeLa cells transfected for 48 h with a plasmid expressing pcDNA3 (Control) or TFEB 3xflag (TFEB). (B) ORAI1-YFP representative images and ORAI1 clusters quantification of HeLa cells transfected with a plasmid expressing pcDNA3 (Control) or TFEB 3xflag (TFEB) before and after treatment with thapsigargin (200 nM) for 15 min in a Ca^{2+}-free medium (KRB/EGTA). (C) STIM1-YFP representative images and STIM1 clusters quantification of HeLa cells transfected with a plasmid expressing pcDNA3 (Control) or TFEB 3xflag (TFEB) before and after treatment with thapsigargin (200 nM) for 15 min in a Ca^{2+}-free medium (KRB/EGTA). Data are presented as the means ± SEM.

Therefore, we induced Ca^{2+} emptying from the ER under the same experimental conditions used for cytosolic Ca^{2+} measurements and assessed the number of ORAI1 clusters using the recombinant reporter ORAI1-EYFP. After treatment with thapsigargin; (200 nM) in Ca^{2+}-free medium (KRB/EGTA), the number of clusters of ORAI1 increased considerably (Fig. 6C) in both control and TFEB-overexpressing HeLa cells, but no significant differences were detected between pcDNA3 and TFEB-transfected cells.

Moreover, we examined the formation of STIM1 puncta resulting from the same treatment (see above) using the recombinant reporter STIM1-ECFP; again, we did not observe significant differences between TFEB-expressing and control HeLa cells (see Fig. 6B), supporting a crucial role for the lysosomal compartment in the TFEB-dependent regulation of Ca^{2+} influx.

6. Modulation of TFEB expression affects lysosomal Ca^{2+} contents after SOCE induction.

As noted above, the increase in the biogenesis of lysosomes and their localization to the PM, induced by overexpression of TFEB affected SOCE, leading to lower calcium uptake in the cytosol and a reduced rate of Ca^{2+} charging of the ER. Conversely, downregulation of TFEB reduced the number of lysosomes and their distribution in the proximity of plasma membrane, associated with increases in cytosolic Ca^{2+} uptake and the Ca^{2+} re-uptake rate of the ER during capacitative Ca^{2+} influx. We thus speculated that lysosomes proximal to the PM take up Ca^{2+} imported into the cell by SOCE, depriving the ER of this ion.

To confirm our hypothesis, we directly assessed lysosomal Ca^{2+} concentrations ($[Ca^{2+}]_{Lys}$) using aequorin fused with the full-length cathepsin D protein, which specifically targets the probe to lysosomes(Ronco, Potenza et al. 2015). If the hypothesis is correct, we expected that TFEB overexpression, a condition able to reduce SOCE would increase $[Ca^{2+}]_{Lys}$. To induce capacitative Ca^{2+} influx via SOCE activation, HeLa cells were treated with ionomycin (3 μM) for 1 h in a Ca^{2+}-free medium (KRB/EGTA) during aequorin reconstitution with coelenterazine to encourage depletion of ER and lysosomal Ca^{2+} stores. When the release of stored Ca^{2+} was complete, Ca^{2+} ($CaCl_2$ 50 μM) was added to the KRB perfusion. In our experimental setting, HeLa cells overexpressing TFEB (Fig. 7A) displayed a significant increase in lysosomal Ca^{2+} compared with control cells. Accordingly, we detected a significant reduction in $[Ca^{2+}]_{Lys}$ in TFEB-silenced cells compared to siRNA control cells (Fig. 7B), corroborating the role of TFEB in the regulation of SOCE by specifically modulating the lysosomal Ca^{2+}-buffering capacity.

As previously observed, Vac-1 treatment affected the capacity of lysosomes to interact with other organelles(Lopez-Sanjurjo, Tovey et al. 2013), thus reducing the fusion of lysosomes with the PM(Huynh and Andrews 2005). To clarify whether the lack of proximity of lysosomes to the PM under Vac-1 treatment might influence SOCE, we directly assessed the

lysosomal Ca^{2+} concentration in HeLa cells transiently transfected with empty vector (pcDNA3) or TFEB after pretreatment with Vac-1 (10 µM for 1 h) or DMSO (vehicle).

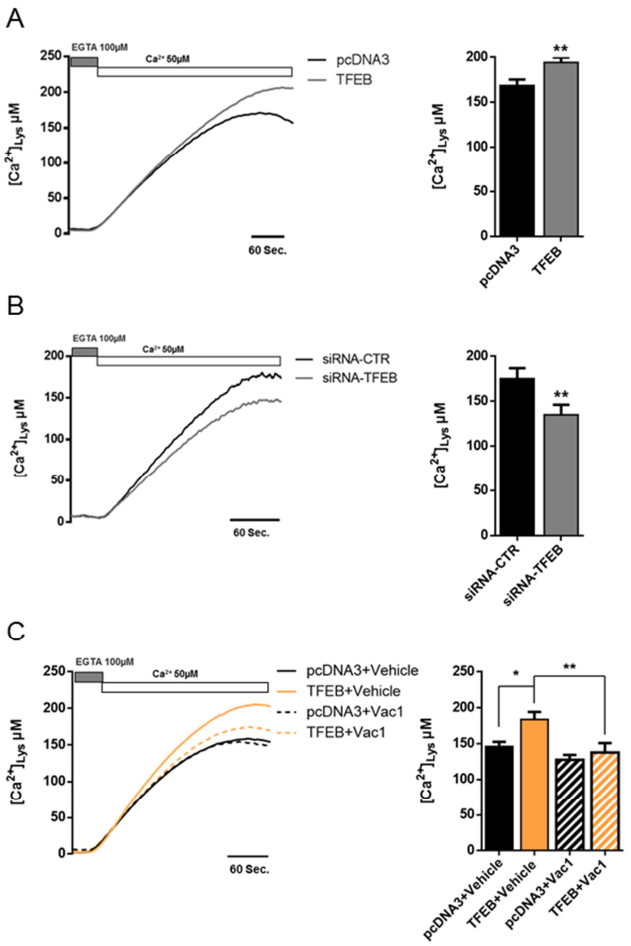

Fig. 7. Lysosomal Ca^{2+} content is affected by TFEB expression. (A) Ca^{2+} reuptake measured with lysosomal aequorin in control HeLa cells (pcDNA3) or HeLa cells overexpressing TFEB for 48 h, after Ca^{2+} (50 µM) administration. (B) Capacitative Ca^{2+} entry was measured using lys-Aeq in HeLa cells with the control siRNA (siRNA-CTR) or siRNA targeting TFEB (siRNA-TFEB) after Ca^{2+} (50 µM) administration. (C) Lysosomal Ca^{2+} uptake measured in HeLa cells transfected with pcDNA3 (control) or with TFEB3xflag (TFEB) and pretreated with 10 µM Vac-1 or DMSO (vehicle) for 1 h. After intracellular Ca^{2+} store depletion, the cells were perfused with 50 µM Ca^{2+} Data are presented as the means ± SEM; *p<0.05, **p<0.01.

Under experimental conditions including only the vehicle, we observed maintenance of the differences in lysosomal Ca^{2+} between control and TFEB-overexpressing samples (Fig. 7C). Importantly, Vac-1 treatment significantly reduces lysosomal Ca^{2+}-buffering capacity exclusively in HeLa cells expressing TFEB, without altering the lysosomal Ca^{2+} levels of control cells. Overall, these data suggest that the effect of TFEB activity on SOCE and on lysosomal Ca^{2+} refilling is strictly dependent on both lysosomal activity and the PM-specific positioning of lysosomes.

7. The calcineurin/TFEB pathway modulates SOCE in TFEB-overexpressing HeLa cells.

As previously demonstrated by Medina et al.(Medina, Di Paola et al. 2015), lysosomal Ca^{2+} release via MCOLN1 controls the activity of the phosphatase calcineurin during starvation.

This pathway activates TFEB, thus promoting its nuclear translocation and lysosomal compartment expansion(Settembre, Di Malta et al. 2011).

To validate our experimental setup, we first performed immunofluorescence staining of HeLa cells overexpressing TFEB before and after 6 h of starvation. Calcineurin activity was inhibited with cyclosporin A (CsA) to prevent TFEB translocation to the nucleus. As expected, analysis of the TFEB distribution revealed a nuclear-enriched pattern upon starvation (Fig. 8A).

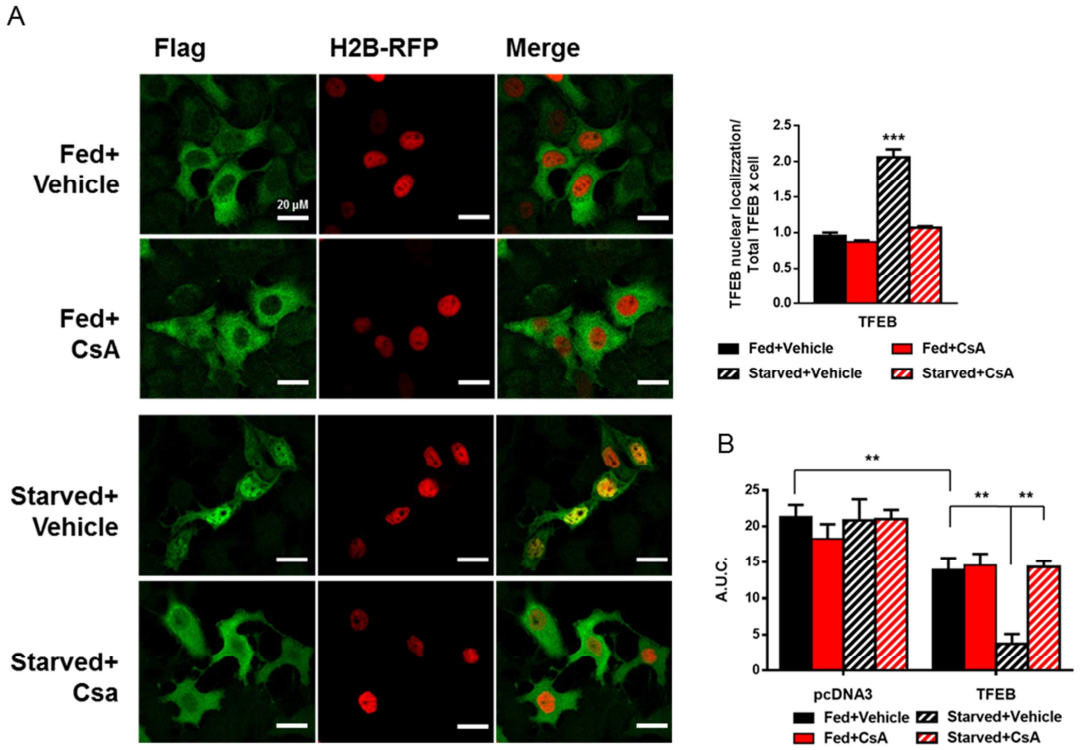

Fig. 8. The calcineurin/TFEB pathway modulates SOCE in TFEB-overexpressing HeLa cells. (A) Representative immunofluorescence images and quantification of TFEB nuclear localization (green) on the total TFEB fraction of HeLa cells overexpressing TFEB 3xflag under basal conditions (fed) or after 6 h of starvation (starved), treated with vehicle (DMSO) or CsA (10 µM). The cells were also transfected with the H2B-RFP construct to mark the nucleus (red). (B) Cytosolic Ca^{2+} measurements of capacitative Ca^{2+} entry measured using cytosolic aequorin in HeLa cells transfected with pcDNA3 or TFEB 3xflag (TFEB) under basal conditions (fed) or after 6 h of starvation (starved), treated with vehicle (DMSO) or CsA (10 µM). After intracellular Ca^{2+} store depletion, 50 µM Ca^{2+} was perfused in solution. Data are presented as the means ± SEM; **p<0.01, ****p<0.0001. a.u.c. = area under the curve.

Then, to investigate the possible role of the lysosomes/calcineurin/TFEB axis in SOCE modulation, we assessed the level of cytosolic Ca^{2+} entering via SOCE in pcDNA3 and TFEB-overexpressing HeLa cells under the same condition described above. Control cells showed no significant differences in SOCE either during starvation (Fig. 8B) or after CsA treatment. Intriguingly, TFEB-mediated reduction of SOCE was amplified by starvation, and

this effect was completely prevented by CsA treatment during starvation. These data indicate that increasing the nuclear localization of TFEB through starvation further stimulates lysosomal biogenesis(Settembre, Di Malta et al. 2011), thereby enhancing the role of lysosomes in the modulation of SOCE.

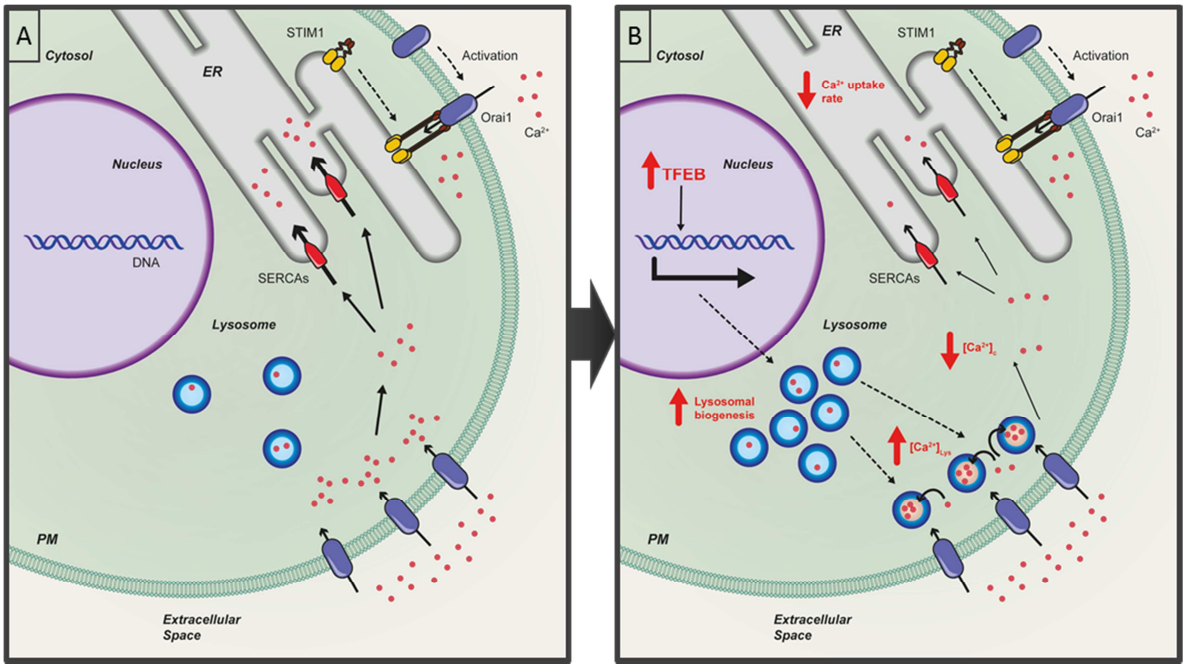

Fig. 9. TFEB modulates SOCE in TFEB-overexpressing HeLa cells. (A) The SOCE activation after ER store depletion due to a regular replenishment of ER. (B) Transient TFEB overexpression induces an increased lysosomal biogenesis and location of lysosome in the proximity of PM. This significantly reduces cytosolic Ca^{2+} levels under a capacitative influx model and ER re-uptake rate of calcium, increasing the lysosomal Ca^{2+} buffering capacity.

Discussion

For a long time, lysosomes have been considered to be merely cellular 'incinerators' involved in the degradation and recycling of cellular waste (Appelqvist, Waster et al. 2013). However, there is now compelling evidence that lysosomes have a much broader function and may assume a pivotal role in intracellular signalling. Indeed, in a recent study, Kilpatrick and coworkers speculate that TRPML1 activation evokes a global Ca^{2+} signal that originates from the ER, lysosomes, and influx from the extracellular environment, suggesting a possible location of a small portion of TRPML1 to the PM (Kilpatrick, Yates et al. 2016).

Lysosomes can accumulate Ca^{2+} released from the ER (Lopez-Sanjurjo, Tovey et al. 2013, Garrity, Wang et al. 2016), and the observation that these two organelles are intimately associated sheds new light on the multiple functions of lysosomes and on their essential roles in cellular homeostasis.

In addition, the identification of TFEB as a master regulator of lysosomal biogenesis and autophagy has revealed how the lysosome adapts to environmental cues such as nutrient availability. Targeting TFEB may provide a novel therapeutic strategy for modulating lysosomal functions in human diseases.

In this thesis, we combined the fundamental role of TFEB in lysosomal biogenesis, to the novel role of lysosomes in Ca^{2+} homeostasis. Through modulation of TFEB expression in HeLa cells, we attempted to better understand the role of lysosomes in maintaining Ca^{2+} homeostasis.

We showed that increases in the number of lysosomes and their proximity to the PM upon TFEB overexpression strongly influence Ca^{2+} entry across the PM (Fig. 1) and lysosomal calcium replenishment (Fig. 5A) after SOCE activation. Using pharmacological approaches to alter both the activity and distribution of lysosomes (Fig. 2B and D), we showed that the TFEB-dependent reduction of SOCE is dependent on lysosomal dynamics. In particular, the reduction in interacting membrane surface after Vac-1 treatment suggests that this buffering role is explained by the proximity of the PM. Conversely, transient TFEB knockdown reduces the number of lysosomes and their localization to the PM, increasing cytosolic Ca^{2+} accumulation, the reticular Ca^{2+} replenishment rate and lysosomal buffering capacity in a location-dependent manner (Fig. 9).

In recent studies, Lopez-Sanjurjo and co-workers (Lopez-Sanjurjo, Tovey et al. 2013, Lopez Sanjurjo, Tovey et al. 2014) revealed that i) the close association between lysosomes and the ER allows lysosomes to selectively accumulate Ca^{2+} released from the ER and that ii) disruption of lysosomal Ca^{2+} uptake does not affect SOCE. The results of the present study confirm these findings; alteration of the lysosomal compartment by different pharmacological approaches did not compromise SOCE in control cells (Fig. 2B and D). However, we observed a restoration of capacitative influx only in TFEB-overexpressing cells treated with both GPN and Vac-1 (Fig. 2B and D and Fig. 5). Therefore, under physiological conditions, lysosomes are prone to sequester Ca^{2+} released by the ER due to the juxtaposition between the two organelles, whereas under specific situations such as TFEB overexpression that undermine the redistribution of lysosomes, different Ca^{2+} sources might represent the primary target of lysosomal Ca^{2+} buffering activity. Interestingly, lysosomes located at different intracellular regions exhibit high heterogeneity(Johnson, Ostrowski et al. 2016). Peripheral lysosomes are more alkaline (pH values $\geq$ 6) than juxtanuclear lysosomes due to increased passive (leak) permeability of H^+ and reduced vacuolar V-ATPase activity. Nevertheless, lysosomal buffering capacity appears to be comparable between central and marginal lysosomes, whereas peripheral lysosomes display reduced cathepsin L activity. Based on the widely accepted view that lysosomal acidification drives Ca^{2+} into lysosomes(Lopez-Sanjurjo, Tovey et al. 2013), it is reasonable to assume that peripheral lysosomes possess a decreased capacity for Ca^{2+} uptake due to their higher pH. However, a recent paper by Garrity et al. contests the 'pH hypothesis' of lysosomal Ca^{2+} accumulation by elegantly demonstrating that under normal conditions, lysosome Ca^{2+} stores are refilled from the ER through IP3 receptors in a manner independent of lysosomal pH(Garrity, Wang et al. 2016). Moreover, in secretory granules and the ER, increasing the luminal pH raised the Ca^{2+} buffering capacity of both compartments(Dickson, Duman et al. 2012). Taken together, these findings suggest that the primary effects of TFEB expression on extracellular Ca^{2+} entry might be precisely due to the lower acidification of the lysosomes closest to the PM, which in turn might result in a higher Ca^{2+} buffering capacity.

The principal activity of perimetral lysosomes is fusion with the PM to complete the process of exocytosis in a Ca^{2+}-dependent manner(Xu and Ren 2015). Lysosomes likely provide the Ca^{2+} required for lysosomal fusion(Xu and Ren 2015). Interestingly, TFEB modulates exocytosis, causing increased expression/activity of tethering factors or proteins involved in lysosome mobility, docking(Settembre, Fraldi et al. 2013) and fusion to the PM(Settembre, Di Malta et al. 2011). In particular, upregulation of the lysosomal Ca^{2+} channel TRPML1 triggers

the final fusion of these organelles through localized Ca^{2+} release(Settembre, Di Malta et al. 2011). Therefore, the buffering capacity of lysosomes close to the PM, which we observed in TFEB-overexpressing cells, could be critical for promoting lysosomal Ca^{2+} refilling, thereby favouring lysosomal exocytosis.

Moreover, a recent study by Medina et al.(Medina, Di Paola et al. 2015) revealed that lysosomes could release Ca^{2+} via MCOLN1 during starvation. This lysosomal Ca^{2+} efflux triggers the phosphatase calcineurin, which de-phosphorylates TFEB, thus promoting its nuclear translocation and autophagy. In this work, we demonstrate that TFEB increases $[Ca^{2+}]_{Lys}$, which would, in turn, potentiate calcineurin activation during starvation. It is therefore proposed that TFEB modulation of SOCE and $[Ca^{2+}]_{Lys}$ stimulates a positive feedback loop that maximizes the TFEB-mediated control of lysosomal biogenesis and recruitment to the plasma membrane. In support of this model, we showed that starvation exacerbates the role of lysosomes in the modulation of SOCE, and this phenomenon is completely prevented by CsA-mediated inhibition of calcineurin (Fig. 8).

Importantly, the TFEB-mediated regulation of SOCE was observed only in the presence of a low extracellular Ca^{2+} concentration (50 μM) (Fig. 1). Although studies on the role of lysosomes in Ca^{2+} signalling have significantly increased in number over the last decade, the nature of the exchanger/channel responsible for lysosomal Ca^{2+} uptake remains unknown. Based on our data, we suggest that the lysosomal compartment represents a system that responds well to low concentrations of Ca^{2+} and has a high affinity for the cation, as speculated in other works(Christensen, Myers et al. 2002, Lopez-Sanjurjo, Tovey et al. 2013).

Moreover, in a recent work Zhen-Dong Zhu and co-worker (Zhu, Yu et al. 2018) prove the existence of a functional link between SOCE, calcineurin and TFEB in the pathogenesis of acute pancreatitis. They suggest caerulein-induced SOCE activated CaN, which in turn dephosphorylated TFEB and NFAT and respectively regulated autophagic and inflammatory injury in the development of acute pancreatitis. These data reveal that targeting CaN may be potential for arresting SOCE-induced pancreatic injury. So in this scenario, our model may represent a modulation system in TFEB activation by SOCE. In addition, it is tempting to speculate that, just as in acute pancreatitis, SOCE-regulating TFEB activation may also exist in some other SOCE-related diseases (Lacruz and Feske 2015) like Duchenne's dystrophy, neurofibromatosis or some neurodegenerative disorders.

In conclusion, we provide new evidence for the role of TFEB in shaping extracellular Ca^{2+} entry through the re-distribution of the lysosomal compartment to the PM. These findings not only describe TFEB as a new regulator of intracellular Ca^{2+} homeostasis but also propose

lysosomal control of SOCE as an important aspect of lysosomal function and cellular health (Sbano, Bonora et al. 2017).

Materials and Methods

Immunoblotting

For immunoblotting, cells were scraped into ice-cold, phosphate buffered saline (PBS) and lysed in a buffer containing 50 mM Tris HCl pH 7.4, 150 mM NaCl, 1% Triton X-100, 0.2% SDS, protease and phosphatase inhibitor cocktail. After 30 min of incubation on ice and centrifugation at 2,500 rpm at 4°C for 5 min, proteins were quantified by the Lowry method, and 10 µg of each sample was loaded onto a Novex NuPage Bis-Tris 4–12% precast gel (Life Technologies). The separated proteins were transferred to nitrocellulose membranes. After incubation with TBS-Tween-20 (0.05%) supplemented with 5% non-fat powdered milk for 1 h to saturate unspecific binding sites, the membranes were incubated overnight with primary antibodies. Detection was achieved using appropriate horseradish peroxidase-labelled secondary antibodies (Santa Cruz Biotechnology), followed by biochemiluminescence (ThermoScientific) using an ImageQuant LAS4000 (GE Healthcare).

Antibodies

The following primary antibodies were used for Western blotting: rabbit anti-FLAG [F7425] (1:2,000) and mouse anti-b-actin [A1978] (1:10,000) from Sigma-Aldrich; rabbit anti-GAPDH [#2118] (1:5,000) and rabbit anti-TFEB [#4240] (1:1000) from Cell Signaling; rabbit anti-STIM1 [sc-68897] (1:1,000) and rabbit anti-ORAI1 [sc-68895] (1:1,000) from Santa Cruz Biotechnology.

Analysis of lysosomal morphology

HeLa cells expressing a lysosomal-targeted variant of GFP (LAMP1-GFP) were imaged using an IX-81 automated epifluorescence microscope (Olympus) equipped with a 60× oil-immersion objective (N.A. 1.35, from Olympus) and an ORCA-R2 CCD camera (Hamamatsu Photonics K.K.). Selected cells were followed over time, and z-stacks were subjected to digital deconvolution using a Wiener deconvolution filter and a theoretical point-spread function provided by Xcellence software (Olympus). GFP-positive objects were quantified using BITPLANE Imaris 4.

Reagents and solutions

The following chemicals were used: di-peptide glycyl-L-phenylalanine 2-naphthylamide (GPN; Bachem), vacuolin 1 (Vac-1; Calbiochem), thapsigargin (Sigma-Aldrich), ethylene glycol-bis (β-aminoethyl ether)-N,N,N',N'-tetraacetic acid (EGTA; Sigma-Aldrich), cyclosporin a (CsA; Sigma-Aldrich).

Cell culture and transient transfection

HeLa cells were grown in Dulbecco's modified Eagle's medium (DMEM) supplemented with 10% fetal bovine serum (FBS; Life Technologies), 2 mM L-glutamine, and 100 U/ml penicillin (EuroClone), and 100 mg/ml streptomycin (EuroClone) in 75 cm^2 Corning flasks. All cells were maintained at 37°C under 90% relative humidity with 5% CO_2. Before transfection, cells were seeded onto 13 mm glass coverslips for intracellular Ca^{2+} measurements with aequorin and onto 24 mm glass coverslips for microscopic analysis. Cells were grown to 70% confluence and then transfected for 12 h at 37° C for transient plasmid overexpression. Transfection was performed via the standard Ca^{2+}phosphate procedure(Pinton, Ferrari et al. 2000). All experiments were performed 48 h after transfection. For siRNA experiments, cells were seed onto 13 mm glass coverslips for intracellular Ca^{2+} measurements with aequorin and onto 24 mm glass coverslips for microscopic analysis. siRNA for TFEB (siRNA-TFEB, Thermo, D-009798-03) and non-targeting siRNA (siRNA-CTR, Thermo, D-001810-10-05) were transfected with Lipofectamine RNAiMAX (Invitrogen) using a reverse transfection protocol. After 24 h, the cells were transfected for 12 h at 37° C to achieve transient plasmid overexpression, via the standard Ca^{2+} phosphate procedure (Pinton, Ferrari et al. 2000), and siRNA experiments were performed 48 h after the last transfection.

Aequorin measurements

The probes used in these experiments were chimeric aequorins targeted to the cytosol (cyt-Aeq), PM (PM-Aeq), ER (ER-Aeq) and lysosomes (lys-Aeq). To evaluate the capacitative Ca^{2+} entry current in the experiments with cyt-Aeq, at 48 h post-transfection, the coverslips were incubated with 5 μM coelenterazine (Fluka) for 1.5 h in Krebs–Ringer modified buffer (KRB; 125 mM NaCl, 5 mM KCl, 1 mM Na_3PO_4, 1 mM $MgSO_4$, 5.5 mM glucose, and 20 mM 4-(2-hydroxyethyl)-1-piperazineethanesulfonic acid [HEPES], pH 7.4, at 37° C)

supplemented with 1 mM $CaCl_2$. For the PM-Aeq experiments, the coverslips were incubated in KRB supplemented with 5 μM coelenterazine and 100 μM EGTA for 1 h.

Then, to induce ER Ca^{2+} emptying, cells were incubated with 200 nM thapsigargin (SERCA inhibitor) and 1 mM EGTA in Ca^{2+}-free KRB for 15 min at 4°C. A coverslip with transfected cells was subsequently placed in a perfused thermostat-controlled chamber located in close proximity to a low-noise photomultiplier with a built-in amplifier/discriminator. After 30" of perfusion with KRB supplemented with 100 μM EGTA, Ca^{2+} was added to KRB, as specified in the figure legends. All experiments were terminated by lysing cells with X-100 Triton in a hypotonic Ca^{2+}-containing solution (10 mM $CaCl_2$ in H_2O), thus discharging the remaining aequorin pool.

To reconstitute ER-Aeq and lys-Aeq with high efficiency, the luminal [Ca^{2+}] of the intracellular Ca^{2+} stores was first reduced by incubating the cells for 45 min at 4°C in KRB supplemented with 5 μM coelenterazine N, the Ca^{2+} ionophore ionomycin, and 600 μM EGTA. After incubation, the cells were extensively washed with KRB supplemented with 2% bovine serum albumin and 2 mM EGTA before luminescence measurements were initiated. After 180" of perfusion with KRB supplemented with 100 μM EGTA, 50 μM Ca^{2+} was added to KRB, as specified in the figure legends. For the ER-Aeq experiments, the agonist (histamine at 100 μM) was added to the same medium after a Ca^{2+} plateau was reached.

All experiments were terminated by lysing cells with X-100 Triton in a hypotonic Ca^{2+}-containing solution (10 mM $CaCl_2$ in H_2O), thus discharging the remaining aequorin pool.

For the experiments with GPN, the cells were pretreated for 30' during the period of incubation using coelenterazine and 200 μM GPN to induce emptying of the ER or DMSO in control cells. For experiments with Vac-1, the cells were pretreated with coelenterazine for 1 h during the period of incubation, and emptying of the ER was induced with 10 μM Vac1; control cells were treated with DMSO.

The output of the discriminator was captured with a Thorn EMI photon-counting board and stored in an IBM-compatible computer for further analyses. The aequorin luminescence data were calibrated into [Ca^{2+}] values offline, using a computer algorithm based on the Ca^{2+} response curve of wild-type aequorin. Further experimental details were previously described(Bonora, Giorgi et al. 2013).

Acquisition of fluorescence microscopy observations of the treatments

HeLa cells expressing lysosomal-targeted GFP (LAMP1-GFP) were stained with LysoTracker RED (Invitrogen) and treated with GPN, Vac1 or vehicle alone, as indicated in the text and figures. For all treated cells, digital images were acquired in a 37° C thermostat-controlled incubation chamber with a confocal microscope (Zeiss LSM510), using a 40 × 1.4 NA Plan-Apochromat oil-immersion objective. The acquired images were subsequently analyzed using the open source software Fiji.

Measurements of ER Ca^{2+} dynamics with D1ER

Luminal Ca^{2+} dynamics were measured using single-cell Ca^{2+} imaging and the Ca^{2+}-sensitive FRET (fluorescence resonance energy transfer)-based chameleon protein D1ER(Palmer, Jin et al. 2004). HeLa cells were co-transfected with D1ER and TFEB-3xFLAG or empty vector (pcDNA3). After 40 h, coverslips were placed in 1 ml of KRB, and images were captured with METAFLUOR 7.0 Software (Universal Imaging) at $\lambda_{excitation}$=430 nm and $\lambda_{emission}$= 470 and 535 nm every 2 s using a Zeiss Axiovert 200M inverted microscope equipped with a C-Apochromat 40x/1.2 W CORR objective and a cooled CCD camera (Photometrics). CFP emission and yellow fluorescent protein (YFP) FRET emission were alternately collected at 470 and 535 nm, respectively. The FRET signal was normalized to the CFP emission intensity, and changes in ER Ca^{2+} were expressed as the ratio of the emissions at 535 and 470 nm. Cells were perfused with KRB with 50 μM Ca^{2+} at the beginning of the experiment, and the baseline of the FRET ratio was measured, which corresponds to resting Ca^{2+}. Then, 100 μM histamine was added to the perfusion, thus stimulating Ca^{2+} release from the ER through IP3Rs (R_{min}). Finally, the agonist as washed out using KRB with 50 μM Ca^{2+}, and the rate of Ca^{2+} re-uptake in the ER was measured. Cells were pre-treated with GPN, Vac1 or DMSO (vehicle), as previously described for cytosolic Ca^{2+} measurement with aequorin and indicated in the text and figures.

Cell treatment in the starvation experiment

For starvation experiments, cells were cultured in the following media for 6 h: (normal) DMEM high glucose supplemented with 10% FBS; (starvation) HBSS with Ca^{2+} and Mg^{2+} supplemented with 10 mM HEPES. During starvation, cells were treated with CsA (10 μM) or DMSO (vehicle) to inhibit the phosphatase calcineurin.

Immunofluorescence

Cells, transfected or treated as described, were washed with PBS and fixed with 4% formaldehyde for 10 min at room temperature. After washing three times with PBS, the cells were permeabilized with 0.1% Triton X-100 in PBS (PBST) at room temperature for 10 min and blocked with PBST containing 5% BSA at room temperature for 1 h. The cells were incubated with an anti-FLAG primary antibody (Sigma-Aldrich, dilution 1:100) in PBST containing 5% BSA overnight at 4°C, washed three times with PBS, and then incubated with appropriate isotype-matched, AlexaFluor 488-conjugated secondary antibodies (Life Technologies, dilution 1:1000) at room temperature for 1 h. Digital images were acquired using a confocal microscope (Zeiss LSM510) with a 63 × 1.4 NA Plan-Apochromat oil-immersion objective and analyzed using Fiji open-source software.

Statistical analysis

Statistical analyses were performed using an unpaired two-tailed t-test (two groups) or one-way ANOVA with Tukey correction (for groups of three or more). For grouped analyses, two-way ANOVA was performed; $p<0.05$ was considered significant. All data are reported as the means ± SEs.

Chapter 2. Down-regulation of the AGC1 inhibits proliferation and N-acetylaspartate synthesis in Neuro2A cells

Abstract

The mitochondrial aspartate-glutamate carrier isoform 1 (AGC1) catalyzes a Ca^{2+}-stimulated export of aspartate to the cytosol in exchange for glutamate and is a key component of the malate-aspartate shuttle which transfers NADH reducing equivalents from the cytosol to mitochondria. By sustaining the complete glucose oxidation, AGC1 is thought to be critical in providing energy for cells, in particular in the central nervous system (CNS) and muscle where this protein is mainly expressed. Defects in the AGC1 gene cause AGC1 deficiency, an infantile encephalopathy with delayed myelination and reduced brain N-acetylaspartate (NAA) levels, the precursor of myelin synthesis in the CNS. Here, we show that undifferentiated Neuro2A cells with down-regulated AGC1 display a significant proliferation deficit associated with reduced mitochondrial respiration, and are unable to synthesize NAA properly. In the presence of high glutamine oxidation, cells with reduced AGC1 restore cell proliferation, although oxidative stress increases and NAA synthesis deficit persists. Our data suggest that the cellular energetic deficiency due to AGC1 impairment is associated with inappropriate aspartate levels to support neuronal proliferation when glutamine is not used as metabolic substrate, and we propose that delayed myelination in AGC1 deficiency patients could be attributable, at least in part, to neuronal loss combined with lack of NAA synthesis occurring during the nervous system development.

Introduction

1. Mitochondria: structure and functions

Mitochondria are organelles with complex structures and functions. They are derived from an α-proteobacterium-like ancestor, due to an ancient "invasion" that occurred more than a billion years ago (Dyall, Brown et al. 2004). The acquisition of mitochondria (and plastids) was a key event in the evolution of the eukaryotic cell, supplying it with bioenergetic and biosynthetic factors. At subcellular resolution, mitochondria are composed of an outer membrane (OMM), mostly permeable to ions and metabolites up to 10 kDa, and a highly selective inner mitochondrial membrane (IMM), characterized by invaginations called cristae. The space between these two structures is called the intermembrane space (IMS). Together, the OMM and IMM enclose the mitochondrial matrix. The IMM is further subdivided into two compartments: the peripheral inner boundary membrane and the cristae (Frey and Mannella 2000). Cristae are not simply random folds, but rather internal compartments formed by deep invaginations originating from very tiny "point-like structures" in the inner membrane. These narrow tubular structures, called cristae junctions, can limit the diffusion of molecules from the intra-cristae space towards the IMS, thus creating a microenvironment where mitochondrial electron transport chain (ETC) complexes (as well as other proteins) are hosted and protected from random diffusion. The inner boundary membrane is enriched with structural proteins and components of the import machinery of mitochondria (Vogel, Bornhovd et al. 2006). Mitochondrial morphology in living cells is heterogeneous and can range from small spheres to interconnected tubules. This heterogeneity results from the balance between fusion and fission processes and represents a phenomenon termed mitochondrial dynamics *(Benard and Rossignol 2008)*. A growing body of evidence indicates that mitochondrial morphology is critical for the physiology of the cell and changes in mitochondrial shape have been related to many different processes such as development, neurodegeneration, calcium (Ca^{2+}) signalling, reactive oxygen species (ROS) production, cell division, and apoptotic cell death (Cereghetti and Scorrano 2006). The mitochondrial shape is controlled by the identified "mitochondria-shaping proteins", which regulate the fusion-fission equilibrium of the organelle. In mammals, critical components of the fusion machinery include the homologues MFN1 and MFN2 (Cereghetti and Scorrano 2006). The only dynamin-like GTPase currently identified in the IMM is OPA1, a fusion protein that is

mutated in dominant optic atrophy (DOA), the most common cause of inherited optic neuropathy. Post-transcriptional mechanisms, including proteolytic processing, tightly regulate OPA1 activity. In mammalian cells, the mitochondrial division is controlled by DRP1 and FIS1 (James, Parone et al. 2003) (Smirnova, Griparic et al. 2001). The large GTPase DRP1 is a cytosolic dynamin-related protein, whose inhibition or downregulation results in a highly interconnected mitochondrial network. The same phenotype is caused by the downregulation of FIS1, a protein of the OMM, proposed to act as a mitochondrial receptor for DRP1 (Yoon, Krueger et al. 2003). For example, mitochondrial dynamics seem to influence the production of ROS and cellular longevity. DRP1-dependent fragmentation of the mitochondrial reticulum is a crucial component for the accumulation of ROS in pathological conditions (Yu, Robotham et al. 2006). How mitochondrial fission is required for ROS production and lifespan remains unclear, although a link between the two processes seems plausible.

Hence, factors other than mitochondrial metabolism *per se* could have a role in the pathogenesis of ROS-related diseases. Interestingly, many ROS (as well as Reactive Nitrogen Species, RNS) sources and targets are localized in the mitochondria and ER with are relevant consequences for different pathways (Csordas and Hajnoczky 2009).

2. Mitochondria as site for major energy production

Within cells, energy is provided by oxidation of "metabolic fuels" such as carbohydrates, lipids and proteins. It is then used to sustain energy-dependent processes, such as the synthesis of macromolecules, muscle contraction, active ion transport or thermogenesis. The oxidation process results in free energy production that can be stored in phosphoanhydrine "high-energy bonds" within molecules such as nucleoside diphosphate and nucleoside triphosphate (*i.e.*, adenosine 5' diphosphate and adenosine 5' trisphosphate, ADP and ATP, respectively), phosphoenolpyruvate, carbamoyl phosphate, 2,3-bisphosphoglycerate, and other phosphates like phosphoarginine or phosphocreatine.

Among them, ATP is the effective central link-the exchange coin-between energy producing and the energy demanding processes that effectively involve formation, hydrolysis or transfer of the terminal phosphate group. In general, the primary energy source for cellular metabolism is glucose, which is catabolized in the three subsequent processes: glycolysis, tricarboxylic acid cycle (TCA or Krebs cycle), and finally oxidative phosphorylation to produce ATP. In the first process, which takes place in the cytosol, glucose is converted into

pyruvate: this generates a low amount of ATP produced. Only 5% of ATP generate by glucose is provided by glycolysis. Subsequently, pyruvate is converted to acetyl coenzyme A (acetyl-CoA), which enters the TCA cycle, enabling the production of NADH. Finally, NADH is used by the respiratory chain complexes to generate a proton gradient across the inner mitochondrial membrane, necessary for the production of large amounts of ATP by mitochondrial ATP synthase. In addition, it should be mentioned that acetyl-CoA could be generated also by lipid and protein catabolism.

3. Citric acid cycle

The citric acid cycle (TCA) was elucidated by Sir Hans Krebs in 1940 (Krebs and Eggleston 1940). The triose deriving from glycolysis is wholly oxidized into three molecules of CO_2 during a sequence of reactions that allow the reduction of cofactors NAD and flavin adenine nucleotide (FAD), providing energy for the respiratory chain in the form of electrons. In 1949 Kennedy and Lehningher demonstrated that the entire cycle occurs inside mitochondria (Krebs and Eggleston 1940). The first reaction of the citric acid cycle (See Fig. 1) is the condensation of one Acetyl-CoA and a molecule of citrate to generate oxaloacetate and is catalysed by citrate synthase. Citrate is then transformed into isocitrate by aconitase through the formation of cis-aconitate. This step is reversible and could lead to the formation of both citrate and isocitrate. Only the fast consumption of isocitrate by its dehydrogenase can force the reaction to the proper direction. Isocitrate dehydrogenase catalyses the first irreversible oxidation leading to the decarboxylation of isocitrate, generating CO_2 and α-ketoglutarate. The second carbon leaves the cycle in the following step when the newly generated α-ketoglutarate is immediately decarboxylated by the α-ketoglutarate dehydrogenase complex in a reaction similar to the pyruvate decarboxylation. In fact, both these complexes share high similarities in enzyme amino acid composition and in the organization of the different subunits. The energy released from both oxidations is used to generate NADH from NAD that directly feeds into the respiratory chain. The following step is catalysed by succinyl-CoA synthetase and utilizes the energy derived from the CoA removal to phosphorylate GDP (or ADP) to GTP (or ATP).

The first of these steps is the oxidation of succinate to fumarate by succinate dehydrogenase. This enzyme, tightly bound to the inner mitochondrial membrane (IMM), catalyses FAD reduction to $FADH_2$ that provides electrons for the respiratory chain. Fumarate is then hydrated by fumarate hydratase to L-malate. Both succinate dehydrogenase and fumarate

hydratase are oncosuppressor genes and their inactivation leads to the accumulation of succinate and fumarate that spread in the cytosol and promote hypoxia-inducible factor 1α (HIF1α) accumulation by inactivating prolyl hydroxylase enzymes (promoter of HIF1α degradation); HIF1α, promotes a pseudo-hypoxic condition that favours tumour development (Amemori, Iwakiri et al. 2006).

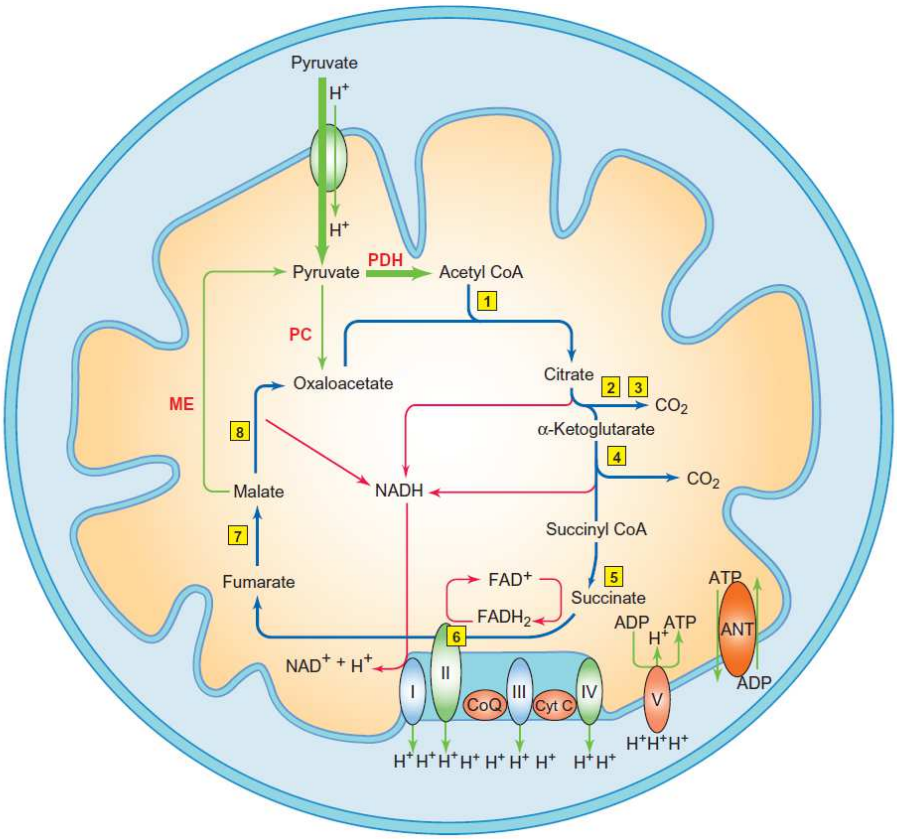

Fig. 1. Tricarboxylic acid cycle and oxidative phosphorylation. Pyruvate is carried into the mitochondrial matrix for oxidative decarboxylation to acetyl-CoA via the pyruvate dehydrogenase complex (PDH) or for carboxylation to oxaloacetate via pyruvate carboxylase (PC). Acetyl-CoA is condensed with oxaloacetate via citrate synthase (1) to form citrate, which is converted to α-ketoglutarate via aconitase (2) and isocitrate dehydrogenase (3). α-Ketoglutarate is subsequently decarboxylated via the α-ketoglutarate dehydrogenase complex (4) to succinyl- CoA. Succinate is formed from succinyl-CoA via succinyl CoA synthase (5). Complex II of the respiratory chain/succinate dehydrogenase (6) oxidizes succinate to fumarate, which is converted into malate via fumarase (7). Malate is oxidized to oxaloacetate via malate dehydrogenase (8), or it can be converted to pyruvate via malic enzyme (ME). NADH is re-oxidized in complex I, and FADH in complex II of the electron transport chain. The electrons are carried by the complexes, coenzyme Q (CoQ), and cytochrome C (Cyt c) to O2, which is reduced to H2O in complex IV. The electron transport generates a proton gradient over the inner membrane driving the ATP synthesis in complex V. Proton leakage across the membrane back into the matrix reduces the net yield of ATP (Brady, Siegel et al. 2012).

The last event that completes the citric acid cycle is the oxidation of L-malate to oxaloacetate. This reaction is performed by L-malate dehydrogenase, which induces the reduction of

another molecule of NAD to NADH. The resulting molecule of oxaloacetate is suitable for starting another cycle through condensation with an acetyl group.

During all these processes, only one molecule of ATP (or GTP) is produced, but three molecules of NADH and one of $FADH_2$ (plus one molecule of NADH from pyruvate dehydrogenase), which provide electrons for respiratory chain, are also generated and subsequently result in the production of large amounts of ATP (Bonora, Patergnani et al. 2012).

4. Respiratory chain and oxidative phosphorylation

Respiratory chain comprises a series of hydrophobic complexes conducting electron transfer across the membrane and involved in oxidative phosphorylation (OXPHOS), a process that occurs in aerobic conditions. In eukaryotic cells, electron transport occurs in mitochondria and chloroplasts, whereas in bacteria it is carried out across the plasma membrane. As mentioned, the electron transfer is considered a part OXPHOS, the process through which ADP is phosphorylated into ATP by dint of energy derived from the oxidation of nutrients. The majority of the complexes are integral membrane proteins containing prosthetic groups capable of accepting or donating one or two electrons. Respiratory chain complexes I, III and IV, located in the IMM, and are able to produce an electrochemical potential across the mitochondrial membrane by creating a concentration gradient of H^+ ions between the two sides of the membrane. This potential is exploited to activate the transport channels present on the membrane and to promote the synthesis of ATP by ATP synthase. The electron carriers of the respiratory chain are organized in separated supramolecular intramembrane complexes, and each of them represents a fraction of the respiratory chain (Fig. 1).

The complexes of the respiratory chain are:

- Complex I: NADH dehydrogenase
- Complex II: Succinate dehydrogenase
- Complex III: cytochrome c reductase
- Complex IV: Cytochrome c oxidase

All complexes are formed by multiple subunits and contain proteins encoded by nuclear or mitochondrial DNA, except the Complex II which is entirely encoded by nuclear DNA. The first complex, the NADH:ubiquinone oxidoreductase, transfers electrons from NADH (produced in the citric acid cycle) and passes them on to the first shuttle, Coenzyme Q (ubiquinone), a liposoluble cofactor located within the phospholipid bilayer of the IMM.

Succinate dehydrogenase is another entrance site for electrons into the respiratory chain. In this case, electrons derived from the oxidation of succinate are passed through FAD to Coenzyme Q. Coenzyme Q is located between Complex I and Complex III and can accept only one electron, becoming a semiquinone radical, or two electrons acquiring the entirely reduced ubiquinol form. Since ubiquinone is small in size and hydrophobic, it is freely diffusible in the lipid bilayer of the IMM and can act as a bridge between less mobile electron carriers in the same membrane. Coenzyme Q transfers the electrons previously transported in complex I and complex II from NADH and $FADH_2$ to complex III; here, electrons are moved through several heme groups from the liposoluble shuttle ubiquinone to the water-soluble shuttle which is cytochrome c and hence they will be conducted to complex IV. Cytochrome c eventually transfers electrons directly to oxygen, leading to H_2O production.

Cytochrome c is a peripheral membrane protein of 12.5 kDa soluble in water and weakly associated with the external surface of IMM due to interaction with cardiolipin (Quinn and Dawson 1969). This protein transfers electrons between complexes III and IV. Like all cytochromes, it has a prosthetic group (heme group) and it is constituted by a tetrapyrrolic ring with an iron atom covalently bonded to the centre. Cytochrome c allows the passage of electrons to oxygen through the oscillation of the iron from the ferric form Fe^{3+} to the ferrous form Fe^{2+}. Oxygen is then reduced to water. This constitutes the bulk of oxygen consumption in all aerobic life. Electron transport through complexes I, III and IV induces the pumping of protons from the matrix to the IMS. Specifically, for every two electrons coming from one molecule of NADH, four H^+ are moved by complex I, four by complex III, and two by complex IV. The respiratory complex II does not generate any proton movement (Lenaz and Genova 2010). The chemical mechanism which couples the proton flow with the phosphorylation is called Chemiosmotic Model and it was proposed by Peter Mitchell (Mitchell 1979). In agreement with this model the electrochemical energy contained in the difference of proton concentration and in the charge separation across the IMM leads to the synthesis of ATP when the proton flow reverses its direction and protons back into the matrix through a proton channel associated to the ATP synthase. The mechanism of action of ATP synthase (called also as complex V) was elucidated by the Nobel Prizes Paul Boyer and John Walker. ATP synthase could be divided into two main components: Fo that allows the channelling of protons, and F1 that catalyses ATP phosphorylation. The Fo is embedded in the IMM, while the F1 resides in the mitochondrial matrix and is bound to the Fo through a γ subunit (which drives conformational changes) and a b2δ dimer (that holds Fo and F1 together). The protons flow from the intermembrane space to the matrix through the Fo

inducing its rotation; the movement is transmitted from the γ subunit to the F1 causing conformational rearrangements. The Fo region consists of three main subunits a (ATP6 gene), b (ATP5F1 gene) and c (ATP5G1, ATP5G2 and ATP5G3 genes), and in humans six additional subunits d, e, f, g, F6 and 8. The F1 has a trimeric structure consisting of αβ dimers. The following changes are linked to the binding of substrates, phosphorylation and release of ATP. The three available dimers are never in the same conformational state and the conformational changes in one dimer drive rearrangements in the other (Boyer 2000). This region consists of different protein subunits, α (ATP5A1 and ATPAF2 genes), β (ATP5B, ATPAF1 and C16orf7 genes), γ (ATP5C1gene), δ (ATP5D gene) and ε (ATP5E gene).

It has been calculated that for the synthesis of one ATP molecule, 4 protons are required (Ferguson 2010). Once synthesized, ATP can locate inside mitochondrial matrix or be transported into the IMS by the nucleotide exchanger adenine nucleotide translocase (ANT) that passively exchanges ATP with ADP. Once in the IMS, ATP can freely pass the OMM through the voltage-dependent anion channel (VDAC).

The concentration gradient of H^+ ions that is created between the two sides of the membrane is equivalent to a proton motive force and this is defined mitochondrial trans-membrane potential which corresponds to -150/-180 mV in the cytosol (Duchen 2004). This is essential for many processes, including the production of ATP by ATP synthase and the accumulation of Ca^{2+}. Dysfunction of the respiratory chain are associated with mitochondrial disorders and affect tissues that require a large amount of energy as the brain, heart and skeletal muscle (DiMauro and Schon 2003). Mitochondrial DNA encodes thirteen polypeptides, each of which is an integral subunit of respiratory chain complexes (Anderson, Bankier et al. 1981).

5. The malate-aspartate shuttle

The malate-aspartate shuttle (MAS) is a biochemical system for translocation of electrons produced during glycolysis across the semipermeable IMM of the mitochondrion for oxidative phosphorylation in eukaryotes. These electrons enter the electron transport chain of the mitochondria via reduction equivalents to generate ATP. The MAS comprises a transport-transamination-redox cycle in both cytosolic and mitochondrial domains.

The shuttle system is required because the mitochondrial inner membrane is impermeable to NADH, the primary reducing equivalent of the electron transport chain. To circumvent this, malate carries the reducing equivalents across the membrane.

In this way MAS involves both the cytosolic and mitochondrial forms of aspartate aminotransferase (respectively cMDH and mAAT) and malate dehydrogenases (respectively cMDH and mMDH), the mitochondrial aspartate-glutamate carriers (AGCs), and the dicarboxylic acid carrier (OGC, 2-oxoglutarate/malate carrier) (Fig. 2) (McKenna, Waagepetersen et al. 2006). The electrogenic exchange of glutamate and a proton for aspartate via the ACG is irreversible (LaNoue and Tischler 1974); the transfer favours entry of glutamate into and efflux of aspartate from mitochondria.

The primary enzyme in the MAS is malate dehydrogenase. The two malate dehydrogenases are differentiated by their location and structure and catalyze their reactions in opposite directions in this process.

First, in the cytosol, malate dehydrogenase catalyses the reaction of oxaloacetate and NADH to produce malate and NAD^+. In this process, two electrons generated from NADH, and an accompanying H^+, are attached to oxaloacetate to form malate (Walker 2014).

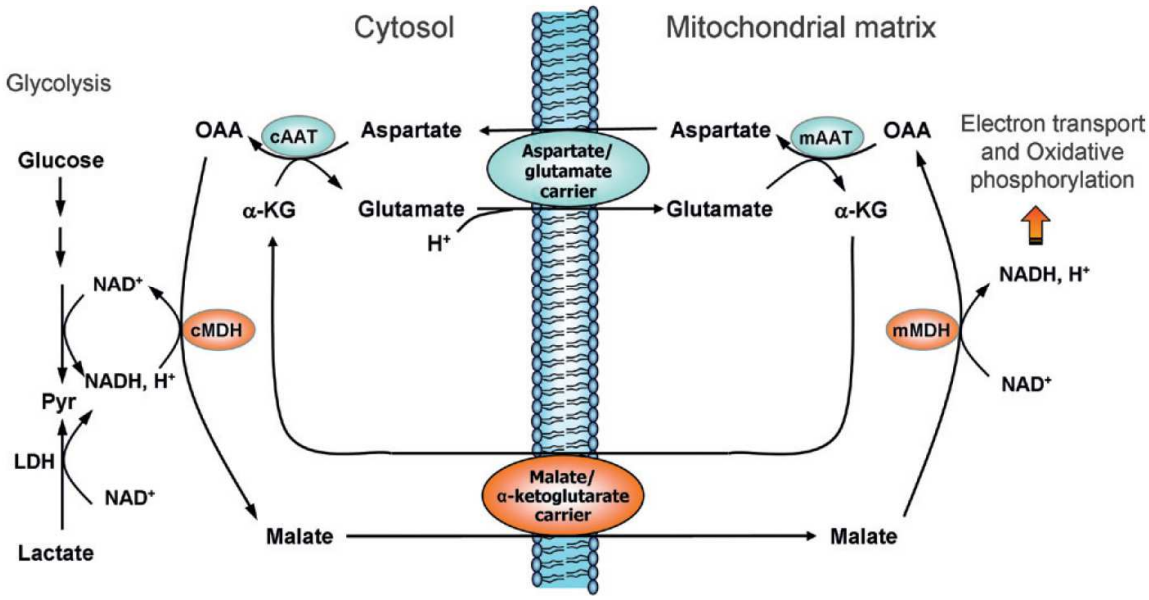

Fig. 2. The malate-aspartate shuttle. NADH is produced in glycolysis and in the conversion of lactate to pyruvate via lactate dehydrogenase (LDH). The reducing equivalents from NADH are transferred via the malate-aspartate shuttle to be oxidized via electron transport to support oxidative phosphorylation. Oxaloacetate (OAA) is converted to malate by cytosolic malate dehydrogenase (cMDH) and NADH is oxidized to NAD^+. Malate is transported into the mitochondrial matrix by a carrier and transformed into OAA, and NAD^+ is reduced to NADH via mitochondrial malate dehydrogenase (mMDH). Within mitochondria, oxaloacetate is converted to aspartate, and α-ketoglutarate (α-KG) is formed from glutamate via mitochondrial aspartate aminotransferase (mAAT). Aspartate leaves the mitochondrial matrix in exchange for a molecule of glutamate + H^+. The irreversible aspartate–glutamate carrier favours glutamate uptake, as the transport is driven in the direction of the mitochondrial membrane potential. In the cytosol, aspartate is converted back to oxaloacetate via cytosolic aspartate aminotransferase (cAAT) (Brady, Siegel et al. 2012).

Once malate is formed, the first antiporter (OGC) imports the malate from the cytosol into the mitochondrial matrix and also exports α-ketoglutarate from the matrix into the cytosol simultaneously. After malate reaches the mitochondrial matrix, it is converted by mitochondrial MDH into oxaloacetate, during which NAD^+ is reduced with two electrons to form NADH. Oxaloacetate is then transformed into aspartate (since oxaloacetate cannot be transported into the cytosol) by mAAT. Since aspartate is an amino acid, an amino radical needs to be added to the oxaloacetate. This is supplied by glutamate, which in the process is transformed into α-ketoglutarate by the same enzyme (Lu, Zhou et al. 2008).

The second antiporter (AGC) imports glutamate from the cytosol into the matrix and exports aspartate from the matrix to the cytosol. Once in the cytosol, aspartate is converted by cMDH to oxaloacetate.

The net effect of the malate-aspartate shuttle is purely redox: NADH in the cytosol is oxidized to NAD^+, and NAD^+ in the matrix is reduced to NADH. The NAD^+ in the cytosol can then be reduced again by another round of glycolysis, and the NADH in the matrix can be used to pass electrons to the electron transport chain so ATP can be synthesized (LaNoue and Schoolwerth 1979).

Since the malate-aspartate shuttle regenerates NADH inside the mitochondrial matrix, it is capable of maximizing the number of ATPs produced in glycolysis (3/NADH), ultimately resulting in a net gain of 38 ATP molecules per molecule of glucose metabolized.

By transferring reducing equivalents from the cytosol into mitochondria, MAS provides an important mechanism to regulate metabolic activity in these two compartments (LaNoue, Meijer et al. 1974, LaNoue and Tischler 1974).

In the healthy heart, the system operates with a net flow of electrons from the cytosol into the mitochondrial matrix that is sufficient to maintain both glycolysis and lactate oxidation, and thus prevent net lactate production (Safer 1975, Rupert, Segar et al. 2000).

6. The malate-aspartate shuttle function in brain

Maintaining a low $NADH/NAD^+$ ratio is essential for the continuation of glycolysis. Without the shuttle system to regenerate cytoplasmic NAD^+, glucose-derived carbon is converted to lactate and released from the cell in order to maintain a high glycolytic rate. Pyruvate only becomes available for mitochondrial metabolism by means of MAS, not LDH activity. Thus, the malate-aspartate shuttle links glycolysis and the TCA cycle in cells (McKenna, Waagepetersen et al. 2006).

This shuttle is also essential for transferring the reducing equivalents from glycolysis to the mitochondrial electron transport chain and subsequent oxidative phosphorylation. The activity of MAS increases during development in parallel with synaptogenesis, which is consistent with the high activity and its importance in neurons and synaptic terminals. The high activity of this shuttle in neurons is in line with the involvement of the shuttle in the synthesis of neurotransmitter glutamate from glutamine. The activity of the malate-aspartate shuttle is impaired in pathological conditions including hypoxic/ischemic brain damage (McKenna, Waagepetersen et al. 2006) and this damage limits the ability of neurons to oxidize lactate for energy (McKenna, Tildon et al. 1998). The presence of isoform 1 of the aspartate-glutamate carrier (AGC1) and activity of the malate-aspartate shuttle are essential for the formation of N–acetylaspartate (NAA) in neurons (Jalil, Begum et al. 2005, Satrustegui, Contreras et al. 2007). Mutations in AGC1 lead to global hypomyelination in animal models and human brain (as we shall see later) since NAA synthesized in neurons is released, taken up by oligodendroglia, and used to provide acetyl groups for synthesis of myelin lipids (Jalil, Begum et al. 2005, Satrustegui, Contreras et al. 2007, Wibom, Lasorsa et al. 2009). Another mechanism to shuttle redox equivalents into mitochondria is the glycerol phosphate shuttle, but it is thought to have a minor role in the brain compared to other tissues (Falkowska, Gutowska et al. 2015). Although the glycerol phosphate shunt can serve to maintain the NAD^+ required for glycolysis, the question of the cellular localization of this shuttle in the brain is unresolved. Glycerol phosphate dehydrogenase (GPDH) is indirectly associated with glycolysis and reduces dihydroxyacetone phosphate to glycerol-3-phosphate, oxidizing NADH in the process.

7. Aspartate-glutamate carriers description: genetics, structure and functions

Aspartate-glutamate carriers (AGCs) are nuclear-coded proteins of the mitochondrial carrier family (MCF) (Palmieri 2013) and they supply the aspartate synthesized within the mitochondrial matrix to the cytosol in exchange for the cytosolic glutamate plus a proton (Palmieri, Pardo et al. 2001). These proteins have to be translocated from the cytosol to the inner mitochondrial membrane. Like other mitochondrial carriers (MCs) are not synthesized with targeting pre-sequence but are characterized by internal targeting signals that allow the penetration of the OMM and subsequent folding and localization in IMM through the TOM/TIM complex(Ferramosca and Zara 2013).

Two genes coding for AGCs have been found in Homo sapiens, namely SLC25A12 (AGC1 also named aralar) and SLC25A13 (AGC2 also named citrin) (Palmieri, Pardo et al. 2001).
AGC1 and AGC2 are differently expressed among tissues, (Fig. 3) (Amoedo, Punzi et al. 2016), and the observed differences in the expression levels may be related to the development stage, the status of cell proliferation and tissue-specific energy and REDOX requirements (Iijima, Jalil et al. 2001). Notably, AGC1 appears to be highly expressed in the adult central nervous system (CNS) and in the skeletal muscle (SM) (Iijima, Jalil et al. 2001). AGC1 is also highly expressed in the heart (Fig. 2). Such strong expression of AGC1 in the brain, SM and heart could be ascribed to the specific needs of those tissues in performing an efficient MAS for maintaining the REDOX equilibrium between cytosolic glycolysis, mitochondrial ATP synthesis and, specifically in neurons, myelin biosynthesis. Moreover, both AGCs were found up-regulated in several cancers and their induction was directly associated with glycolytic metabolism, raising a question regarding the role of AGCs in carcinogenesis and related metabolic remodelling.
Due to their implication in energy metabolism and REDOX homeostasis, AGCs were among the most studied MCs.
Both AGCs are proteins of about 675 amino-acids (aa) (the longer transcript of AGC1 encodes a protein of 678 aa, whereas the longest transcript of AGC2 encodes a protein of 676 aa) (Iijima, Jalil et al. 2001, Palmieri, Pardo et al. 2001, Pierri, Palmieri et al. 2014). The N-terminal domain of AGCs contains 8 EF-hands for calcium binding (Thangaratnarajah, Ruprecht et al. 2014). Notably, cytosolic calcium has a direct role in the regulation of SLC25A12 gene expression via CREB (cAMP response element-binding protein) in neuronal cells, underlining the crucial role of AGC1 in the central nervous system, both in physiology (up-regulation in neuronal differentiation) and pathology (down-regulation in neuroinflammation) (Menga, Iacobazzi et al. 2015).

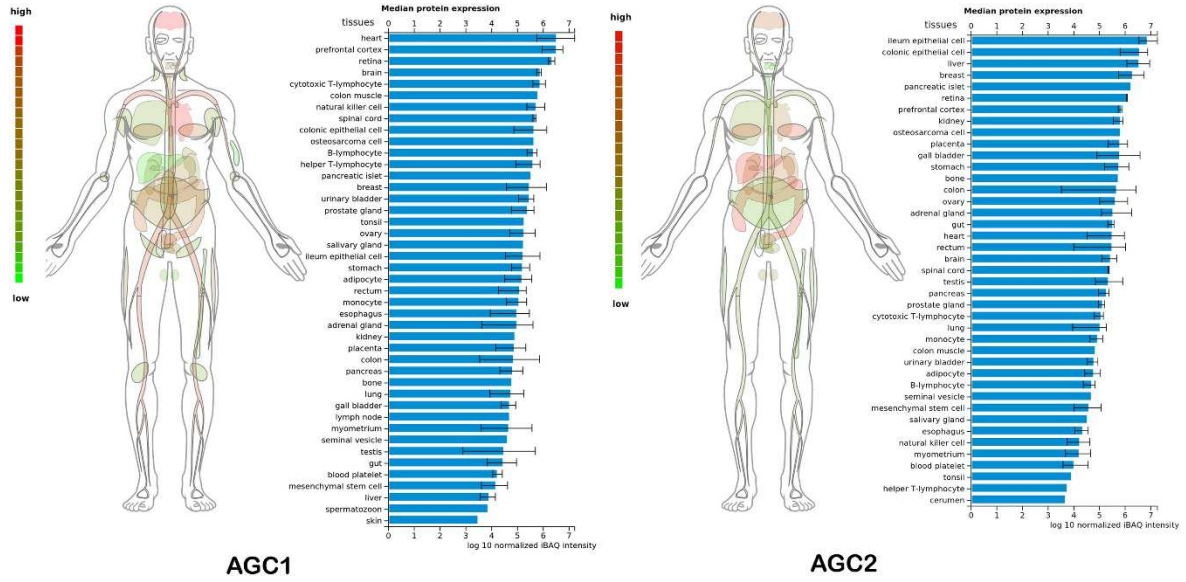

Fig. 2. Tissue expression profile of AGC1 and AGC2 mitochondrial carrier proteins. (Amoedo, Punzi et al. 2016).

The C-terminal domain contains the transmembrane domain (of approximately 300 aa) that catalyzes the electrogenic exchange of aspartate for glutamate plus a proton (H^+) across the inner mitochondrial membrane (Wibom, Lasorsa et al. 2009, Fiermonte, Parisi et al. 2011) and a further cytosolic domain (of approximately 40 aa). Given the co-transport of glutamate with a proton in exchange for mitochondrial aspartate, the export of aspartate is obliged in energized mitochondria (Palmieri, Pardo et al. 2001).

It was shown that AGC1 is required to stimulate mitochondrial respiration in the presence of glutamate and aspartate (and ADP). In such conditions of activated AGC1, a decrease in ROS production could be expected given the opposite relationship between the magnitude of the $\Delta\Psi$ and ROS production (Quinlan, Treberg et al. 2012). Also, given that glutamate entry through AGC1 requires one proton in co-transport, the loss of membrane potential is compensated by the extrusion of 4 protons by the respiratory chain when one molecule of glutamate is processed through the Krebs cycle (which generates one molecule of NADH). Moreover, AGC1 and AGC2 were found to harbour different types of post-translational modifications as ubiquitination (K55, K406, K482 and K485), methylation (K370) and acetylation (K112, K377 and K578) (Pierri, Palmieri et al. 2014). Yet, the actual regulation of AGCs by those modifications remains unknown. Regarding acetylation, the mitochondrial sirtuin (sirt 3) may not be involved since the study of the lysine acetylome performed in mouse liver mitochondria did not identify AGC1 nor AGC2 (Rardin, Newman et al. 2013), but a similar study could be conducted in the brain given the major role of AGC1 in this tissue.

8. AGCs in human physiology

The well-described role of AGCs concern their participation to MAS underlines their centrality as pivotal modulators in REDOX homeostasis in numerous tissues. In neurons, the lactate (produced by the astrocytes) can be used as energy substrate for oxidative phosphorylation, and the activity of AGC1 is required to allow the lactate dehydrogenase to generate pyruvate since this reaction produces a molecule of NADH that needs to be reoxidized. In pancreatic β-cells, the shuttling of cytosolic NADH into the mitochondrion by the MAS was shown to participate to insulin secretion, since this process depends on the synthesis of ATP by the mitochondrion (Ramos, del Arco et al. 2003, Cahoy, Emery et al. 2008, Solar, Cardalda et al. 2009). Lastly, the central role of AGC in the MAS was shown to be critical for zygote early development during embryogenesis (Lane and Gardner 2005).

Another well-documented function of AGCs is their participation in the calcium-mediated regulation of mitochondrial respiration (Gellerich, Gizatullina et al. 2012). Gellerich F. discovered that the glutamate/malate-dependent oxidative phosphorylation of brain mitochondria is regulated by cytosolic Ca^{2+} via regulatory Ca^{2+} binding sites of AGC1. The extent of this activation by Ca^{2+} was strong as it reached 500 % of the control respiration value.

The origin of the glutamate imported by AGC1 is also an essential question in the field of brain bioenergetics. It was proposed that astrocytes produce glutamate from pyruvate using the pyruvate carboxylase anaplerotic reaction, and convert glutamate to glutamine using the glutamine synthetase (Shank, Bennett et al. 1985, Sonnewald and Rae 2010). The glutamine is then transported to neurons where it is converted back into glutamate and can serve for oxidative phosphorylation (Rothman, De Feyter et al. 2011). Therefore, AGC1, as part of the MAS, plays a central role in neuron bioenergetics, and this is further supported by the analysis of the phenotype of AGC1 deficient neurons, which showed decreased respiration levels and the incapacity to regulate their respiration rates in response to Ca^{2+} during stimulation (Llorente-Folch, Sahun et al. 2013).

Another indirect function of AGCs concerns the fate of the aspartate exported from the mitochondrion to produce NADPH and to regenerate the antioxidant capacity of glutathione (Amoedo, Punzi et al. 2016). In this case, the AGC is decoupled from the MAS, as the malate generated by the aspartate does not re-enter the mitochondrion by the malate carrier, but is rather transformed in pyruvate and NADPH by the malic enzyme in the cytosol. In this

context, it remains to be understood how the previously described regulation of AGC by calcium could participate in the modulation of the antioxidant defences.

Lastly, AGC1 could play a role in dopamine handling and glutamate-induced excitotoxicity. Glutamate is the major excitatory neuromediator in the central nervous system, and prolonged activation of synaptic receptors by glutamate is neurotoxic and can result in neurodegeneration. The deleterious mechanisms involve a continued increase in calcium concentration in the post-synaptic neuron which triggers ROS generation and subsequent mitochondrial insult, leading to the cellular energy crisis. In support to the central role of AGC1 in neuron physiology, the AGC1 deficient mice models (Sakurai, Ramoz et al. 2010) showed a phenotype characterized by growth delay, generalized tremor and motor coordination defects with impaired myelinization in the central nervous system. In the study of Jalil et al. [50], the mitochondrial respiration was impaired when glutamate and aspartate were used as energy substrates, while respiration remained unchanged when using succinate.

9. AGCs and alterations in human diseases

NADH cannot penetrate mitochondrial membranes, and regeneration of NAD^+ in the cytoplasm depends on the activities of the LDH reaction and a shuttle system that transfers reducing equivalents to mitochondria. The malate-aspartate shuttle involves both the cytosolic and mitochondrial forms of aspartate aminotransferase and malate dehydrogenase, the mitochondrial aspartate-glutamate carrier, and the dicarboxylic acid carrier in the brain (McKenna, Waagepetersen et al. 2006). The electrons exchange of glutamate and a proton for aspartate via the aspartate–glutamate carrier is irreversible (LaNoue and Tischler 1974); the transfer favours entry of glutamate into and efflux of aspartate from mitochondria. The activities of the mitochondrial aspartate-glutamate carrier, which is the overall rate-limiting step of the shuttle, is stimulated by Ca^{2+} binding to a domain on the outer side of the inner mitochondrial membrane; the concentration of Ca^{2+} inducing half-maximal activation is approximately 320 nM (Satrustegui, Contreras et al. 2007). Given the central role of AGCs in cell metabolism, it is not surprising that AGC gene defects are associated with human diseases.

AGC1 mitochondrial carrier is encoded by the nuclear gene SLC25A12 (see above) and known mutations of this gene (1769A > C) are responsible glutamine-arginine substitution at position 590 (Q590R) of the AGC1 deficiency. It alters a highly conserved residue in the aspartate/glutamate MC subfamily, protruding into the cavity of the carrier just above the

common substrate-binding site, and causes a complete loss of the protein's ability to transport aspartate and glutamate in reconstituted liposomes. Main features of the disease are severe global hypomyelination and marked reduction of N-acetyl aspartate in the brain (NAA).
The patient manifested a wide spectrum of clinical symptoms related to the AGC1 deficit, like severe hypotonia, psychomotor developmental arrest and seizures beginning at a few months of age, followed later by spasticity and hypomyelination (Palmieri 2013).
Interestingly, Slc25a12 knockout mice showed impaired myelination, a marked decrease of the myelin lipid precursor NAA and lower aspartate concentration in the brain (Wibom, Lasorsa et al. 2009). Thus, in healthy individuals, the aspartate exported from neuronal mitochondria is mainly utilized for the production of N-acetyl aspartate, the precursor of myelin lipids. Those results obtained on AGC1 knockout mice thus provide genetic evidence in support of an essential role for AGC1 in myelin formation. The described mutations concerned two crucial regions for mitochondrial carrier function.
Similarly, mutations in the SLC25A13 gene encoding AGC2 cause the adult-onset type 2 citrullinemia (CTLN2) and neonatal intrahepatic cholestasis (NiCCD). About symptoms of NiCCD and CTLN2, it is worth noting that the NiCCD led to intrahepatic cholestasis, fatty liver, hepatomegaly, growth retardation, citrullinemia, ketotic hypoglycemia, hypoproteinemia, aminoacidemias (elevated methionine, threonine, tyrosine, phenylalanine, lysine and arginine), and an increased threonine-to-serine ratio and galactose concentration. Some patients present with hepatitis, jaundice, failure to thrive, decreased coagulation factors, hemolytic anaemia and bleeding diathesis. CTLN2 usually manifests in adults between the ages of 20 and 50 years and it is characterized by hypoproteinemia, hyperammonemia and citrullinemia. In patients affected by CTLN2, the lack of cytosolic aspartate and inhibition of the MAS (as a consequence of the inhibition of cytosolic NADH oxidation) causes hyperlipidemia and fatty liver, dislike for carbohydrates, preference for high-protein diets and inhibition of alcohol metabolism. AGC2 impairment is also responsible for both the inhibition of the argininosuccinate synthetase (ASS) reaction (caused by the lack of cytosolic aspartate provided by mitochondria). Instead, white matter showed abnormal and globally lowered myelination, indicating a role of AGC1 in cerebral myelination (Palmieri 2013).

Starting from these observations, we studied the role of AGC1 in proliferation and control of metabolism in an undifferentiated model of neuronal cells (mouse neuroblastoma Neuro2, N2A). Consistently with the importance of AGC in MAS, we showed that AGC1 down-regulation is detrimental to the survival of undifferentiated N2A cells albeit addition of

glutamine rescued the proliferation of N2A cells with reduced AGC1. Furthermore, we demonstrated that NAA levels in undifferentiated N2A neuroblastoma cells are strongly reduced if AGC1 is down-regulated preventing the formation of appropriate acetyl-CoA levels for NAA synthesis.

Results

1. AGC1 is the only isoform of the mitochondrial aspartate/glutamate carrier expressed in undifferentiated N2A cells

To investigate the role of AGC1 in neurons we first evaluate the level expression of the protein in mouse brain-derived N2A cells that is a reliable model of neuron proliferation, metabolism and differentiation (Ma'ayan, Jenkins et al. 2009, Wu, Lin et al. 2009, Wesley, Hatcher et al. 2015). In agreement with Ramos and coworkers (Ramos, del Arco et al. 2003), immunoblot analysis (Fig. 1A) performed revealed the increasing expression of AGC1 after differentiation with dibutiryl-AMPc. AGC2 isoform was instead detected at constant levels only after cell differentiation, thus suggesting that in undifferentiated proliferating N2A cells MAS works uniquely in the presence of AGC1. Therefore, we stably down-regulated AGC1 expression in N2A cells by using two lentiviral constructs (LVshAGC1- N2A.1 and LVshAGC1-N2A.2) that individually allowed a ~75% reduction of AGC1 protein even after cell differentiation and without affecting AGC2 expression, as compared to N2A cells stably transduced with a lentiviral control construct (LVshMM-N2A) (Fig. 1B). It should be noted that in Fig. 1B, as well as in all other reported results, only data referred to LVshAGC1-N2A.1 silenced cells are shown, unless otherwise indicated, and similar results were also obtained with LVshAGC1-N2A.2 silenced cells. As measured with mitochondrial extracts reconstituted in liposomes (Fig. 1C), AGC1 silencing in undifferentiated LVshAGC1-N2A cells reduced both the aspartate/glutamate and the glutamate/glutamate exchange activities by ~80% and ~50%, respectively, when compared to those measured with mitochondria isolated from control cells. These data suggested the presence of alternative mitochondrial proteins able to perform glutamate transport in N2A cells, such as the mitochondrial glutamate carrier (GC) isoforms (Fiermonte, Palmieri et al. 2002).

It is noteworthy that AGC1 activity in LVshAGC1-N2A cells is basically similar to that revealed in patients with AGC1 function dramatically reduced, but not abolished entirely (Falk, Li et al. 2014). The effect of reduced AGC1 activity on the transfer of the NADH reducing equivalents from the cytosol to mitochondria was then tested by measuring lactic acid secreted by N2A cells grown in complete DMEM (Fig. 1D). As expected, after 24 h incubation the lactic acid released in the conditioned DMEM harvested from undifferentiated LVshAGC1-N2A cells was from 70% to 120% higher than that of control cells, while in

media from differentiated LVshAGC1-N2A cells, lactic acid was ~40% more than in medium from differentiated LVshMMN2A cells (Fig. 1D).

Therefore, these data suggested that LVshAGC1-N2A cells consume glucose preferentially in the cytosol, as revealed by the increasing the production of lactate from glycolysis-derived pyruvate (necessary to regenerates NAD^+) since the down-regulation of AGC1 inhibits MAS activity. This effect, due to the AGC1 deficit, may partially compensate by AGC2 expression only after differentiation.

2. Down-regulation of AGC1 inhibits proliferation and mitochondrial respiration of N2A cells

The altered glucose metabolism in AGC1-silenced cells suggested that LVshAGC1-N2A growth was sustained by alternative utilization of other metabolites. Therefore, N2A cells were cultured for several days in minimal growth media (MEM) containing glucose in combination with other substrates for neurons, such as lactate or pyruvate in the presence or absence of glutamine (Fig. 2A). LVshAGC1- N2A and control LVshMM-N2A cell number was not significantly different when grown in the presence of glucose with either pyruvate or lactate supplemented with glutamine, with the exception of the first measurements at 24 h and 48 h. Interestingly, when MEM was deprived of glutamine, LVshAGC1-N2A cells failed to proliferate at the same rate of control cells. In particular, in the presence of glucose and pyruvate LVshAGC1-N2A cell number was markedly lower than that of LVshMM-N2A cells, while in the presence of glucose and lactate LVshAGC1-N2A cells started to die after 24–36 h of incubation.

As shown in Fig. 3A and B, the measurements of cell respiration parameters in the presence of the above-mentioned substrates revealed a diminished respiratory capacity of N2A cells with impaired AGC1 activity in the absence of glutamine. More in detail, the basal (routine) respiration of LVshAGC1-N2A cells incubated for 1 h with minimal medium supplemented with glucose plus either pyruvate or lactate was ~25% and ~45% decreased, respectively, when compared to control LVshMM-N2A cells, as in part previously described for intact cortical neurons with deficient AGC1 (Llorente-Folch, Rueda et al. 2013). On the other hand, no difference in basal respiration of both cell types was found when glutamine was added to the medium (Fig. 3A and B).

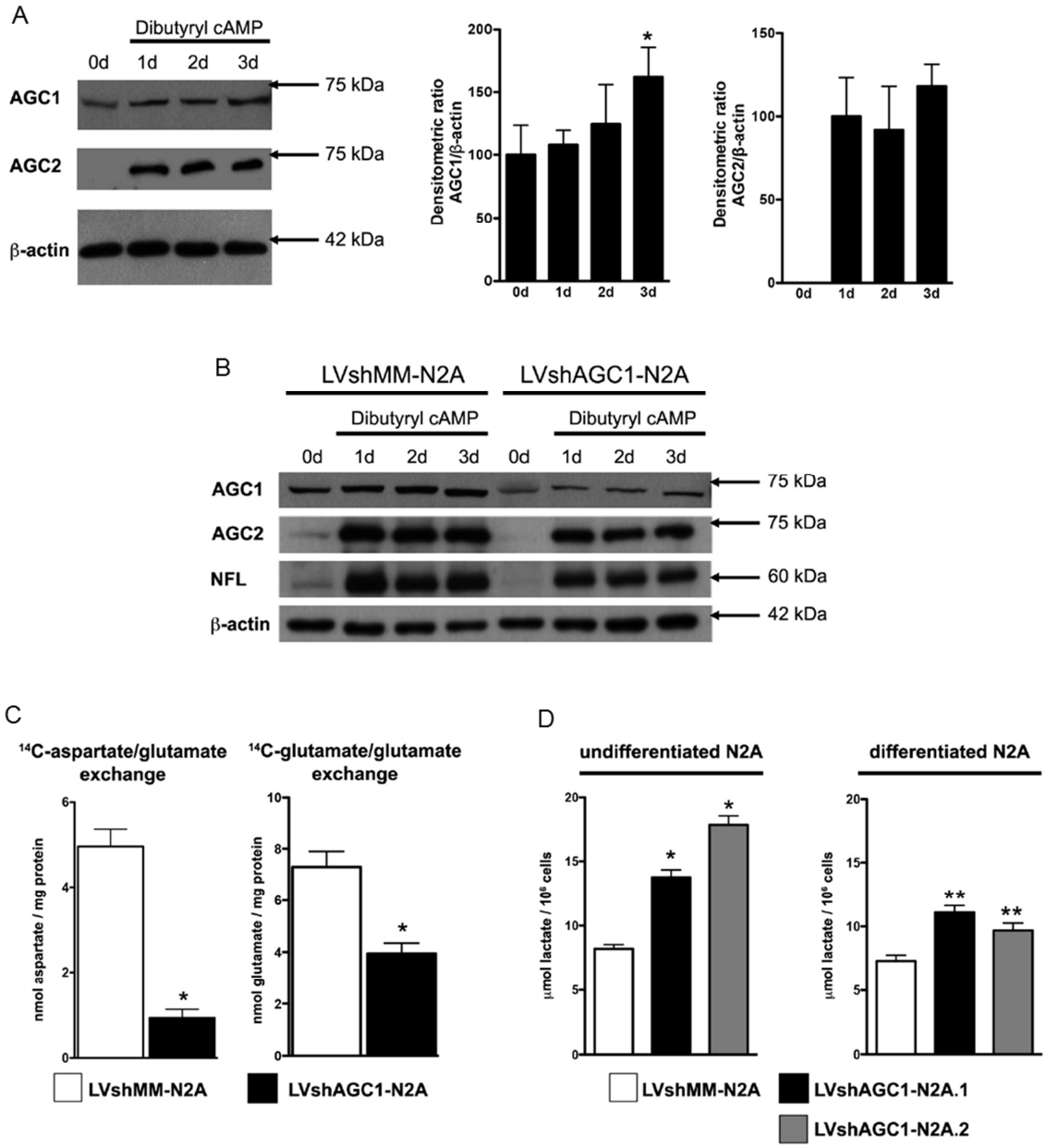

Fig. 1. Down-regulation of AGC1 increases lactate release in conditioned medium of N2A cells. (A) Representative immunoblot images of protein expression levels of AGC1 and AGC2 in N2A cells treated with 1 mM dibutyryl-cAMP, as differentiating agent, and harvested every 24 h for western the analysis. Histogram graphs show the means of the densitometric ratios between either AGC1 or AGC2 and β-actin. (B) Immunoblot images of protein expression levels of AGC1 and AGC2 and The neurofilament light chain protein (NFL) (a marker of neuronal maturation) in N2A cells stably transduced with either control LVshMM or LVshAGC1 construct and differentiated with 1 mM dibutyryl-cAMP. (C) Aspartate/glutamate and glutamate/glutamate exchange activities were assayed in liposomes reconstituted with mitochondrial extracts from undifferentiated N2A cells stably transduced with control LVshMM (white bars) or LVshAGC1 (black bars) construct. Transport was initiated by adding 50 µM ^{14C}aspartate (left panel) or 0.2 mM ^{14C}glutamate (right panel) to reconstituted liposomes both preloaded with 20 mM glutamate. (D) Lactic acid was quantified in conditioned complete DMEM harvested from control LVshMM-N2A cells (white bars) or LVshAGC1-N2A.1 and LVshAGC1-N2A.2 cells (black and grey bars). Conditioned media from undifferentiated cells were harvested after 24 h incubation; conditioned media from differentiated cells were harvested 24 h after addition of 1 mM dibutyryl-cAMP. Data are presented as the means ± SEM, **p<0.05, *p<0.01.

Moreover, the absence of glutamine in the incubation medium caused a significant decrease in both mitochondrial Electron Transfer System (ETS) capacity, i.e., maximal respiration with FCCP, and ATP turnover of LVshAGC1-N2A cells (Fig. 3A and B). To verify whether bioenergetics deficits and the reduced proliferation of LVshAGC1-N2A cells could be associated with higher cell mortality, in the same experimental conditions we estimated the cleavage of PARP1 and Caspase 3 proteins (Fig. 2B), as markers of an occurring apoptotic process.

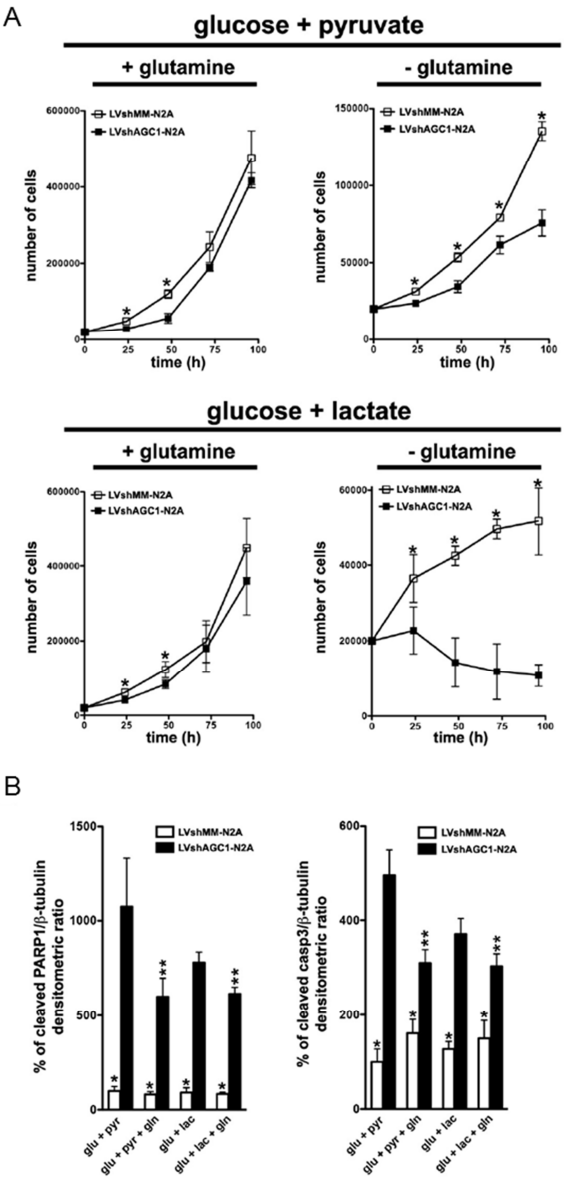

Fig. 2. Glutamine deprivation reduces proliferation of N2A cells with down-regulated AGC1. (A) Cell count for LVshMM-N2A (white squares) and LVshAGC1-N2A (black squares) cells grown in MEM supplemented with 1 g/l glucose + 1 mM pyruvate or 5 mM lactate ± 2 mM glutamine. (B) Relative quantitative analysis of apoptotic markers in LVshMM-N2A cells (white columns) and LVshAGC1-N2A (black columns) incubated 1 h in MEM supplemented with 1 g/l glucose + 1 mM pyruvate or 5 mM lactate ± 2 mM glutamine. Data are means of relative densities of 89 kDa cleaved PARP1 (upper panel) and 17 kDa cleaved caspase-3 (lower panel) proteins versus β-tubulin from 3 independent western blots. Data are presented as the means ± SEM, **p<0.05, *p<0.01.

After 1 h incubation in MEM supplemented with glucose and either pyruvate or lactate, LVshAGC1-N2A cells displayed a dramatic increase of both apoptotic markers, as compared

to control LVshMM-N2A cells. Notably, in the presence of glutamine, the apoptosis in LVshAGC1-N2A cells, while still enhanced, was significantly reduced. All together these data suggested a role of glutamine to sustain mitochondrial respiration and cell viability in undifferentiated N2A cell when AGC1 levels are impaired.

3. Down-regulation of AGC1 alters mitochondrial Ca^{2+} homeostasis in N2A cells

AGCs are Ca^{2+}-stimulated carriers that allow higher mitochondrial pyruvate oxidation when $[Ca^{2+}]$ increases in the cytosol (see above). Therefore, we simultaneously measured the extracellular acidification rate (ECAR) and OCR of N2A cells challenged by ATP that elicits IP3-mediated mobilization of Ca^{2+} from intracellular stores. ECAR significantly decreased in stimulated LVshMM-N2A cells when compared to that of LVshAGC1-N2A cells independently whether glucose and pyruvate (Fig. 4A) ± glutamine were used as incubation substrates. Surprisingly, in the same experimental conditions, the expected increase of OCR after ATP stimulation was virtually the same in both control and AGC1 silenced N2A cells (Fig. 4B). ECAR data confirmed that in the presence of higher $[Ca^{2+}]_c$, mitochondrial pyruvate consumption underlying cell respiration cannot be boosted when MAS is deficient and suggest that glutamine supply does not modify the mitochondrial Ca^{2+}-stimulated pyruvate metabolism.

On the other hand, OCR measurements suggested that in undifferentiated N2A cells with reduced AGC1, additional factors might maintain a high respiration rate when intracellular Ca^{2+} signals are triggered. As measured with Ca^{2+}-sensitive recombinant aequorins (Fig. 4C), in both stimulated control and AGC1-silenced N2A cells expressing cytosolic aequorin (cytAEQ), $[Ca^{2+}]_c$ peaks were virtually the same. Instead, LVshAGC1-N2A cells expressing the mitochondrial targeted aequorin (mtAEQmut) showed a two-fold increased mitochondrial Ca^{2+} accumulation as compared to control LVshMM-N2A cells. Remarkably, the higher mitochondrial Ca^{2+} uptake in due to a more elevated mitochondrial membrane potential ($\Delta\psi_m$) which acts as driving force for divalent cations. Mitochondrial membrane potential measurement with TMRM revealed an increased $\Delta\psi_m$, in response to the agonist (Fig. 4D), and accompanied by a significant enhancement of the Ca^{2+}-induced mitochondrial ATP synthesis in silenced LVshAGC1-N2A cells (Fig. 4E). All together these results indicated that in cells with down-regulated AGC1 a stronger activation of the mitochondrial Ca^{2+}-dependent pyruvate, isocitrate and 2-oxoglutarate dehydrogenases may take place, thus in turn further stimulating the mitochondrial metabolic machinery.

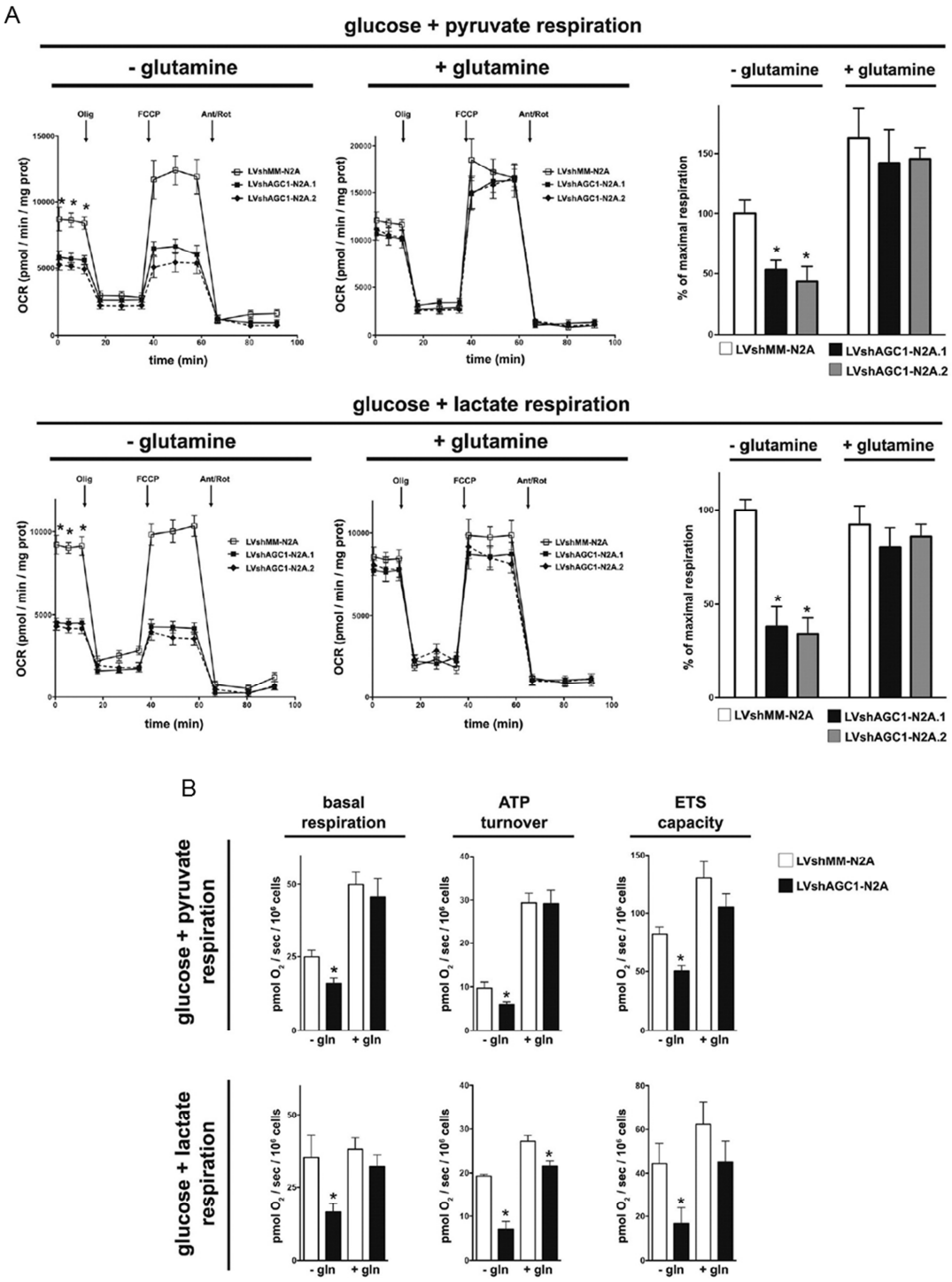

Fig. 3. Glutamine deprivation inhibits mitochondrial respiration in N2A cells with down-regulated AGC1. Oxygen consumption rates (OCR) were measured with XF96 extracellular flux analyzer (SeaHorse) (A) and O2k oxygraph (Oroboros) (B) in LVshMM-N2A and LVshAGC1-N2A cells incubated for 1 h in base medium supplemented with 1 g/l glucose + 1 mM pyruvate or 5 mM lactate ± 2 mM glutamine. N2A cells were exposed to sequential additions of 2 μM oligomycin, 0.2 μM FCCP, and 1 μM antimycin A + 1 μM rotenone. In Seahorse experiments, maximal respiration data with FCCP have been expressed as percentage of values compared with those of LVshMM-N2A cells incubated in the absence of glutamine. Data are presented as the means ± SEM, *p<0.01.

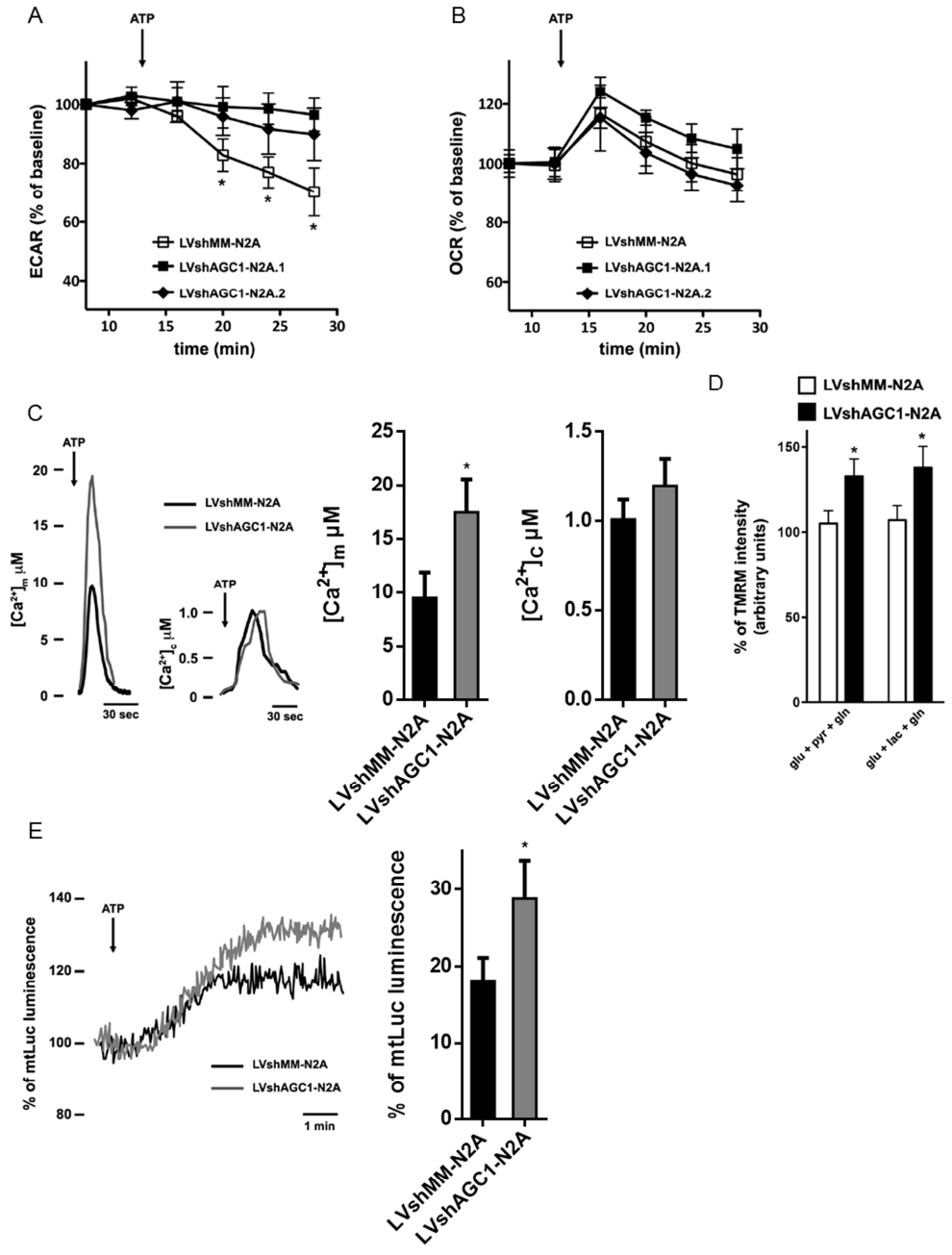

Fig. 4. The enhanced Ca^{2+}-dependent mitochondrial response in stimulated N2A cells with down-regulated AGC1. ECAR (A) and OCR (B) were simultaneously measured with XF96 extracellular flux analyzer (SeaHorse) in LVshMM-N2A or LVshAGC1-N2A.1 or LVshAGC1-N2A.2 cells incubated for 1 h in base medium supplemented with 1 g/l glucose + 1 mM pyruvate + 2 mM glutamine and stimulated with 1 mM ATP at the indicated time. ECAR and OCR were normalized to basal values before agonist stimulation. (C) The mitochondrial (left traces and histogram graph) and cytosolic (right traces and histogram graph) Ca^{2+} concentration were measured with mitochondrial- and cytosolic- targeted aequorin respectively in control N2A cells. Cells are challenged with ATP (1 mM). (D) Relative increases of $\Delta\psi m$ after Ca^{2+}-releasing agonist stimulation were measured by fluorescence microscopy in LVshMM-N2A and LVshAGC1-N2A cells incubated for 1 h in base medium supplemented with 1 g/l glucose, either 1 mM pyruvate or 5 mM lactate and 2 mM glutamine. (E) ATP-dependent luminescence was measured in LVshMM-N2A and LVshAGC1-N2A cells expressing mtLuc and incubated for 1 h in KRB supplemented with 1 mM $CaCl_2$, 1 g/l glucose, 1 mM pyruvate and 2 mM glutamine. In the luminometer, cells were perfused in the same medium and challenged with 1 mM ATP. Data are expressed as percentage of mtLuc light output increase from cells normalized to the pre-stimulatory values. Data are presented as the means ± SEM; *p<0.01.

4. Metabolomic analysis of AGC1-silenced N2A cells reveals an increased consumption of TCA cycle intermediates

Taken together, our data suggested that AGC1-silenced N2A cells might adapt their metabolism to stimulate mitochondrial activity, in particular by strengthening both mitochondrial Ca^{2+}-sensitivity and glutamine oxidation.

By LC-MS/MS analysis, we studied whether increased glutamine expenditure occurs in N2A cells with down-regulated AGC1. As shown in Fig. 5A and C, the uptake of glutamine in LVshAGC1-N2A cells was markedly increased compared to LVshMM-N2A cells.

Consequently, the relative glutamine content in LVshAGC1-N2A cells was higher than in control cells, although not significantly (Fig. 5B and D). These data indicated that glutamine is not only efficiently imported, but also highly consumed by N2A cells when AGC1 is silenced. Interestingly, when cells were deprived of glutamine (Fig. 5E), LVshAGC1-N2A took ~50% more glutamate from the culture medium and the intracellular glutamate content was ~50% reduced (Fig. 5F), as compared to control cells. By extending our analysis to other amino acids and TCA cycle intermediates, after 1 h incubation, LVshAGC1-N2A cells showed a significant increase of intracellular alanine which is consistent with reduced mitochondrial pyruvate oxidation, and marked decrease of aspartate as well as of 2-oxoglutarate, succinate, fumarate and malate, but not of citrate, as compared to LVshMM-N2A cells (Fig. 5B and F). Similar results were obtained when measurements were performed after 6 h incubation in medium containing glutamine with the only exception for alanine content which appeared restored to values similar to those of control cells (Fig. 5D). Therefore, although in the presence of inhibited pyruvate oxidation, N2A cells with low AGC1 activity appear able to consume at a higher rate the TCA cycle intermediates downstream of glutamate deamination.

5. Changes in mitochondrial protein activity are associated with higher ROS generation in AGC1-silenced N2A cells

Mass spectrometry data prompted us to investigate the activity of members of the mitochondrial carrier family that may potentially lower or increase the concentration of TCA cycle intermediates in anaplerosis and/or cataplerosis (Palmieri and Monne 2016). As shown in Fig. 6A, the expression of mitochondrial carriers CIC, GC, AAC and DIC resulted unvaried in both LVshMM-N2A and LVshAGC1-N2A cells.

The mitochondrial UCP2 carrier, a mitochondrial exchanger of aspartate with other C4 metabolites, appeared somewhat reduced in LVshAGC1-N2A cells, although not significantly. Most notably, N2A cells with reduced AGC1 revealed a striking increase in both expression and transport activity of the mitochondrial carriers for phosphate (PiC) and 2-oxoglutarate/malate (OGC), the latter participating together with AGC in the MAS (see above).

Furthermore, we investigated whether the mitochondrial respiratory chain was affected by AGC1 silencing. The activity of mitochondrial respiratory chain complexes II, II+III, IV and ATP synthase were not significantly different in both LVshMM-N2A and LVshAGC1-N2A cells.

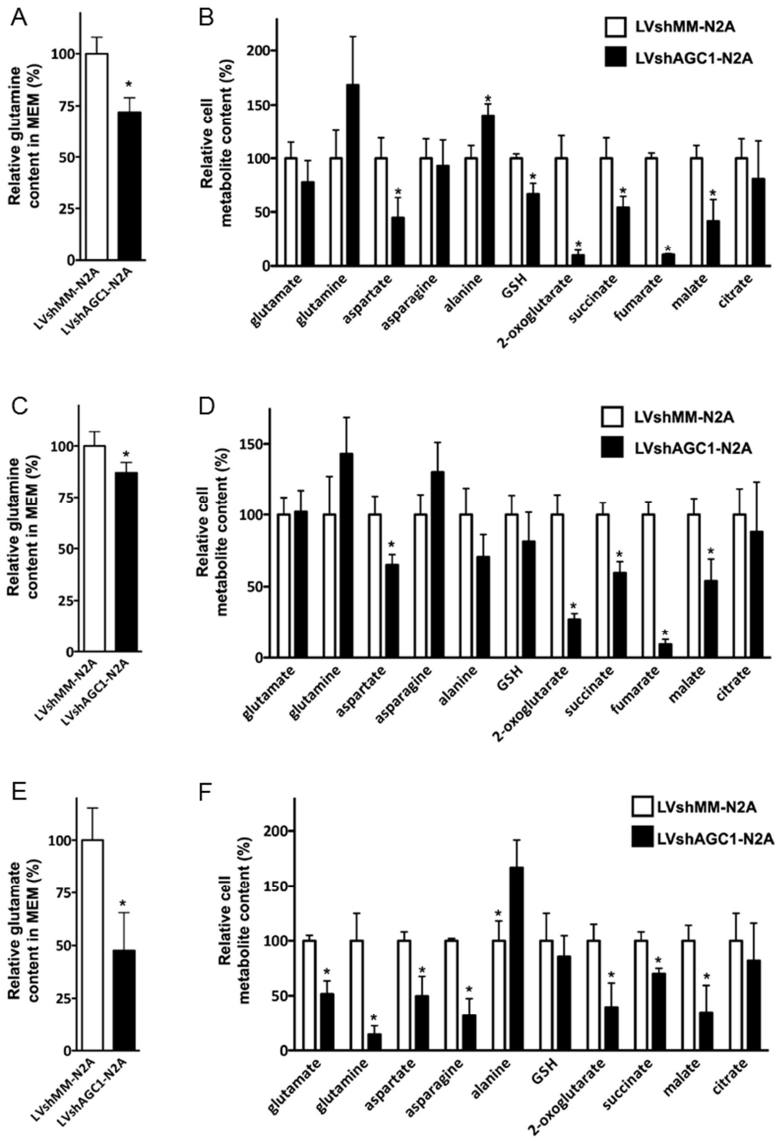

Fig. 5. Relative metabolite content in N2A cells with down-regulated AGC1. Media from LVshMM-N2A and LVshAGC1-N2A cells were harvested after 1 h (A and B) and 6 h (C and D) incubation with MEM supplemented with 1 g/l glucose, 5 mM lactate and 2 mM glutamine. Media and cells were also harvested after 1 h incubation with the same medium deprived of glutamine (E and F). Glutamine (A and C) and glutamate (E) levels in MEM, and the total cell pools of L-glutamate, L-glutamine, L-aspartate, L-asparagine, L-alanine, reduced glutathione, 2-oxoglutarate, succinate, fumarate, L-malate and citrate (B, D and F) were determined by mass spectrometry. Data are presented as the means ± SEM; *p<0.01.

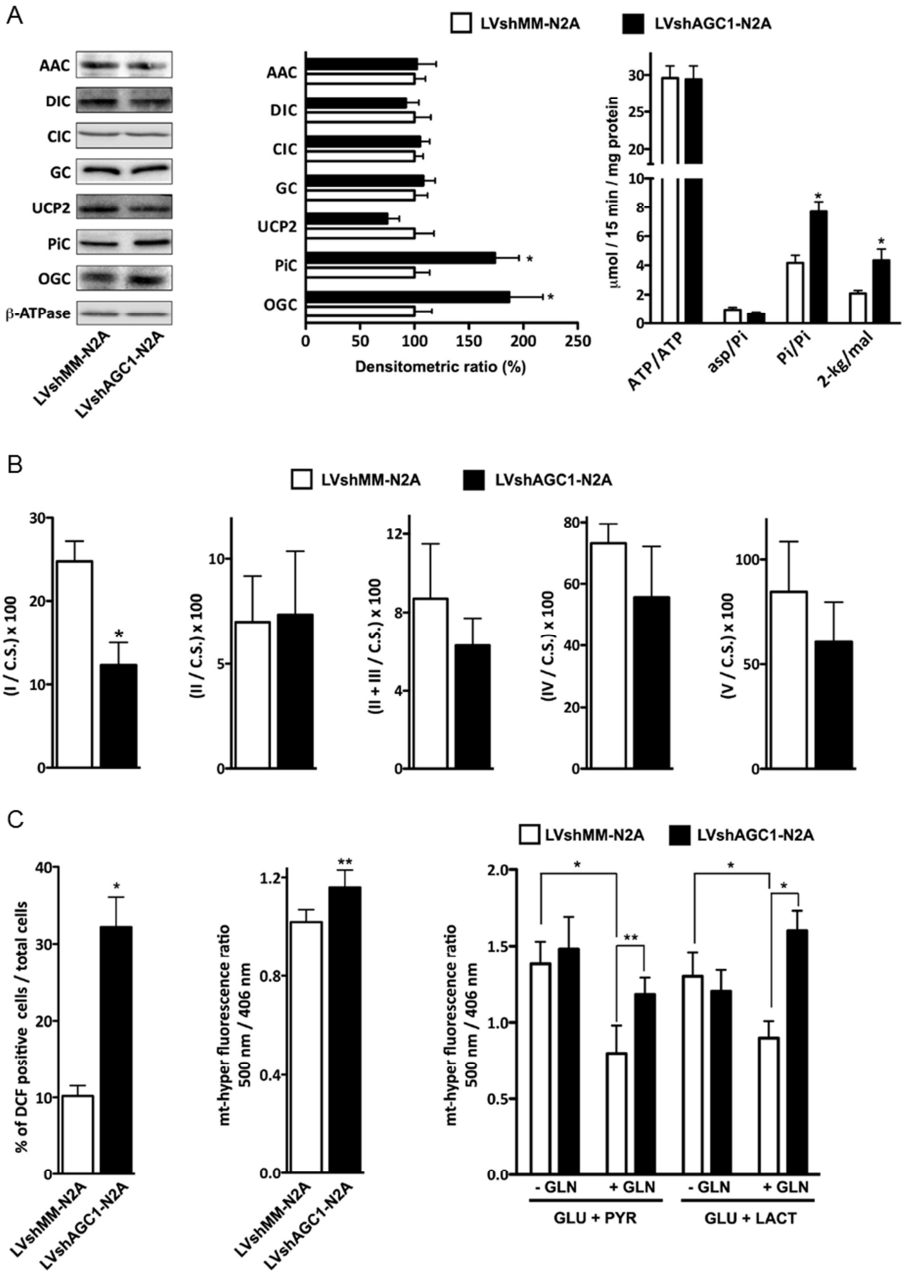

Fig. 6. Activities of mitochondrial carriers and respiratory chain complexes in N2A cells with down-regulated AGC1. Representative immunoblot images of protein expression levels mitochondrial carriers and activities in undifferentiated AGC1-silenced N2A cells. Histogram graph (middle panel) shows the means of the densitometric analysis on western blots performed on mitochondrial extracts from LVshMM-N2A (white bars) and LVshAGC1-N2A cells (black bars). The activities of the ^{14C}ATPext/ATPint, ^{14C}aspartateext/phosphateint, ^{33P}phosphateext/phosphateint and ^{14C}2-oxoglutarateext/malateint exchanges (right panel) catalyzed by AAC, UCP2, PiC and OGC proteins, respectively, and assayed in liposomes reconstituted with the mitochondrial extracts of LVshMM-N2A or LVshAGC1-N2A cells. (B) Mitochondrial respiratory chain complex activities in undifferentiated AGC1-silenced N2A cells. Activities of the indicated complexes in LVshMM-N2A (white bars) or LVshAGC1-N2A cells (black bars) were determined by spectrophotometry and related to citrate synthase (C.S.) activity which resulted unvaried in both cell types. (C) Cytosolic and mitochondrial hydrogen peroxide measurement in LVshMM-N2A (white bars) and LVshAGC1-N2A cells (black bars) loaded with 5 µM CM-H2DCFDA (left panel) or expressing the ratiometric H_2O_2-sensitive mt-HyPer protein (central and right panel). Measurements were performed in cells in complete rich DMEM (left and central panel) or incubated 1 h in MEM with 1 g/l glucose, 1 mM pyruvate or 5 mM lactate ± 2 mM glutamine. Data are presented as the means ± SEM; **p<0.05, *p<0.01.

By contrast, a significant decrease in complex I activity in LVshAGC1-N2A cells was found (Fig. 6B). Since increased production of hydroxyl radicals has been ascertained in mitochondrial pathologies with complex I deficiency (Verkaart, Koopman et al. 2007, Hirst and Roessler 2016), ROS generation in both cytosol and mitochondria of AGC1-silenced N2A cells was measured (Fig. 6C).We detected a more pronounced mitochondrial ROS generation in LVshAGC1-N2A cells compared to control cells grown in complete rich DMEM. To better understand whether ROS production was dependent on substrate supply, ratiometric fluorescence of mitochondrial localized probe mtHyper was measured in cells incubated in minimal growth medium. When N2A cells were supplemented with glucose plus either pyruvate or lactate, there was no significant difference in the high ROS synthesis between LVshAGC1-N2A and LVshMMN2A cells.

By contrast, the addition of glutamine to the medium significantly mitigated mitochondrial ROS production in control cells, but, importantly, not in LVshAGC1-N2A cells which appeared subjected to higher oxidative stress in each tested condition. As a result, these data suggested a protective role of glutamine against ROS synthesis in mitochondria that lacks in N2A cells with knocked-down AGC1. All together these data denote that undifferentiated N2A cells with low AGC1 activity may survive only by adapting their metabolism, expending more glutamine with the deleterious consequence of increased oxidative stress. By interpreting OCR and HPLC/MS data (Figs. 3A, B and 5), higher glutamine utilization by AGC1-silenced N2A cells would both enforce the Krebs cycle and provide metabolites for biosyntheses and cell proliferation.

6. Impaired AGC1 activity inhibits N-acetylaspartate synthesis in N2A cells

Aspartate along with acetyl-CoA is required for the synthesis of N-acetylaspartate (NAA) by the neuronal aspartate N-acetyltransferase (ANAT) (Madhavarao, Chinopoulos et al. 2003, Lu, Chakraborty et al. 2004, Tahay, Wiame et al. 2012). NAA is the precursor of myelin lipids in the brain and is severely reduced in patients affected by AGC1 deficiency where AGC1 activity is either absent (Wibom, Lasorsa et al. 2009) or significantly inhibited (Falk, Li et al. 2014). Indeed, N2A cells with silenced AGC1 revealed a striking deficit of NAA content compared to control cells, which was not rescued even when cells were incubated with glutamine for a longer time (6 h) (Fig. 7). These data suggested that aspartate produced in N2A cells with reduced AGC1 might be preferably utilized for proliferation process. However, it could be also argued that AGC1 activity impairment, which in turn inhibits

pyruvate oxidation in N2A mitochondria, might generate insufficient levels of acetyl-CoA to participate in ANAT reaction, thus unable to synthesize appropriate NAA levels.

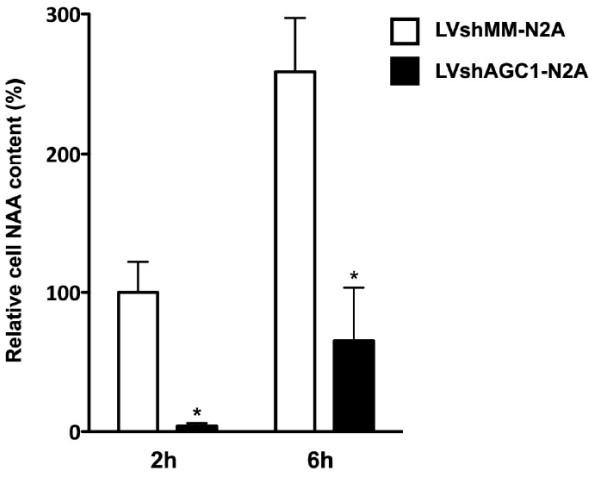

Fig. 7. Down-regulation of AGC1 reduces the content of N-acetylaspartate in N2A cells. Relative N-acetylaspartate concentrations were determined by mass spectrometry in LVshMM-N2A and LVshAGC1-N2A cells harvested after 1- or 6-h incubation with MEM supplemented with 1 g/l glucose, 5 mM lactate and 2 mM glutamine. Data are presented as the means ± SEM; **p<0.01.

Discussion

The human brain is an 'expensive' organ that represents ~2% of body weight but accounts for ~20% of the body's resting metabolic rate; most of this energy is used to maintain or re-establish membrane potentials. About 75% of the brain's calculated energy consumption is related to signalling, with the remainder ascribed to essential cellular activities including turnover of proteins, nucleotides, phospholipids, and other compounds, and axoplasmic transport (Attwell and Laughlin 2001).

Given the high needed of energy, new increasing evidence suggests a pivotal role of mitochondrial dysfunction in the pathogenesis of major neurodegenerative disorders. The bioenergetic defects, mtDNA mutations/polymorphism, altered mitochondrial dynamics, transcriptional dysregulation, and altered Ca^{2+} homeostasis are associated with mitochondrial dysfunction in neurodegenerative diseases (Mlody, Lorenz et al. 2016). The significant number of the neurological pathologies related with inborn mitochondrial dysfunctions in humans (Rafalski and Brunet 2011) further suggests the primary importance of the correct fulfilment of bioenergetics processes in order to sustain healthy brain maturation.

Oxidative metabolism provides most of the energy required for the brain's activities and oxygen is also needed for catecholamine neurotransmitter synthesis and degradation by the enzymes, tyrosine hydroxylase, dopamine-β-hydroxylase, tryptophan hydroxylase, and monoamine oxidase.

Therefore, mitochondria emerge as central organelles to allow the metabolic changes underpinning neuronal and glial cells function in the different stages of brain differentiation. In particular, it has been recently demonstrated that improved bioenergetics with increased mitochondrial activity is required when neuronal differentiation takes place (Agostini, Romeo et al. 2016).

Neurons usually oxidize almost exclusively glucose through the combined activity of glycolysis and TCA cycle for subsequent ATP synthesis (Attwell and Laughlin 2001). Oxidation of either glucose- or lactate-derived pyruvate in neurons requires the correct transfer of NADH reducing equivalents from the cytosol to mitochondria. Therefore, being the malate/aspartate NADH shuttle the main redox shuttle system in the brain (Attwell and Laughlin 2001), the activity of Ca^{2+}-regulated AGC isoforms becomes crucial for healthy brain functions. However, the relative contribution of AGC1 and AGC2 in the modulation of

bioenergetics and mitochondrial metabolism in neurons and other brain cells has not yet been fully elucidated.

In the present study, we have identified in undifferentiated mouse brain-derived N2A cells, a neuronal cell model expressing uniquely AGC1. In our hands, diversely to AGC1, AGC2 is virtually undetectable in proliferating N2A cells, whereas both AGC isoforms are simultaneously expressed when cells are committed to complete differentiation (Fig. 1A). This experimental evidence suggested that AGC1 might have an irreplaceable energetic function during N2A cell proliferation, while AGC2 could be recruited to sustain increased mitochondrial bioenergetics in the subsequent stages of neuronal differentiation. Indeed, when pyruvate or lactate where used with glucose as the sole respiratory substrates, AGC1 impairment brings undifferentiated N2A cells to an energetic deficit (Fig. 3A and B)which may underlie the boosted apoptotic processes compromising normal cell viability (Fig. 2A and B).

The oxidation of this substrate generates an additional quota of cytosolic NADH, which cannot be re-oxidized in mitochondria with impaired AGC1, thus further unbalancing the cellular redox state. Conversely, we observed that even in the absence of functional MAS, the addition of glutamine to the cellular medium apparently re-establishes a normal energetic profile of N2A cells, as shown in terms of basal respiration, ATP turnover and mitochondrial respiration capacity, and restores cell survival.

It has been documented that in hypoglycemic conditions neurons actively use glutamine and in turn glutamate as alternative fuels to sustain energy production by entering the TCA cycle at the level of 2-oxoglutarate dehydrogenase [61]. Accordingly, our data demonstrated that undifferentiated N2A cells with down-regulated AGC1 scarcely oxidize pyruvate, but have a higher disposition to take and consume glutamine (Fig. 5). As expected, glutamine consumption appears not to interfere with pyruvate oxidation, since higher lactate synthesis occurs in AGC1-silenced N2A cells either grown in rich medium with glutamine (Fig. 1D) or with TCA enhancement after ATP stimulation even in the presence of glutamine (see ECAR changes in Fig. 4A).

According to our data, it could be suggested that in the brain with impaired AGC1 (Wibom, Lasorsa et al. 2009, Falk, Li et al. 2014), neuronal progenitors could survive only if appropriate glutamine concentrations are available. Interestingly, astrocytes can supply glutamine to neurons (Hertz, Peng et al. 2007) by a process called glutamate-glutamine cycle where part of the neuronally released glutamate is converted by the enzyme glutamine synthase (GS) in astrocytes to glutamine which is then transferred back to neurons. Moreover,

through aerobic glycolysis, astrocytes carry out net synthesis of glutamate and glutamine, as well as of TCA cycle intermediates and related derivatives whose traffic to neurons has been demonstrated (Erecinska, Zaleska et al. 1990). Therefore, exchange activity of the mitochondrial transporters involved in MAS would represent a potential preferential path to move intermediates required for biosynthesis. As a consequence, AGC1 impairment in N2A cells may result in unbalancing the integration of cytosolic keto and amino acid pools, in particular aspartate. Aspartate is essential for many cell processes since it participates in protein and nucleotide syntheses, and is the main metabolic product of respiration in proliferating cells. Importantly, since the primary site of aspartate production is the mitochondrial matrix, the absence of functional AGC1 in N2A cells proliferating with glutamine would make the inner mitochondrial membrane inaccessible for aspartate exit unless other transporters intervene. Although the mitochondrial UCP2 is the only alternative to transport aspartate out of mitochondria, we observed that in mitochondria from AGC1-silenced N2A cells, aspartate transport catalyzed by UCP2 appears not to compensate the reduction of aspartate/glutamate exchange activity (compare Fig. 1C and 6A). Conversely, we show that N2A cells respond to AGC1 decrease with augmented expression and activity of both mitochondrial PIC and OGC. Increased PIC levels could be required to sustain mitochondrial ATP synthesis rates, as for example measured when cells were triggered with Ca^{2+}-releasing agonists (Fig. 4E). Overexpression of OGC could be interpreted on one side as a biochemical adaptation to sustain the weakened MAS activity. On the other side, in the presence of glutamine supply, increased OGC might diversely favour the exit of C4 metabolites from the TCA cycle, specifically malate.

However, the adaptation mechanism boosted by glutamine oxidation, although preserving cell proliferation, appears to lead AGC1 deficient cells to the metabolic sequela of higher oxidative stress (Fig. 6C), most likely due to the observed lower activity of respiratory complex I, a well-known site of ROS production which may inaccurately handle the flux of NADH generated by glutamine oxidation.

The reduced aspartate content revealed in proliferating AGC1-silenced cells (Fig. 5), could, therefore, be interpreted as high utilization of this amino acid for protein and nucleotide synthesis purposes during cell growth and division (Sullivan, Gui et al. 2015). In addition, the required aspartate synthesis might likely be less efficient in AGC1-silenced cells than in normal cells affecting other aspartate-requiring cellular processes. This may explain the reduced NAA synthesis measured in AGC1 deficient N2A cells (Fig. 7). NAA is formed from aspartate and acetyl-CoA by the neuron-specific aspartate N-acetyltransferase (Asp-NAT).

NAA is thought to be a molecule carrying acetyl groups for the formation of myelin lipids in oligodendrocytes. Reduced NAA content is observed in patients with AGC1 deficiency who suffer of hypomyelination and cerebral volume loss (Wibom, Lasorsa et al. 2009). Indeed, in AGC1 deficient cells, NAA production might be compromised by the limited availability of both Asp-NAT reagents. Furthermore, when AGC1 is inactivated, the subsequent MAS impairment may impede efficient pyruvate oxidation and may prevent the formation of appropriate acetyl- CoA levels for NAA synthesis (Profilo, Pena-Altamira et al. 2017).

Materials and Methods

Cell culture and reagents

Neuro2A cells were purchased from ATCC-LGC Standards (Italy) and cultured in Dulbecco's modified Eagle's medium (DMEM) (D6546 SIGMA - Italy) supplemented with 10% fetal bovine serum, and 100 U/ml penicillin (EuroClone), and 100 mg/ml streptomycin (EuroClone) in 75 cm^2 Corning flasks. All cells were maintained at 37°C under 90% relative humidity with 5% CO_2. Unless otherwise indicated, cell incubations in minimal growth medium were accomplished by using Minimal Essential Medium (MEM, M5650 SIGMA - Italy). Before transfection, cells were seeded onto 13 mm glass coverslips for intracellular Ca^{2+} measurements with aequorin and onto 24 mm glass coverslips for microscopic analysis. Cells were grown to 70% confluence and then transfected for 12 h at 37° C for transient plasmid overexpression. Transfection was performed via Lipofectamine® LTX (Thermo Fisher) according to the manufacturer's instructions (Pinton, Ferrari et al. 2000).

AGC1-silencing shRNA design and lentiviral construct generation for stable transduction of N2A cells.

Two shRNA cassette 5′-TGCTTGTTCGAAAGATCTATAGCTCGAGCA TAGATCTTTCGAACAAGCTTTTT -3′ and 5′-TGCTTGCAGACCTATATAA TGCCTCGAGGCATTATATAGGTCTGCAAGCTTTTT-3′ were designed as a hairpin-loop structure from the mouse Slc25a12 cDNA sequence encoding AGC1 protein according to the guidelines described in http://sirna.wi.mit.edu/ and AgeI/EcoRI cloned into the pLKO.1 vector (Sigma - Italy). In parallel, a mismatch shRNA 5′-TACAACCAACGCACGCTAATCTCGAGATTAGCGTGCGTTGGT TGTTTTTT-3′ was cloned into the same vector to generate unsilencing control plasmid. The resulting constructs were sequenced and used to transfect HEK293T cells with the Lentiviral Packaging mix (SIGMA - Italy) according to the manufacturer's instructions for the recombinant generation of control LVshMM, and AGC1-silencing LVshAGC1.1 and LVshAGC1.2 lentiviral particles. 4 days after transfection, cell conditioned media containing the virus were harvested, their titer estimated and used for the transduction. N2A cells were transduced with

the recombinant LVshMM and LVshAGC1 particles at a viral titer of ~5 plaque-forming units/ml for 24 h at 37 °C and treated with 1 µg/ml puromycin for stable selection.

Immunoblotting

For immunoblotting, cells were scraped into ice-cold, phosphate buffered saline (PBS) and lysed in a buffer containing 50 mM Tris HCl pH 7.4, 150 mM NaCl, 1% Triton X-100, 0.2% SDS, protease and phosphatase inhibitor cocktail. After 30 min of incubation on ice and centrifugation at 2,500 rpm at 4°C for 5 min, proteins were quantified by the Lowry method, and 10 µg of each sample was loaded onto a Novex NuPage Bis-Tris 4–12% precast gel (Life Technologies). The separated proteins were transferred to nitrocellulose membranes. After incubation with TBS–Tween-20 (0.05%) supplemented with 5% non-fat powdered milk for 1 h to saturate unspecific binding sites, the membranes were incubated overnight with primary antibodies. Detection was achieved using appropriate horseradish peroxidase-labeled secondary antibodies (Santa Cruz Biotechnology), followed by biochemiluminescence (ThermoScientific) using an ImageQuant LAS4000 (GE Healthcare). AGC1, AGC2, UCP2, α-actin and NFL antibodies were purchased from Santa Cruz Biotechnology, Inc. (Dallas, TX USA). AAC antibody was purchased from Mitoscience (Eugene, OR USA). Caspase 3 and PARP-1 antibodies were purchased from Cell Signaling Technology (Danvers, MA USA). Homemade antibodies raised in rabbit against mitochondrial carriers for dicarboxylates (DIC), citrate (CIC), glutamate (GC), phosphate (PiC) and 2-oxoglutarate/malate (OGC) were used. Densitometric analyses were accomplished by using the Image Lab™ Touch software (Bio-Rad Laboratories, CA USA).

Mitochondrial carriers transport activity measurements

30 µg of isolated mitochondria from N2A cells were solubilized (0.5 mg/ml) in a buffer containing 3% TX-114, 1 mM EDTA, 10 mM PIPES, pH 7.0 for 45 min on ice, and reconstituted in liposomes. Transport measurements at 25 °C were initiated by adding radioactive substrates at the indicated concentrations to liposomes reconstituted with mitochondrial extracts containing 20mMunlabeled substrates and terminated by adding 10mMpyridoxal 5′-phosphate and 8mMbathophenanthroline, according to the inhibitor stop method. The incorporated radioactivity was quantified by an LS 6500 liquid scintillation counter (Beckman Coulter, CA USA).

Measurements of oxygen consumption (OCR) and extracellular acidification rates (ECAR)

Oxygen consumption rates and extracellular acidification rates were measured using the SeahorseXF96 instrument (Seahorse Biosciences, North Billerica, MA) according to the manufacturer's protocols.

Respiration parameters were also determined through the high-resolution O2k respirometer (OROBOROS Instruments, Austria). In Seahorse experiments, 25.000 cells/well were washed three times with unbuffered XF base medium (Seahorse Bioscience, MA USA) without added substrates and then incubated for 1 h in humidified incubator at 37 °C in the presence of unbuffered XF base medium supplemented with 1 g/l glucose + 1 mM pyruvate or 5 mM lactate ± 2 mM glutamine. After incubation, basal OCR/ECAR were recorded three times for total 12 min prior to the sequential injections of 2 μM oligomycin, as inhibitor of ATP synthase (three measurements for total 25 min), 0.2 μM FCCP, as mitochondrial uncoupler (three measurements for total 25 min), and 1 μM antimycin A + 1 μM rotenone, as mitochondrial respiratory chain inhibitors (three measurements for total 25 min). In O2k oxygraphy experiments, 1 × 10 cells were trypsinized and the cell suspension, treated for 1 h in the same incubation media used for Seahorse experiments,was subsequently subjected to sequential addition of the above-mentioned reagents.

Aequorin and luciferase luminescence measurements

N2A cells were transiently transfected with plasmids carrying the coding sequence of recombinant aequorins selectively targeted to the cytosol (cytAEQ) or mitochondria (mtAEQmut), and of the recombinant luciferase targeted to mitochondria (mtLuc).

To evaluate the [Ca^{2+}] in the experiments with cytAEQ and mtAEQ, the coverslips were incubated with 5 μM coelenterazine (Fluka) for 1.5 h in Krebs–Ringer modified buffer (KRB; 125 mM NaCl, 5 mM KCl, 1 mM Na_3PO_4, 1 mM $MgSO_4$, 5.5 mM glucose, and 20 mM 4-(2-hydroxyethyl)-1-piperazineethanesulfonic acid [HEPES], pH 7.4, at 37° C) supplemented with 1 mM $CaCl_2$. A coverslip with transfected cells was subsequently placed in a perfused thermostat-controlled chamber located in close proximity to a low-noise photomultiplier with a built-in amplifier/discriminator.

Cells were perfused in the same buffer (+20 mM luciferin for luciferase assays) and subsequently they were stimulated with 1 mM ATP. Aequorin experiments were terminated by lysing cells with X-100 Triton in a hypotonic Ca^{2+}-containing solution (10 mM $CaCl_2$ in

H_2O), thus discharging the remaining aequorin pool. In luciferase assays, data are expressed as mtLuc light output percentage of cells before agonist stimulus. The output of the discriminator was captured with a Thorn EMI photon-counting board and stored in an IBM-compatible computer for further analyses. The aequorin luminescence data were calibrated into [Ca^{2+}] values offline, using a computer algorithm based on the Ca^{2+} response curve of wild-type aequorin. Further experimental details were previously described

Cell fluorescence analysis

Measurements of intracellular reactive oxygen species were performed by loading cells with 5 μM 5-(and-6)-chloromethyl-2′,7′- dichlorodihydrofluorescein diacetate, acetyl ester (CM-H2DCFDA; Life Technologies, C-6827) for 20 min at 37 °C, and green fluorescence of cells was analyzed with a Tali® Image-Based Cytometer. Mitochondrial hydrogen peroxide levels were measured in N2A cells cultured on 24mmglass coverslips and transfected with the ratiometric fluorescent probe with mitochondrial localization pHyPer-dMito (mt-HyPer). After 24 h expression, cells were maintained in KRB supplemented with 1 mM CaCl2 and the indicated carbon sources and placed in an open Leyden chamber on a 37 °C thermostated stage. 494/406 nm excitation filters and a 500-nm long-pass beam splitter were used, and an image pair was obtained in every 200 ms with a ×40 objective. For a ratiometric measurement, at the end of each measurement, the efficiency of the probe was ascertained by adding H2O2 as reference. Fluorescence data were expressed as emission ratios. The experiments were performed on a Cell^R Olympus multiple wavelength high-resolution epi-fluorescence microscope. Mitochondrial inner membrane potential (Ψm) was measured by loading the cells with 20 nM tetramethyl rhodamine methyl ester (TMRM; Life Technologies, T-668) for 30 min at 37 °C. Images were taken on an inverted Nikon LiveScan Swept Field Confocal Microscope (SFC) Eclipse Ti equipped with NIS-Elements microscope imaging software (Nikon Instruments). TMRM fluorescence intensities (exc. 560 nm; emis. 590–650 nm) were imaged every 5 s with a fixed 20 ms exposure time. At the end of the experiments, 10 μM FCCP was added after 240 acquisitions to completely collapse the Ψm and to subtract the non-mitochondrial TMRM fluorescence, as previously described.

Metabolite determinations by mass spectrometry

For metabolite quantification, LVshMM-N2A and LVshAGC1-N2A cells were starved for 1 h in KRB without carbon sources and subsequently incubated in Minimum Essential Medium

Eagle (MEM (Sigma M5650) supplemented with 1 g/l glucose, 5 mM lactate, and with or without 2 mM glutamine. After the indicated incubation times, conditioned MEM and cells were harvested, extracted with methanol/ water (50–50), and the aqueous phase was centrifuged at 13,000 g for 20 min at 4 °C to precipitate the protein fraction. A Quattro Premier mass spectrometer with an Acquity UPLC system (Waters - Italy) was used for electrospray ionization LC-MS/MS analysis in the multiple reaction monitoring (RMR) mode, as previously described. The MRM transitions in the negative-ion mode were m/z 190.95 N 110.89 for citrate, m/z 116.88 N 73.20 for succinate, m/z 115.07 N 71.31 for fumarate, m/z 132.95 N 115.20 for malate, m/z 144.9 N 101.10 for 2-oxoglutarate, and m/z 174.1 N 88.0 for NAA. The MRM transitions in the positive-ion mode were m/z 134.16 N 73.76 for aspartate, m/z 148.20 N 83.80 for glutamate, m/z 90.00 N 44.24 for alanine, and m/z 308.28 N 179.02 for reduced glutathione. Calibration curves of standards were used for metabolites quantifications.

Respiratory chain complex analysis

Mitochondrial respiratory chain complex and citrate synthase activities were measured in permeabilized cells using a Cary 50 spectrophotometer (Agilent Technologies Santa Clara, CA USA), as previously described with some modification. The NADH-ubiquinone oxidoreductase activity of complex I was measured quantifying the decrease in UV absorbance accompanying the oxidation of NADH. Any rotenone-insensitive activity was measured. Succinate dehydrogenase/complex II activity was measured following the reduction of 2.6-dichlorophenolindophenol (DCPIP) at 600 nm after the addition of succinate. Complex II+III (succinate cytochrome c reductase) activity was measured following the reduction of oxidized cytochrome c at 550 nm coupled to succinate oxidation. The activity of complex IV was carried out by evaluating the oxidation of reduced cytochrome c at 550 nm. ATPase activity was measured at 340 nm by coupling the production of ADP to the oxidation of NADH via pyruvate Kinase and lactate dehydrogenase. The reactions were measured for 2 min under controlled temperature, with a linear slope in the presence or absence of inhibitor when present and enzymatic activity of each complex was normalized to that of citrate synthase.

Statistical analysis

Statistical analyses were performed using an unpaired two-tailed t-test (two groups) or one-way ANOVA with Tukey correction and one-way analysis with Bonferroni t-test (for groups of three or more). For grouped analyses, two-way ANOVA was performed; $p<0.05$ was considered significant. All data are reported as the means ± SEs.

References

Agostini, M., F. Romeo, S. Inoue, M. V. Niklison-Chirou, A. J. Elia, D. Dinsdale, N. Morone, R. A. Knight, T. W. Mak and G. Melino (2016). "Metabolic reprogramming during neuronal differentiation." Cell Death Differ **23**(9): 1502-1514.

Amemori, S., R. Iwakiri, H. Endo, A. Ootani, S. Ogata, T. Noda, S. Tsunada, H. Sakata, H. Matsunaga, M. Mizuguchi, Y. Ikeda and K. Fujimoto (2006). "Oral dimethyl sulfoxide for systemic amyloid A amyloidosis complication in chronic inflammatory disease: a retrospective patient chart review." J Gastroenterol **41**(5): 444-449.

Amoedo, N. D., G. Punzi, E. Obre, D. Lacombe, A. De Grassi, C. L. Pierri and R. Rossignol (2016). "AGC1/2, the mitochondrial aspartate-glutamate carriers." Biochim Biophys Acta **1863**(10): 2394-2412.

Anderson, S., A. T. Bankier, B. G. Barrell, M. H. de Bruijn, A. R. Coulson, J. Drouin, I. C. Eperon, D. P. Nierlich, B. A. Roe, F. Sanger, P. H. Schreier, A. J. Smith, R. Staden and I. G. Young (1981). "Sequence and organization of the human mitochondrial genome." Nature **290**(5806): 457-465.

Appelqvist, H., P. Waster, K. Kagedal and K. Ollinger (2013). "The lysosome: from waste bag to potential therapeutic target." J. Mol. Cell Biol. **5**(4): 214-226.

Attwell, D. and S. B. Laughlin (2001). "An energy budget for signaling in the grey matter of the brain." J Cereb Blood Flow Metab **21**(10): 1133-1145.

Bainton, D. F. (1981). "The discovery of lysosomes." J Cell Biol **91**(3 Pt 2): 66s-76s.

Ballabio, A. (2016). "The awesome lysosome." EMBO Mol Med **8**(2): 73-76.

Ballabio, A. and V. Gieselmann (2009). "Lysosomal disorders: from storage to cellular damage." Biochim Biophys Acta **1793**(4): 684-696.

Bargal, R., H. H. Goebel, E. Latta and G. Bach (2002). "Mucolipidosis IV: novel mutation and diverse ultrastructural spectrum in the skin." Neuropediatrics **33**(4): 199-202.

Benard, G. and R. Rossignol (2008). "Ultrastructure of the mitochondrion and its bearing on function and bioenergetics." Antioxid Redox Signal **10**(8): 1313-1342.

Berg, T., T. Gjoen and O. Bakke (1995). "Physiological functions of endosomal proteolysis." Biochem J **307 (Pt 2)**: 313-326.

Berg, T. O., E. Stromhaug, T. Lovdal, O. Seglen and T. Berg (1994). "Use of glycyl-L-phenylalanine 2-naphthylamide, a lysosome-disrupting cathepsin C substrate, to distinguish between lysosomes and prelysosomal endocytic vacuoles." Biochem. J. **300 (Pt 1)**: 229-236.

Berridge, M. J. (2012). "Calcium signalling remodelling and disease." Biochem. Soc. Trans. **40**(2): 297-309.

Berridge, M. J., M. D. Bootman and H. L. Roderick (2003). "Calcium signalling: dynamics, homeostasis and remodelling." Nat. Rev. Mol. Cell Biol. **4**(7): 517-529.

Berridge, M. J., P. Lipp and M. D. Bootman (2000). "The versatility and universality of calcium signalling." Nat Rev Mol Cell Biol **1**(1): 11-21.

Bonora, M., C. Giorgi, A. Bononi, S. Marchi, S. Patergnani, A. Rimessi, R. Rizzuto and P. Pinton (2013). "Subcellular calcium measurements in mammalian cells using jellyfish photoprotein aequorin-based probes." Nat. Protoc. **8**(11): 2105-2118.

Bonora, M., C. Giorgi and P. Pinton (2015). "Novel frontiers in calcium signaling: A possible target for chemotherapy." Pharmacol. Res. **99**: 82-85.

Bonora, M., S. Patergnani, A. Rimessi, E. De Marchi, J. M. Suski, A. Bononi, C. Giorgi, S. Marchi, S. Missiroli, F. Poletti, M. R. Wieckowski and P. Pinton (2012). "ATP synthesis and storage." Purinergic Signal **8**(3): 343-357.

Bossi, G. and G. M. Griffiths (2005). "CTL secretory lysosomes: biogenesis and secretion of a harmful organelle." Semin Immunol **17**(1): 87-94.

Boyer, P. D. (2000). "Catalytic site forms and controls in ATP synthase catalysis." Biochim Biophys Acta **1458**(2-3): 252-262.

Brady, S. T., G. J. Siegel, R. W. Albers, D. L. Price and J. Benjamins (2012). Basic neurochemistry : principles of molecular, cellular, and medical neurobiology. Amsterdam ; Boston, Elsevier/Academic Press.

Brailoiu, E., R. Hooper, X. Cai, G. C. Brailoiu, M. V. Keebler, N. J. Dun, J. S. Marchant and S. Patel (2010). "An ancestral deuterostome family of two-pore channels mediates nicotinic acid adenine dinucleotide phosphate-dependent calcium release from acidic organelles." J Biol Chem **285**(5): 2897-2901.

Braulke, T. and J. S. Bonifacino (2009). "Sorting of lysosomal proteins." Biochim Biophys Acta **1793**(4): 605-614.

Bursch, W. (2001). "The autophagosomal-lysosomal compartment in programmed cell death." Cell Death Differ **8**(6): 569-581.

Cahoy, J. D., B. Emery, A. Kaushal, L. C. Foo, J. L. Zamanian, K. S. Christopherson, Y. Xing, J. L. Lubischer, P. A. Krieg, S. A. Krupenko, W. J. Thompson and B. A. Barres (2008). "A transcriptome database for astrocytes, neurons, and oligodendrocytes: a new resource for understanding brain development and function." J Neurosci **28**(1): 264-278.

Calcraft, P. J., M. Ruas, Z. Pan, X. Cheng, A. Arredouani, X. Hao, J. Tang, K. Rietdorf, L. Teboul, K. T. Chuang, P. Lin, R. Xiao, C. Wang, Y. Zhu, Y. Lin, C. N. Wyatt, J. Parrington, J. Ma, A. M. Evans, A. Galione and M. X. Zhu (2009). "NAADP mobilizes calcium from acidic organelles through two-pore channels." Nature **459**(7246): 596-600.

Cang, C., Y. Zhou, B. Navarro, Y. J. Seo, K. Aranda, L. Shi, S. Battaglia-Hsu, I. Nissim, D. E. Clapham and D. Ren (2013). "mTOR regulates lysosomal ATP-sensitive two-pore Na(+) channels to adapt to metabolic state." Cell **152**(4): 778-790.

Cea, M., A. Cagnetta, M. Fulciniti, Y. T. Tai, T. Hideshima, D. Chauhan, A. Roccaro, A. Sacco, T. Calimeri, F. Cottini, J. Jakubikova, S. Y. Kong, F. Patrone, A. Nencioni, M. Gobbi, P. Richardson, N. Munshi and K. C. Anderson (2012). "Targeting NAD+ salvage pathway induces autophagy in multiple myeloma cells via mTORC1 and extracellular signal-regulated kinase (ERK1/2) inhibition." Blood **120**(17): 3519-3529.

Cereghetti, G. M. and L. Scorrano (2006). "The many shapes of mitochondrial death." Oncogene **25**(34): 4717-4724.

Cerny, J., Y. Feng, A. Yu, K. Miyake, B. Borgonovo, J. Klumperman, J. Meldolesi, P. L. McNeil and T. Kirchhausen (2004). "The small chemical vacuolin-1 inhibits Ca(2+)-dependent lysosomal exocytosis but not cell resealing." EMBO Rep. **5**(9): 883-888.

Chan, E. Y., S. Kir and S. A. Tooze (2007). "siRNA screening of the kinome identifies ULK1 as a multidomain modulator of autophagy." J Biol Chem **282**(35): 25464-25474.

Chieregatti, E. and J. Meldolesi (2005). "Regulated exocytosis: new organelles for non-secretory purposes." Nat Rev Mol Cell Biol **6**(2): 181-187.

Christensen, K. A., J. T. Myers and J. A. Swanson (2002). "pH-dependent regulation of lysosomal calcium in macrophages." J. Cell Sci. **115**(Pt 3): 599-607.

Christensen, K. A., J. T. Myers and J. A. Swanson (2002). "pH-dependent regulation of lysosomal calcium in macrophages." J Cell Sci **115**(Pt 3): 599-607.

Clapham, D. E. (1995). "Intracellular calcium. Replenishing the stores." Nature **375**(6533): 634-635.

Clapham, D. E. (2007). "Calcium signaling." Cell **131**(6): 1047-1058.

Clapper, D. L., T. F. Walseth, P. J. Dargie and H. C. Lee (1987). "Pyridine nucleotide metabolites stimulate calcium release from sea urchin egg microsomes desensitized to inositol trisphosphate." J Biol Chem **262**(20): 9561-9568.

Conner, S. D. and S. L. Schmid (2003). "Regulated portals of entry into the cell." Nature **422**(6927): 37-44.

Csordas, G. and G. Hajnoczky (2009). "SR/ER-mitochondrial local communication: calcium and ROS." Biochim Biophys Acta **1787**(11): 1352-1362.

de Duve, C. (2005). "The lysosome turns fifty." Nat Cell Biol **7**(9): 847-849.

Dickson, E. J., J. G. Duman, M. W. Moody, L. Chen and B. Hille (2012). "Orai-STIM-mediated Ca2+ release from secretory granules revealed by a targeted Ca2+ and pH probe." Proc. Natl. Acad. Sci. USA **109**(51): E3539-3548.

DiMauro, S. and E. A. Schon (2003). "Mitochondrial respiratory-chain diseases." N Engl J Med **348**(26): 2656-2668.

Duchen, M. R. (2004). "Mitochondria in health and disease: perspectives on a new mitochondrial biology." Mol Aspects Med **25**(4): 365-451.

Dyall, S. D., M. T. Brown and P. J. Johnson (2004). "Ancient invasions: from endosymbionts to organelles." Science **304**(5668): 253-257.

Erecinska, M., M. M. Zaleska, D. Nelson, I. Nissim and M. Yudkoff (1990). "Neuronal glutamine utilization: glutamine/glutamate homeostasis in synaptosomes." J Neurochem **54**(6): 2057-2069.

Falk, M. J., D. Li, X. Gai, E. McCormick, E. Place, F. M. Lasorsa, F. G. Otieno, C. Hou, C. E. Kim, N. Abdel-Magid, L. Vazquez, F. D. Mentch, R. Chiavacci, J. Liang, X. Liu, H. Jiang, G. Giannuzzi, E. D. Marsh, G. Yiran, L. Tian, F. Palmieri and H. Hakonarson (2014). "AGC1

Deficiency Causes Infantile Epilepsy, Abnormal Myelination, and Reduced N-Acetylaspartate." JIMD Rep **14**: 77-85.

Falkowska, A., I. Gutowska, M. Goschorska, P. Nowacki, D. Chlubek and I. Baranowska-Bosiacka (2015). "Energy Metabolism of the Brain, Including the Cooperation between Astrocytes and Neurons, Especially in the Context of Glycogen Metabolism." Int J Mol Sci **16**(11): 25959-25981.

Ferguson, S. J. (2010). "ATP synthase: from sequence to ring size to the P/O ratio." Proc Natl Acad Sci U S A **107**(39): 16755-16756.

Ferramosca, A. and V. Zara (2013). "Biogenesis of mitochondrial carrier proteins: molecular mechanisms of import into mitochondria." Biochim Biophys Acta **1833**(3): 494-502.

Ferri, K. F. and G. Kroemer (2001). "Organelle-specific initiation of cell death pathways." Nat Cell Biol **3**(11): E255-263.

Ferron, M., C. Settembre, J. Shimazu, J. Lacombe, S. Kato, D. J. Rawlings, A. Ballabio and G. Karsenty (2013). "A RANKL-PKCbeta-TFEB signaling cascade is necessary for lysosomal biogenesis in osteoclasts." Genes Dev **27**(8): 955-969.

Fiermonte, G., L. Palmieri, S. Todisco, G. Agrimi, F. Palmieri and J. E. Walker (2002). "Identification of the mitochondrial glutamate transporter. Bacterial expression, reconstitution, functional characterization, and tissue distribution of two human isoforms." J Biol Chem **277**(22): 19289-19294.

Fiermonte, G., G. Parisi, D. Martinelli, F. De Leonardis, G. Torre, C. L. Pierri, A. Saccari, F. M. Lasorsa, A. Vozza, F. Palmieri and C. Dionisi-Vici (2011). "A new Caucasian case of neonatal intrahepatic cholestasis caused by citrin deficiency (NICCD): a clinical, molecular, and functional study." Mol Genet Metab **104**(4): 501-506.

Finck, B. N. and D. P. Kelly (2006). "PGC-1 coactivators: inducible regulators of energy metabolism in health and disease." J Clin Invest **116**(3): 615-622.

Frey, T. G. and C. A. Mannella (2000). "The internal structure of mitochondria." Trends Biochem Sci **25**(7): 319-324.

Galione, A., A. J. Morgan, A. Arredouani, L. C. Davis, K. Rietdorf, M. Ruas and J. Parrington (2010). "NAADP as an intracellular messenger regulating lysosomal calcium-release channels." Biochem Soc Trans **38**(6): 1424-1431.

Garrity, A. G., W. Wang, C. M. Collier, S. A. Levey, Q. Gao and H. Xu (2016). "The endoplasmic reticulum, not the pH gradient, drives calcium refilling of lysosomes." Elife **5**: e15887.

Gellerich, F. N., Z. Gizatullina, S. Trumbekaite, B. Korzeniewski, T. Gaynutdinov, E. Seppet, S. Vielhaber, H. J. Heinze and F. Striggow (2012). "Cytosolic Ca2+ regulates the energization of isolated brain mitochondria by formation of pyruvate through the malate-aspartate shuttle." Biochem J **443**(3): 747-755.

Ghosh, P., N. M. Dahms and S. Kornfeld (2003). "Mannose 6-phosphate receptors: new twists in the tale." Nat Rev Mol Cell Biol **4**(3): 202-212.

Graves, A. R., P. K. Curran, C. L. Smith and J. A. Mindell (2008). "The Cl-/H+ antiporter ClC-7 is the primary chloride permeation pathway in lysosomes." Nature **453**(7196): 788-792.

Gruenberg, J. and F. R. Maxfield (1995). "Membrane transport in the endocytic pathway." Curr Opin Cell Biol **7**(4): 552-563.

Guicciardi, M. E., M. Leist and G. J. Gores (2004). "Lysosomes in cell death." Oncogene **23**(16): 2881-2890.

Haller, T., P. Dietl, P. Deetjen and H. Volkl (1996). "The lysosomal compartment as intracellular calcium store in MDCK cells: a possible involvement in InsP3-mediated Ca2+ release." Cell Calcium **19**(2): 157-165.

Haller, T., H. Volkl, P. Deetjen and P. Dietl (1996). "The lysosomal Ca2+ pool in MDCK cells can be released by ins(1,4,5)P3-dependent hormones or thapsigargin but does not activate store-operated Ca2+ entry." Biochem. J. **319 (Pt 3)**: 909-912.

Hertz, L., L. Peng and G. A. Dienel (2007). "Energy metabolism in astrocytes: high rate of oxidative metabolism and spatiotemporal dependence on glycolysis/glycogenolysis." J Cereb Blood Flow Metab **27**(2): 219-249.

Hinton, A., S. Bond and M. Forgac (2009). "V-ATPase functions in normal and disease processes." Pflugers Arch **457**(3): 589-598.

Hirst, J. and M. M. Roessler (2016). "Energy conversion, redox catalysis and generation of reactive oxygen species by respiratory complex I." Biochim Biophys Acta **1857**(7): 872-883.

Huynh, C. and N. W. Andrews (2005). "The small chemical vacuolin-1 alters the morphology of lysosomes without inhibiting Ca2+-regulated exocytosis." EMBO Rep. **6**(9): 843-847.

Iijima, M., A. Jalil, L. Begum, T. Yasuda, N. Yamaguchi, M. Xian Li, N. Kawada, H. Endou, K. Kobayashi and T. Saheki (2001). "Pathogenesis of adult-onset type II citrullinemia caused by deficiency of citrin, a mitochondrial solute carrier protein: tissue and subcellular localization of citrin." Adv Enzyme Regul **41**: 325-342.

Jadot, M., C. Colmant, S. Wattiaux-De Coninck and R. Wattiaux (1984). "Intralysosomal hydrolysis of glycyl-L-phenylalanine 2-naphthylamide." Biochem. J. **219**(3): 965-970.

Jaffe, L. F. and R. Creton (1998). "On the conservation of calcium wave speeds." Cell Calcium **24**(1): 1-8.

Jaiswal, J. K., N. W. Andrews and S. M. Simon (2002). "Membrane proximal lysosomes are the major vesicles responsible for calcium-dependent exocytosis in nonsecretory cells." J Cell Biol **159**(4): 625-635.

Jalil, M. A., L. Begum, L. Contreras, B. Pardo, M. Iijima, M. X. Li, M. Ramos, P. Marmol, M. Horiuchi, K. Shimotsu, S. Nakagawa, A. Okubo, M. Sameshima, Y. Isashiki, A. Del Arco, K. Kobayashi, J. Satrustegui and T. Saheki (2005). "Reduced N-acetylaspartate levels in mice lacking aralar, a brain- and muscle-type mitochondrial aspartate-glutamate carrier." J Biol Chem **280**(35): 31333-31339.

James, D. I., P. A. Parone, Y. Mattenberger and J. C. Martinou (2003). "hFis1, a novel component of the mammalian mitochondrial fission machinery." J Biol Chem **278**(38): 36373-36379.

Johnson, D. E., P. Ostrowski, V. Jaumouille and S. Grinstein (2016). "The position of lysosomes within the cell determines their luminal pH." J. Cell Biol. **212**(6): 677-692.

Kasper, D., R. Planells-Cases, J. C. Fuhrmann, O. Scheel, O. Zeitz, K. Ruether, A. Schmitt, M. Poet, R. Steinfeld, M. Schweizer, U. Kornak and T. J. Jentsch (2005). "Loss of the

chloride channel ClC-7 leads to lysosomal storage disease and neurodegeneration." EMBO J **24**(5): 1079-1091.

Kilpatrick, B. S., E. Yates, C. Grimm, A. H. Schapira and S. Patel (2016). "Endo-lysosomal TRP mucolipin-1 channels trigger global ER Ca2+ release and Ca2+ influx." J. Cell. Sci. **129**(20): 3859-3867.

Kiselyov, K., S. Yamaguchi, C. W. Lyons and S. Muallem (2010). "Aberrant Ca2+ handling in lysosomal storage disorders." Cell Calcium **47**(2): 103-111.

Koziel, K., M. Lebiedzinska, G. Szabadkai, M. Onopiuk, W. Brutkowski, K. Wierzbicka, G. Wilczynski, P. Pinton, J. Duszynski, K. Zablocki and M. R. Wieckowski (2009). "Plasma membrane associated membranes (PAM) from Jurkat cells contain STIM1 protein is PAM involved in the capacitative calcium entry?" Int. J. Biochem. Cell Biol. **41**(12): 2440-2449.

Krebs, H. A. and L. V. Eggleston (1940). "The oxidation of pyruvate in pigeon breast muscle." Biochem J **34**(3): 442-459.

Lacruz, R. S. and S. Feske (2015). "Diseases caused by mutations in ORAI1 and STIM1." Ann N Y Acad Sci **1356**: 45-79.

Lane, M. and D. K. Gardner (2005). "Mitochondrial malate-aspartate shuttle regulates mouse embryo nutrient consumption." J Biol Chem **280**(18): 18361-18367.

LaNoue, K. F., A. J. Meijer and A. Brouwer (1974). "Evidence for electrogenic aspartate transport in rat liver mitochondria." Arch Biochem Biophys **161**(2): 544-550.

LaNoue, K. F. and A. C. Schoolwerth (1979). "Metabolite transport in mitochondria." Annu Rev Biochem **48**: 871-922.

LaNoue, K. F. and M. E. Tischler (1974). "Electrogenic characteristics of the mitochondrial glutamate-aspartate antiporter." J Biol Chem **249**(23): 7522-7528.

LaPlante, J. M., J. Falardeau, M. Sun, M. Kanazirska, E. M. Brown, S. A. Slaugenhaupt and P. M. Vassilev (2002). "Identification and characterization of the single channel function of human mucolipin-1 implicated in mucolipidosis type IV, a disorder affecting the lysosomal pathway." FEBS Lett **532**(1-2): 183-187.

LaPlante, J. M., M. Sun, J. Falardeau, D. Dai, E. M. Brown, S. A. Slaugenhaupt and P. M. Vassilev (2006). "Lysosomal exocytosis is impaired in mucolipidosis type IV." Mol Genet Metab **89**(4): 339-348.

Laplante, M. and D. M. Sabatini (2012). "mTOR signaling in growth control and disease." Cell **149**(2): 274-293.

Lee, H. C. (1997). "Mechanisms of calcium signaling by cyclic ADP-ribose and NAADP." Physiol Rev **77**(4): 1133-1164.

Leist, M. and M. Jaattela (2001). "Triggering of apoptosis by cathepsins." Cell Death Differ **8**(4): 324-326.

Lenaz, G. and M. L. Genova (2010). "Structure and organization of mitochondrial respiratory complexes: a new understanding of an old subject." Antioxid Redox Signal **12**(8): 961-1008.

Lewis, R. S. (2007). "The molecular choreography of a store-operated calcium channel." Nature **446**(7133): 284-287.

Li, W., X. Yuan, G. Nordgren, H. Dalen, G. M. Dubowchik, R. A. Firestone and U. T. Brunk (2000). "Induction of cell death by the lysosomotropic detergent MSDH." FEBS Lett **470**(1): 35-39.

Llorente-Folch, I., C. B. Rueda, I. Amigo, A. del Arco, T. Saheki, B. Pardo and J. Satrustegui (2013). "Calcium-regulation of mitochondrial respiration maintains ATP homeostasis and requires ARALAR/AGC1-malate aspartate shuttle in intact cortical neurons." J Neurosci **33**(35): 13957-13971, 13971a.

Llorente-Folch, I., I. Sahun, L. Contreras, M. J. Casarejos, J. M. Grau, T. Saheki, M. A. Mena, J. Satrustegui, M. Dierssen and B. Pardo (2013). "AGC1-malate aspartate shuttle activity is critical for dopamine handling in the nigrostriatal pathway." J Neurochem **124**(3): 347-362.

Logan, M. R., S. O. Odemuyiwa and R. Moqbel (2003). "Understanding exocytosis in immune and inflammatory cells: the molecular basis of mediator secretion." J Allergy Clin Immunol **111**(5): 923-932; quiz 933.

Lopez-Sanjurjo, C. I., S. C. Tovey, D. L. Prole and C. W. Taylor (2013). "Lysosomes shape Ins(1,4,5)P3-evoked Ca2+ signals by selectively sequestering Ca2+ released from the endoplasmic reticulum." J. Cell Sci. **126**(Pt 1): 289-300.

Lopez Sanjurjo, C. I., S. C. Tovey and C. W. Taylor (2014). "Rapid recycling of Ca2+ between IP3-sensitive stores and lysosomes." PLoS One **9**(10): e111275.

Lu, M., L. Zhou, W. C. Stanley, M. E. Cabrera, G. M. Saidel and X. Yu (2008). "Role of the malate-aspartate shuttle on the metabolic response to myocardial ischemia." J Theor Biol **254**(2): 466-475.

Lu, Z. H., G. Chakraborty, R. W. Ledeen, D. Yahya and G. Wu (2004). "N-Acetylaspartate synthase is bimodally expressed in microsomes and mitochondria of brain." Brain Res Mol Brain Res **122**(1): 71-78.

Lubke, T., P. Lobel and D. E. Sleat (2009). "Proteomics of the lysosome." Biochim Biophys Acta **1793**(4): 625-635.

Luzio, J. P., P. R. Pryor and N. A. Bright (2007). "Lysosomes: fusion and function." Nat Rev Mol Cell Biol **8**(8): 622-632.

Ma'ayan, A., S. L. Jenkins, A. Barash and R. Iyengar (2009). "Neuro2A differentiation by Galphai/o pathway." Sci Signal **2**(54): cm1.

Madhavarao, C. N., C. Chinopoulos, K. Chandrasekaran and M. A. Namboodiri (2003). "Characterization of the N-acetylaspartate biosynthetic enzyme from rat brain." J Neurochem **86**(4): 824-835.

Marchi, S., S. Patergnani and P. Pinton (2014). "The endoplasmic reticulum-mitochondria connection: one touch, multiple functions." Biochim. Biophys. Acta. **1837**(4): 461-469.

Marsault, R., M. Murgia, T. Pozzan and R. Rizzuto (1997). "Domains of high Ca2+ beneath the plasma membrane of living A7r5 cells." EMBO J. **16**(7): 1575-1581.

Martina, J. A. and R. Puertollano (2013). "Rag GTPases mediate amino acid-dependent recruitment of TFEB and MITF to lysosomes." J Cell Biol **200**(4): 475-491.

Massari, M. E. and C. Murre (2000). "Helix-loop-helix proteins: regulators of transcription in eucaryotic organisms." Mol Cell Biol **20**(2): 429-440.

McCombs, J. E. and A. E. Palmer (2008). "Measuring calcium dynamics in living cells with genetically encodable calcium indicators." Methods **46**(3): 152-159.

McKenna, M. C., J. T. Tildon, J. H. Stevenson, I. B. Hopkins, X. Huang and R. Couto (1998). "Lactate transport by cortical synaptosomes from adult rat brain: characterization of kinetics and inhibitor specificity." Dev Neurosci **20**(4-5): 300-309.

McKenna, M. C., H. S. Waagepetersen, A. Schousboe and U. Sonnewald (2006). "Neuronal and astrocytic shuttle mechanisms for cytosolic-mitochondrial transfer of reducing equivalents: current evidence and pharmacological tools." Biochem Pharmacol **71**(4): 399-407.

McNeil, P. L. and T. Kirchhausen (2005). "An emergency response team for membrane repair." Nat Rev Mol Cell Biol **6**(6): 499-505.

Meadows, N. A., S. M. Sharma, G. J. Faulkner, M. C. Ostrowski, D. A. Hume and A. I. Cassady (2007). "The expression of Clcn7 and Ostm1 in osteoclasts is coregulated by microphthalmia transcription factor." J Biol Chem **282**(3): 1891-1904.

Medina, D. L., S. Di Paola, I. Peluso, A. Armani, D. De Stefani, R. Venditti, S. Montefusco, A. Scotto-Rosato, C. Prezioso, A. Forrester, C. Settembre, W. Wang, Q. Gao, H. Xu, M. Sandri, R. Rizzuto, M. A. De Matteis and A. Ballabio (2015). "Lysosomal calcium signalling regulates autophagy through calcineurin and TFEB." Nat Cell Biol **17**(3): 288-299.

Medina, D. L., S. Di Paola, I. Peluso, A. Armani, D. De Stefani, R. Venditti, S. Montefusco, A. Scotto-Rosato, C. Prezioso, A. Forrester, C. Settembre, W. Wang, Q. Gao, H. Xu, M. Sandri, R. Rizzuto, M. A. De Matteis and A. Ballabio (2015). "Lysosomal calcium signalling regulates autophagy through calcineurin and TFEB." Nat. Cell Biol. **17**(3): 288-299.

Medina, D. L., A. Fraldi, V. Bouche, F. Annunziata, G. Mansueto, C. Spampanato, C. Puri, A. Pignata, J. A. Martina, M. Sardiello, M. Palmieri, R. Polishchuk, R. Puertollano and A. Ballabio (2011). "Transcriptional activation of lysosomal exocytosis promotes cellular clearance." Dev. Cell **21**(3): 421-430.

Medina, D. L., A. Fraldi, V. Bouche, F. Annunziata, G. Mansueto, C. Spampanato, C. Puri, A. Pignata, J. A. Martina, M. Sardiello, M. Palmieri, R. Polishchuk, R. Puertollano and A. Ballabio (2011). "Transcriptional activation of lysosomal exocytosis promotes cellular clearance." Dev Cell **21**(3): 421-430.

Mellman, I. (1996). "Endocytosis and molecular sorting." Annu Rev Cell Dev Biol **12**: 575-625.

Menga, A., V. Iacobazzi, V. Infantino, M. L. Avantaggiati and F. Palmieri (2015). "The mitochondrial aspartate/glutamate carrier isoform 1 gene expression is regulated by CREB in neuronal cells." Int J Biochem Cell Biol **60**: 157-166.

Mindell, J. A. (2012). "Lysosomal acidification mechanisms." Annu Rev Physiol **74**: 69-86.

Mitchell, P. (1979). "Keilin's respiratory chain concept and its chemiosmotic consequences." Science **206**(4423): 1148-1159.

Mlody, B., C. Lorenz, G. Inak and A. Prigione (2016). "Energy metabolism in neuronal/glial induction and in iPSC models of brain disorders." Semin Cell Dev Biol **52**: 102-109.

Morgan, A. J., F. M. Platt, E. Lloyd-Evans and A. Galione (2011). "Molecular mechanisms of endolysosomal Ca2+ signalling in health and disease." Biochem. J. **439**(3): 349-374.

Morgan, A. J. and A. P. Thomas (1999). "Single cell and subcellular measurement of intracellular Ca2+ concentration ([Ca2+]i)." Methods Mol Biol **114**: 93-123.

Mostov, K. and Z. Werb (1997). "Journey across the osteoclast." Science **276**(5310): 219-220.

Mukherjee, S., R. N. Ghosh and F. R. Maxfield (1997). "Endocytosis." Physiol Rev **77**(3): 759-803.

Mullins, C. and J. S. Bonifacino (2001). "The molecular machinery for lysosome biogenesis." Bioessays **23**(4): 333-343.

Mullock, B. M., J. H. Perez, T. Kuwana, S. R. Gray and J. P. Luzio (1994). "Lysosomes can fuse with a late endosomal compartment in a cell-free system from rat liver." J Cell Biol **126**(5): 1173-1182.

Naylor, E., A. Arredouani, S. R. Vasudevan, A. M. Lewis, R. Parkesh, A. Mizote, D. Rosen, J. M. Thomas, M. Izumi, A. Ganesan, A. Galione and G. C. Churchill (2009). "Identification of a chemical probe for NAADP by virtual screening." Nat Chem Biol **5**(4): 220-226.

Nishi, T. and M. Forgac (2002). "The vacuolar (H+)-ATPases--nature's most versatile proton pumps." Nat Rev Mol Cell Biol **3**(2): 94-103.

Ohkuma, S., Y. Moriyama and T. Takano (1982). "Identification and characterization of a proton pump on lysosomes by fluorescein-isothiocyanate-dextran fluorescence." Proc Natl Acad Sci U S A **79**(9): 2758-2762.

Palmer, A. E., C. Jin, J. C. Reed and R. Y. Tsien (2004). "Bcl-2-mediated alterations in endoplasmic reticulum Ca2+ analyzed with an improved genetically encoded fluorescent sensor." Proc. Natl. Acad. Sci. USA **101**(50): 17404-17409.

Palmieri, F. (2013). "The mitochondrial transporter family SLC25: identification, properties and physiopathology." Mol Aspects Med **34**(2-3): 465-484.

Palmieri, F. and M. Monne (2016). "Discoveries, metabolic roles and diseases of mitochondrial carriers: A review." Biochim Biophys Acta **1863**(10): 2362-2378.

Palmieri, L., B. Pardo, F. M. Lasorsa, A. del Arco, K. Kobayashi, M. Iijima, M. J. Runswick, J. E. Walker, T. Saheki, J. Satrustegui and F. Palmieri (2001). "Citrin and aralar1 are Ca(2+)-stimulated aspartate/glutamate transporters in mitochondria." EMBO J **20**(18): 5060-5069.

Parekh, A. B. and J. W. Putney, Jr. (2005). "Store-operated calcium channels." Physiol Rev **85**(2): 757-810.

Peiter, E., F. J. Maathuis, L. N. Mills, H. Knight, J. Pelloux, A. M. Hetherington and D. Sanders (2005). "The vacuolar Ca2+-activated channel TPC1 regulates germination and stomatal movement." Nature **434**(7031): 404-408.

Petersen, O. H., D. Burdakov and A. V. Tepikin (1999). "Regulation of store-operated calcium entry: lessons from a polarized cell." Eur J Cell Biol **78**(4): 221-223.

Pierri, C. L., F. Palmieri and A. De Grassi (2014). "Single-nucleotide evolution quantifies the importance of each site along the structure of mitochondrial carriers." Cell Mol Life Sci **71**(2): 349-364.

Pinton, P., D. Ferrari, P. Magalhaes, K. Schulze-Osthoff, F. Di Virgilio, T. Pozzan and R. Rizzuto (2000). "Reduced loading of intracellular Ca(2+) stores and downregulation of capacitative Ca(2+) influx in Bcl-2-overexpressing cells." J. Cell Biol. **148**(5): 857-862.

Profilo, E., L. E. Pena-Altamira, M. Corricelli, A. Castegna, A. Danese, G. Agrimi, S. Petralla, G. Giannuzzi, V. Porcelli, L. Sbano, C. Viscomi, F. Massenzio, E. M. Palmieri, C. Giorgi, G. Fiermonte, M. Virgili, L. Palmieri, M. Zeviani, P. Pinton, B. Monti, F. Palmieri and F. M. Lasorsa (2017). "Down-regulation of the mitochondrial aspartate-glutamate carrier isoform 1 AGC1 inhibits proliferation and N-acetylaspartate synthesis in Neuro2A cells." Biochim Biophys Acta **1863**(6): 1422-1435.

Pryor, P. R., B. M. Mullock, N. A. Bright, M. R. Lindsay, S. R. Gray, S. C. Richardson, A. Stewart, D. E. James, R. C. Piper and J. P. Luzio (2004). "Combinatorial SNARE complexes with VAMP7 or VAMP8 define different late endocytic fusion events." EMBO Rep **5**(6): 590-595.

Quinlan, C. L., J. R. Treberg, I. V. Perevoshchikova, A. L. Orr and M. D. Brand (2012). "Native rates of superoxide production from multiple sites in isolated mitochondria measured using endogenous reporters." Free Radic Biol Med **53**(9): 1807-1817.

Quinn, P. J. and R. M. Dawson (1969). "Interactions of cytochrome c and [14C]." Biochem J **115**(1): 65-75.

Rafalski, V. A. and A. Brunet (2011). "Energy metabolism in adult neural stem cell fate." Prog Neurobiol **93**(2): 182-203.

Ramos, M., A. del Arco, B. Pardo, A. Martinez-Serrano, J. R. Martinez-Morales, K. Kobayashi, T. Yasuda, E. Bogonez, P. Bovolenta, T. Saheki and J. Satrustegui (2003). "Developmental changes in the Ca2+-regulated mitochondrial aspartate-glutamate carrier aralar1 in brain and prominent expression in the spinal cord." Brain Res Dev Brain Res **143**(1): 33-46.

Ramsey, I. S., M. Delling and D. E. Clapham (2006). "An introduction to TRP channels." Annu Rev Physiol **68**: 619-647.

Rao, S. K., C. Huynh, V. Proux-Gillardeaux, T. Galli and N. W. Andrews (2004). "Identification of SNAREs involved in synaptotagmin VII-regulated lysosomal exocytosis." J Biol Chem **279**(19): 20471-20479.

Rardin, M. J., J. C. Newman, J. M. Held, M. P. Cusack, D. J. Sorensen, B. Li, B. Schilling, S. D. Mooney, C. R. Kahn, E. Verdin and B. W. Gibson (2013). "Label-free quantitative proteomics of the lysine acetylome in mitochondria identifies substrates of SIRT3 in metabolic pathways." Proc Natl Acad Sci U S A **110**(16): 6601-6606.

Ren, Q., S. Ye and S. W. Whiteheart (2008). "The platelet release reaction: just when you thought platelet secretion was simple." Curr Opin Hematol **15**(5): 537-541.

Roczniak-Ferguson, A., C. S. Petit, F. Froehlich, S. Qian, J. Ky, B. Angarola, T. C. Walther and S. M. Ferguson (2012). "The transcription factor TFEB links mTORC1 signaling to transcriptional control of lysosome homeostasis." Sci Signal **5**(228): ra42.

Rodriguez, A., P. Webster, J. Ortego and N. W. Andrews (1997). "Lysosomes behave as Ca2+-regulated exocytic vesicles in fibroblasts and epithelial cells." J Cell Biol **137**(1): 93-104.

Rojas, R., T. van Vlijmen, G. A. Mardones, Y. Prabhu, A. L. Rojas, S. Mohammed, A. J. Heck, G. Raposo, P. van der Sluijs and J. S. Bonifacino (2008). "Regulation of retromer recruitment to endosomes by sequential action of Rab5 and Rab7." J Cell Biol **183**(3): 513-526.

Ronco, V., D. M. Potenza, F. Denti, S. Vullo, G. Gagliano, M. Tognolina, G. Guerra, P. Pinton, A. A. Genazzani, L. Mapelli, D. Lim and F. Moccia (2015). "A novel Ca(2)(+)-mediated cross-talk between endoplasmic reticulum and acidic organelles: implications for NAADP-dependent Ca(2)(+) signalling." Cell Calcium **57**(2): 89-100.

Rothman, D. L., H. M. De Feyter, R. A. de Graaf, G. F. Mason and K. L. Behar (2011). "13C MRS studies of neuroenergetics and neurotransmitter cycling in humans." NMR Biomed **24**(8): 943-957.

Roy, D., D. R. Liston, V. J. Idone, A. Di, D. J. Nelson, C. Pujol, J. B. Bliska, S. Chakrabarti and N. W. Andrews (2004). "A process for controlling intracellular bacterial infections induced by membrane injury." Science **304**(5676): 1515-1518.

Rupert, B. E., J. L. Segar, B. C. Schutte and T. D. Scholz (2000). "Metabolic adaptation of the hypertrophied heart: role of the malate/aspartate and alpha-glycerophosphate shuttles." J Mol Cell Cardiol **32**(12): 2287-2297.

Safer, B. (1975). "The Metabolic Significance of the Malate-Aspartate Cycle in Heart." Circ Res **37**(5): 527-533.

Saftig, P. and J. Klumperman (2009). "Lysosome biogenesis and lysosomal membrane proteins: trafficking meets function." Nat Rev Mol Cell Biol **10**(9): 623-635.

Sakurai, T., N. Ramoz, M. Barreto, M. Gazdoiu, N. Takahashi, M. Gertner, N. Dorr, M. A. Gama Sosa, R. De Gasperi, G. Perez, J. Schmeidler, V. Mitropoulou, H. C. Le, M. Lupu, P. R. Hof, G. A. Elder and J. D. Buxbaum (2010). "Slc25a12 disruption alters myelination and neurofilaments: a model for a hypomyelination syndrome and childhood neurodevelopmental disorders." Biol Psychiatry **67**(9): 887-894.

Sancak, Y., L. Bar-Peled, R. Zoncu, A. L. Markhard, S. Nada and D. M. Sabatini (2010). "Ragulator-Rag complex targets mTORC1 to the lysosomal surface and is necessary for its activation by amino acids." Cell **141**(2): 290-303.

Sardiello, M., M. Palmieri, A. di Ronza, D. L. Medina, M. Valenza, V. A. Gennarino, C. Di Malta, F. Donaudy, V. Embrione, R. S. Polishchuk, S. Banfi, G. Parenti, E. Cattaneo and A. Ballabio (2009). "A gene network regulating lysosomal biogenesis and function." Science **325**(5939): 473-477.

Satrustegui, J., L. Contreras, M. Ramos, P. Marmol, A. del Arco, T. Saheki and B. Pardo (2007). "Role of aralar, the mitochondrial transporter of aspartate-glutamate, in brain N-acetylaspartate formation and Ca(2+) signaling in neuronal mitochondria." J Neurosci Res **85**(15): 3359-3366.

Sbano, L., M. Bonora, S. Marchi, F. Baldassari, D. L. Medina, A. Ballabio, C. Giorgi and P. Pinton (2017). "TFEB-mediated increase in peripheral lysosomes regulates store-operated calcium entry." Sci Rep **7**: 40797.

Schroder, B. A., C. Wrocklage, A. Hasilik and P. Saftig (2010). "The proteome of lysosomes." Proteomics **10**(22): 4053-4076.

Settembre, C., R. De Cegli, G. Mansueto, P. K. Saha, F. Vetrini, O. Visvikis, T. Huynh, A. Carissimo, D. Palmer, T. J. Klisch, A. C. Wollenberg, D. Di Bernardo, L. Chan, J. E. Irazoqui and A. Ballabio (2013). "TFEB controls cellular lipid metabolism through a starvation-induced autoregulatory loop." Nat Cell Biol **15**(6): 647-658.

Settembre, C., C. Di Malta, V. A. Polito, M. Garcia Arencibia, F. Vetrini, S. Erdin, S. U. Erdin, T. Huynh, D. Medina, P. Colella, M. Sardiello, D. C. Rubinsztein and A. Ballabio (2011). "TFEB links autophagy to lysosomal biogenesis." Science **332**(6036): 1429-1433.

Settembre, C., A. Fraldi, D. L. Medina and A. Ballabio (2013). "Signals from the lysosome: a control centre for cellular clearance and energy metabolism." Nat. Rev. Mol. Cell Biol. **14**(5): 283-296.

Settembre, C., A. Fraldi, D. L. Medina and A. Ballabio (2013). "Signals from the lysosome: a control centre for cellular clearance and energy metabolism." Nat Rev Mol Cell Biol **14**(5): 283-296.

Settembre, C., R. Zoncu, D. L. Medina, F. Vetrini, S. Erdin, T. Huynh, M. Ferron, G. Karsenty, M. C. Vellard, V. Facchinetti, D. M. Sabatini and A. Ballabio (2012). "A lysosome-to-nucleus signalling mechanism senses and regulates the lysosome via mTOR and TFEB." EMBO J **31**(5): 1095-1108.

Shank, R. P., G. S. Bennett, S. O. Freytag and G. L. Campbell (1985). "Pyruvate carboxylase: an astrocyte-specific enzyme implicated in the replenishment of amino acid neurotransmitter pools." Brain Res **329**(1-2): 364-367.

Smirnova, E., L. Griparic, D. L. Shurland and A. M. van der Bliek (2001). "Dynamin-related protein Drp1 is required for mitochondrial division in mammalian cells." Mol Biol Cell **12**(8): 2245-2256.

Smyth, J. T., S. Y. Hwang, T. Tomita, W. I. DeHaven, J. C. Mercer and J. W. Putney (2010). "Activation and regulation of store-operated calcium entry." J. Cell Mol. Med. **14**(10): 2337-2349.

Solar, M., C. Cardalda, I. Houbracken, M. Martin, M. A. Maestro, N. De Medts, X. Xu, V. Grau, H. Heimberg, L. Bouwens and J. Ferrer (2009). "Pancreatic exocrine duct cells give rise to insulin-producing beta cells during embryogenesis but not after birth." Dev Cell **17**(6): 849-860.

Sonnewald, U. and C. Rae (2010). "Pyruvate carboxylation in different model systems studied by (13)C MRS." Neurochem Res **35**(12): 1916-1921.

Srinivas, S. P., A. Ong, L. Goon, L. Goon and J. A. Bonanno (2002). "Lysosomal Ca(2+) stores in bovine corneal endothelium." Invest. Ophthalmol. Vis. Sci. **43**(7): 2341-2350.

Steingrimsson, E., N. G. Copeland and N. A. Jenkins (2004). "Melanocytes and the microphthalmia transcription factor network." Annu Rev Genet **38**: 365-411.

Stinchcombe, J., G. Bossi and G. M. Griffiths (2004). "Linking albinism and immunity: the secrets of secretory lysosomes." Science **305**(5680): 55-59.

Stinchcombe, J. C. and G. M. Griffiths (2007). "Secretory mechanisms in cell-mediated cytotoxicity." Annu Rev Cell Dev Biol **23**: 495-517.

Sullivan, L. B., D. Y. Gui, A. M. Hosios, L. N. Bush, E. Freinkman and M. G. Vander Heiden (2015). "Supporting Aspartate Biosynthesis Is an Essential Function of Respiration in Proliferating Cells." Cell **162**(3): 552-563.

Tahay, G., E. Wiame, D. Tyteca, P. J. Courtoy and E. Van Schaftingen (2012). "Determinants of the enzymatic activity and the subcellular localization of aspartate N-acetyltransferase." Biochem J **441**(1): 105-112.

Thangaratnarajah, C., J. J. Ruprecht and E. R. Kunji (2014). "Calcium-induced conformational changes of the regulatory domain of human mitochondrial aspartate/glutamate carriers." Nat Commun **5**: 5491.

Tulsiani, D. R., A. Abou-Haila, C. R. Loeser and B. M. Pereira (1998). "The biological and functional significance of the sperm acrosome and acrosomal enzymes in mammalian fertilization." Exp Cell Res **240**(2): 151-164.

Verhage, M. and R. F. Toonen (2007). "Regulated exocytosis: merging ideas on fusing membranes." Curr Opin Cell Biol **19**(4): 402-408.

Verkaart, S., W. J. Koopman, S. E. van Emst-de Vries, L. G. Nijtmans, L. W. van den Heuvel, J. A. Smeitink and P. H. Willems (2007). "Superoxide production is inversely related to complex I activity in inherited complex I deficiency." Biochim Biophys Acta **1772**(3): 373-381.

Vogel, F., C. Bornhovd, W. Neupert and A. S. Reichert (2006). "Dynamic subcompartmentalization of the mitochondrial inner membrane." J Cell Biol **175**(2): 237-247.

Walker, V. (2014). "Ammonia metabolism and hyperammonemic disorders." Adv Clin Chem **67**: 73-150.

Wang, T., Z. Ming, W. Xiaochun and W. Hong (2011). "Rab7: role of its protein interaction cascades in endo-lysosomal traffic." Cell Signal **23**(3): 516-521.

Wesley, U. V., J. F. Hatcher and R. J. Dempsey (2015). "Sphingomyelin Synthase 1 Regulates Neuro-2a Cell Proliferation and Cell Cycle Progression Through Modulation of p27 Expression and Akt Signaling." Mol Neurobiol **51**(3): 1530-1541.

Wesolowski, J. and F. Paumet (2011). "The impact of bacterial infection on mast cell degranulation." Immunol Res **51**(2-3): 215-226.

Wibom, R., F. M. Lasorsa, V. Tohonen, M. Barbaro, F. H. Sterky, T. Kucinski, K. Naess, M. Jonsson, C. L. Pierri, F. Palmieri and A. Wedell (2009). "AGC1 deficiency associated with global cerebral hypomyelination." N Engl J Med **361**(5): 489-495.

Wu, P. Y., Y. C. Lin, C. L. Chang, H. T. Lu, C. H. Chin, T. T. Hsu, D. Chu and S. H. Sun (2009). "Functional decreases in P2X7 receptors are associated with retinoic acid-induced neuronal differentiation of Neuro-2a neuroblastoma cells." Cell Signal **21**(6): 881-891.

Xu, H. and D. Ren (2015). "Lysosomal physiology." Annu. Rev. Physiol. **77**: 57-80.

Yoon, Y., E. W. Krueger, B. J. Oswald and M. A. McNiven (2003). "The mitochondrial protein hFis1 regulates mitochondrial fission in mammalian cells through an interaction with the dynamin-like protein DLP1." Mol Cell Biol **23**(15): 5409-5420.

Yu, T., J. L. Robotham and Y. Yoon (2006). "Increased production of reactive oxygen species in hyperglycemic conditions requires dynamic change of mitochondrial morphology." Proc Natl Acad Sci U S A **103**(8): 2653-2658.

Zhang, F., S. Jin, F. Yi and P. L. Li (2009). "TRP-ML1 functions as a lysosomal NAADP-sensitive Ca2+ release channel in coronary arterial myocytes." J Cell Mol Med **13**(9B): 3174-3185.

Zhu, Z. D., T. Yu, H. J. Liu, J. Jin and J. He (2018). "SOCE induced calcium overload regulates autophagy in acute pancreatitis via calcineurin activation." Cell Death Dis **9**(2): 50.

Zoncu, R., L. Bar-Peled, A. Efeyan, S. Wang, Y. Sancak and D. M. Sabatini (2011). "mTORC1 senses lysosomal amino acids through an inside-out mechanism that requires the vacuolar H(+)-ATPase." Science **334**(6056): 678-683.